Specific Heat of Unconventional Superconductors

by

Borko Djurkovic

A thesis
presented to the University of Waterloo
in fulfillment of the
thesis requirement for the degree of
Master of Science
in
Physics

Waterloo, Ontario, Canada, 2010

I hereby declare that I am the sole author of this thesis. This is a true copy of the thesis, including any required final revisions, as accepted by my examiners.

I understand that my thesis may be made electronically available to the public.

Abstract

$PrOs_4Sb_{12}$ is the first known heavy fermion superconductor containing Pr. Many experiments show results indicating unconventional superconductivity in this system. Most notably, $PrOs_4Sb_{12}$ exhibits two superconducting transitions. The upper transition occurs at $T_{c1} \approx 1.89K$ and the lower transition occurs at $T_{c2} \approx 1.72K$. There are many features of this system that are not understood and do not have a unified consensus among researchers. Many issues remain unanswered, such as the origin of superconductivity, symmetry of the superconducting energy gap, and the nature of the two superconducting transitions. We present specific heat data for a single $PrOs_4Sb_{12}$ crystal. The data show two superconducting transitions. Variance in the lower superconducting transition (among various samples) suggests multiple superconducting phases. Power law dependence of the low temperature specific heat is indicative of asymmetric energy gap.

Cuprates are unconventional high temperature superconductors. The theory on origin and characteristics of superconductivity in these systems is still a debated issue. Experiments indicate presence of a phase in these systems that occurs above the superconducting transition temperature which exhibits some common characteristics with the superconducting state. An important issue is the nature of this so-called "pseudogap" phase and its relationship to the superconducting state. We have developed an experimental apparatus and procedure for measuring the specific heat of a high temperature superconductor and demonstrated it by measuring the heat capacity of a YBCO high-T_c superconductor sample.

Acknowledgements

I would like to thank Jan Kycia for his excellent guidance and advice as a supervisor, his motivation, and his limitless patience. I will always be in debt to the incredible amount of knowledge he has taught me over the last three years. I would also like to thank Robert Hill for his assistance with the equipment and experiments, as well as helpful discussions on the collected data. Frank Wilhelm taught a course on superconductivity which proved to be an excellent introduction and basis for my understanding of the relevant concepts. I would also like to express my gratitude to Jeff Quilliam. He has helped me in countless ways during my thesis work, and has been a great source of knowledge and inspiration.

A special recognition is deserved by Jeff Hill and Jeff Mason who spent innumerable hours with me working on and operating the dilution refrigerator used in these experiments. I would also like to acknowledge Shuchao Meng and Chas Mugford for all their assistance with various parts of my work. Patrick de Perio needs to be recognized for constructing the probe used in the high-T_c experiments. I need to thank Paul Dube for allowing me to participate and assist in performing the magnetic susceptibility experiments. Other lab personnel that deserve special mention are: Luke Yaraskavitch, Halle Revell, Lauren Persaud, and John Dunn.

I would also like to thank all the members of science machining shop, especially Andy Coglough, Harmen Vander Heide, and Hiruy Haile. They have been of great assistance in manufacturing various experimental components.

I need to acknowledge a few people for their friendship, encouragement and support: Kayla Ryan, Darren Clark, Emily Atkinson, Michael MacKinnon, and Jason Hoyt.

Most importantly, I need to express my gratitude and appreciation to my family who have been incredibly supportive throughout my entire academic career and all of my challenges.

Dedication

This is dedicated to my parents.

Table of contents

List of Tables

List of Figures

Chapter 1

Introduction

Superconductors are materials that, at low enough temperature, have the property of zero electrical resistance. They are able to sustain an electrical current with no dissipation of energy. This trademark property is just one of many remarkable physical characteristics possessed by superconductors. The experimental and theoretical study of superconducting materials has been one of the pivotal undertakings in modern physics. The ultimate goal of expanding our understanding of superconductivity is to develop room temperature superconductors. However, on the road to attaining that goal, we are able to greatly enrich our knowledge and increase our appreciation of the physical world and nature that surrounds us.

The work presented in this thesis consists of two major parts.

The first was concerned with measuring the specific heat of a heavy fermion system $PrOs_4Sb_{12}$. This compound is the first Pr based heavy fermion system that exhibits superconductivity. The transition from normal state to the superconducting state of $PrOs_4Sb_{12}$ is peculiar because it consists of two distinct transitions at two different temperatures. The origin and nature of this double transition behaviour is still a highly contested issue. Additionally, the underlying properties of the superconducting state are unclear. There is a possibility that the superconductivity in this heavy fermion system is unconventional in origin.

The second part of this thesis work appertains to measuring the specific heat of a high temperature cuprate superconductor $YBa_2Cu_3O_7$. The main goal of this work was to design and develop an experimental method to measure the specific heat of a high temperature superconductor and demonstrate it by determining the specific heat of a YBCO sample. Cuprates are high temperature superconductors with possible transition temperatures above the melting point of liquid nitrogen. They are unconventional superconductors and exhibit many interesting properties. The mechanism for the unconventional superconductivity in cuprates is still not fully understood and there are many theoretical and

experimental issues concerning the properties of cuprate systems that are debated and remain unresolved.

The presentation of this work is sectioned in number of chapters. In chapter 2, we briefly describe some of the key empirical properties of superconductors. We also present a very short and qualitative summary of superconductivity theory and some of its most important results. Chapter 3 provides the theoretical background that is relevant to understanding the specific heat of superconductors. A brief overview of the relevant experimental work and results related to $PrOs_4Sb_{12}$ that can be found in literature is summarized in chapter 4. Chapters 5 covers the experimental apparatus and procedure used in performing the specific heat measurements of a $PrOs_4Sb_{12}$ sample. The next chapter presents the discussion and analysis of the results of these measurements. Chapter 7 briefly describes some of the major properties and puzzles of superconductivity in cuprates. Chapters 8 and 9 divulge the experimental method and results related to measuring the specific heat of YBCO. Lastly, the final chapter provides a brief summary and few concluding remarks.

Chapter 2

Superconductivity

In this chapter, we will briefly describe some of the unique empirical properties of superconducting materials. Then, we will give a brief qualitative overview of the BCS theory that explains these unique physical properties, and we will state some of its prominent theoretical predictions.

2.1 Persistent Currents

The most notable property of superconductors is that below a critical temperature T_c, the electrical resistance of a superconducting metal abruptly drops to zero. Above this critical temperature, the metal is in the normal state. The electrical resistance of normal metals is governed by two processes: 1) the scattering due to impurities and defects resulting in a constant minimum resistance ρ_0, and 2) phonon scattering which contributes a temperature dependent term BT^5.[110][1] Therefore, in the normal state, the resistivity is described by $\rho(T) = \rho_0 + BT^5$. When the temperature is lowered below T_c, the metal suddenly enters a new electronically ordered state, the superconducting state. The resistance of the metal in the superconducting state is zero. This behaviour is described pictorially in Figure 2.1. If one establishes an electrical current in a superconducting material, it will continue without any measurable decay indefinitely. This remarkable property of persistent currents is the trademark of superconductors. If the current exceeds a threshold value called the critical current, the material will cease to superconduct and it will become normal.

[1] Electron-electron scattering contributes a T^2 term to the resistivity. However, in metals this term is negligible due to the free electron approximation where electron-electron interactions are ignored.

2.2 Magnetic Properties

Another extraordinary and defining characteristic of superconducting materials is perfect diamagnetism. A material in superconducting state expels all magnetic flux and no magnetic field can pass through its interior. When a superconductor is cooled below its critical temperature, the superconducting transition causes formation of electric currents that expunge any magnetic field that is present inside. This effect is known as the Meissner effect. It should be pointed out that this is not perfect conductivity (resistance being zero). Moving a perfect conductor from a region with zero magnetic field to a region with nonzero magnetic field would cause the creation of screening currents inside the conductor that would negate the magnetic field. Similarly, if a perfect conductor, initially in a magnetic field, is moved to a region with zero magnetic field, it would develop eddy currents in order to prevent the elimination of the magnetic field. This behaviour is expected since Faraday's law of induction

$$\nabla \times \mathbf{E} = -\frac{1}{c}\frac{\partial \mathbf{B}}{\partial t} \tag{2.1}$$

relates time varying magnetic field to the induction of electric field. Accordingly, in a perfect conductor, the magnetic field inside should be time-independent, but its value is undetermined. On the other hand, in a superconducting material, the magnetic field is time-independent and its value is exactly zero.

In zero magnetic field at temperatures below T_c, the superconducting state has lower free energy than the normal state and hence it is energetically favourable. In the presence of a magnetic field, screening eddy currents are created that eliminate the magnetic field inside the superconductor. This process is energy consuming, thus increasing the free energy of the superconducting state. As the magnetic field strength is increased above a critical value H_c, the decrease in the magnetic field energy that would occur if the screening currents disappeared and the magnetic field was allowed to penetrate the superconductor becomes larger than the increase of the free energy caused by the transition from the superconducting state to the normal state. Hence the free energy of the normal state becomes lower than the free energy of the superconducting state. The normal state becomes more energetically advantageous, and the superconducting state is destroyed. The difference between the free energy of the normal state and the free energy of the superconducting state, the so called condensation energy, is related to the critical field:[106]

$$f_n(T) - f_s(T) = \frac{H_c^2(T)}{8\pi} \tag{2.2}$$

where $H_c(T)$ is given by the empirical law depicted in Figure 2.2:[106]

$$H_c(T) \approx H_c(0)\left[1 - \left(\frac{T}{T_c}\right)^2\right] \tag{2.3}$$

Critical currents arise because currents inside the superconducting materials generate magnetic field above H_c causing it to go normal.

The behaviour in which superconducting materials respond to increasing magnetic field strength and allow it to enter its interior differentiates two types of superconductors.

2.2.1 Type I Superconductors

In Type I superconductors, if the magnetic field strength is below a critical value $H_c(T)$, the superconductor is able to create the necessary screening currents and no magnetic field exists in the interior of the specimen. If the magnetic field strength is above $H_c(T)$, the superconductor is unable to expel the magnetic field. It transitions into the normal state, and the magnetic field is allowed to enter the superconductor. The strength of the critical magnetic field $H_c(T)$ increases as temperature decreases below the critical temperature T_c. The $H - T$ phase diagram for Type I superconductors is shown in Figure 2.2.

2.2.2 Type II Superconductors

Type II superconductors exhibit different behaviour when magnetic fields are present. They are characterized by two critical fields. If the magnetic field strength is less then the lower critical field $H_{c1}(T)$, the superconductor is able to cancel the magnetic field perfectly. If the magnetic field strength is above the upper critical field $H_{c2}(T)$, the superconductor becomes normal and the magnetic field penetrates inside. In the intermediate region between $H_{c1}(T)$ and $H_{c2}(T)$, a new superconducting state develops called the mixed state. In the mixed state, it is energetically advantages for the magnetic flux to partially penetrate into the interior of the superconductor. This is accomplished through segregation of the superconducting material into microscopic superconducting domains and normal domains. The normal regions are called vortex lines. The magnetic field lines pass through the cores of vortex lines. They are surrounded by screening currents that trap a quantized amount of magnetic flux inside the cores. Vortex lines form a complex triangular array throughout the superconducting material. In between the vortex lines is superconducting material that contains no magnetic flux.

Figure 2.3 compares the magnetization curves of type I and type II superconductors. In type I superconductors, magnetization is linear up to the critical field H_c; there is no magnetic flux present inside. Above H_c, the sample is normal and there is perfect penetration of flux into the superconductor. In type II superconductors, magnetization is linear up to the lower critical field H_{c1} and superconductor behaves as a type I superconductor. Between H_{c1} and H_{c2}, there is partial penetration of magnetic flux into the specimen.

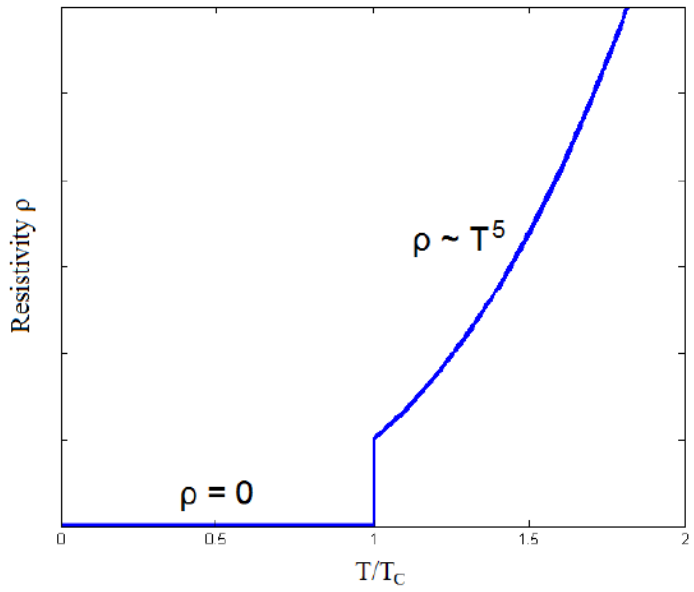

Figure 2.1: Behaviour of resistivity at the superconducting phase transition.

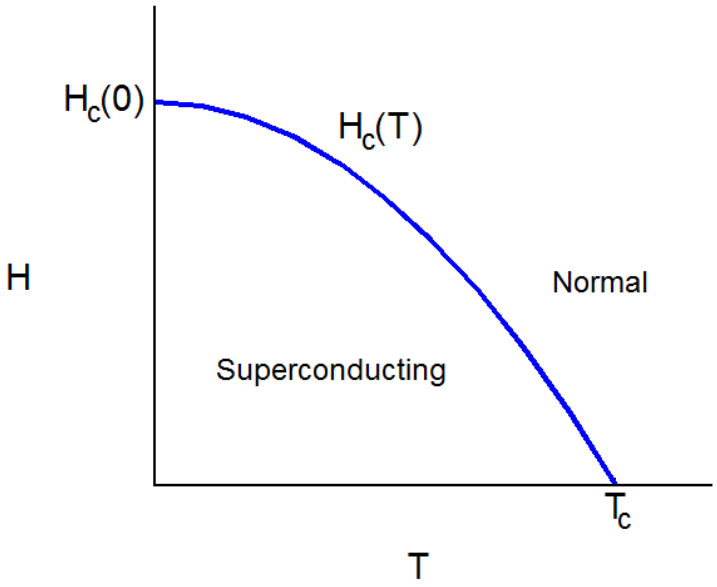

Figure 2.2: Temperature dependence of critical field.

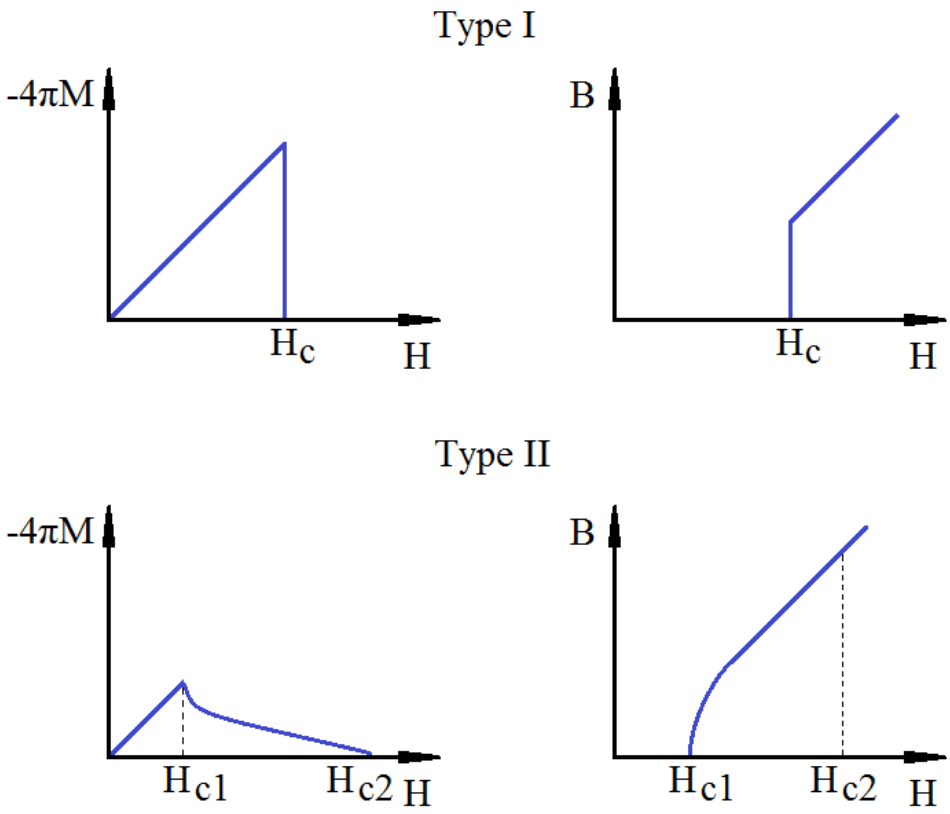

Figure 2.3: Magnetization curves for Type I and Type II superconductors.

Table 2.1: Table of Few Superconductors

Formula	Type	$T_C(K)$	$H_{C1}(mT)$	$H_{C2}(T)$
Al	I	1.18	10.5	
In	I	3.41	22.5	
Nb	II	9.26	248	0.4
Pb	I	7.20	80	
NbTi	II	9.2		12
UBe_{13}	II	0.9	4.4	10
$NbSe_2$	II	7.2	4	17.4

Above the upper critical field H_{c2}, the magnetic flux penetrates perfectly into the sample as it is in normal state.

Table 2.1 lists some superconductors and the corresponding transition temperatures and critical field values.[17]

2.3 Thermoelectric Properties

Another unexpected property of superconductors is that they are very inefficient conductors of heat. Normal metals make for fair thermal conductors because conduction electrons transfer heat while carrying current. Superconductors exhibit completely different behaviour. In superconductors, electrons that carry the persistent current do not transport any entropy making metals in the superconducting state very poor conductors of thermal energy.

2.4 Energy Gap

Superconductors exhibit an energy gap centered about the Fermi energy that represents the difference between the ground state of the superconductor and the excited state of the system. In other words, it takes an energy equal to the energy gap Δ to remove an electron from the superconducting state and into the normal state. The energy gap has its maximum value at low temperatures ($T = 0$) and decreases with increasing temperature.

The most direct indication of the existence of an energy gap is by tunneling experiments. Suppose two metals are brought together into close contact at thermal equilibrium. Electrons will momentarily flow across the contact from one material and into the other material in order to equate the chemical potentials of the two materials. In other words, the Fermi energy of the two levels will be equal.

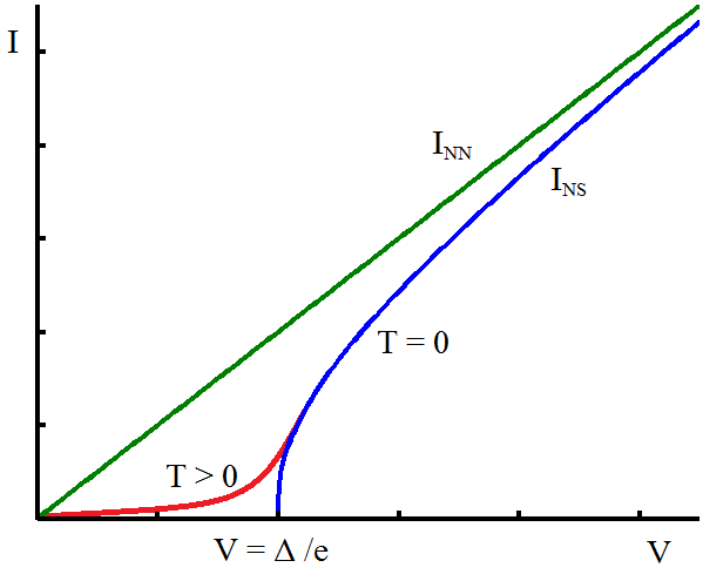

Figure 2.4: Current-Voltage characteristics of a normal-normal tunnel junction (green), normal-superconductor tunnel junction at $T = 0$ (blue) and at finite temperature (red).

If an electrical potential is applied across the two materials, more electrons tunnel across the barrier. This occurs because the chemical potential of one of the materials is increased with respect to the other material by the applied voltage. If the two materials are both normal metals, the current created by the applied voltage obeys Ohm's law. In other words, the conductance across the junction between the two materials is constant (independent of the applied voltage). The situation is very different for the case when one of the materials is a superconductor. Low temperature experiments show no observable tunneling current unless the potential difference is great enough such that $eV > \Delta$.[106] This means that the chemical potential must be lifted enough to provide adequate energy to excite an electron out of the superconducting state and into the normal state. As the temperature increases towards the critical temperature T_c, the required voltage decreases. From this, we can conclude that the energy gap decreases with increasing temperature. This behaviour is illustrated in Figure 2.4.

Specific heat experiments provide further evidence for the existence of the energy gap. The electronic specific heat of a normal-state material is a linear function of temperature $C_{en} = \gamma T$. When a material undergoes the transition into the superconducting state the behaviour of the specific heat is drastically altered. At the critical temperature T_c, a jump in the specific heat is observed. As the temperature decreases below the transition temperature, the electronic specific heat decreases exponentially $e^{-\Delta/k_B T}$. This suggest that the excited (normal) state is an energy equal to 2Δ above the ground (superconducting)

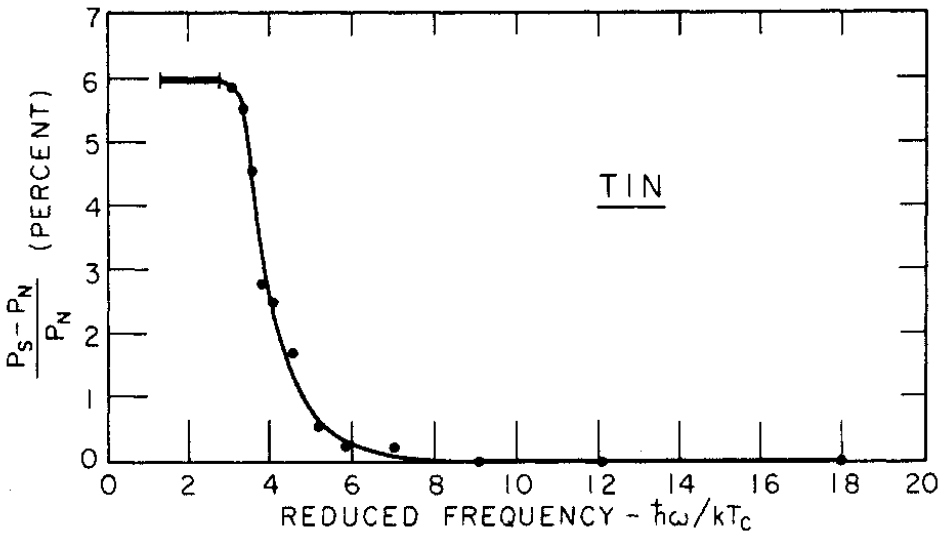

Figure 2.5: Difference in the power reaching the detector between the superconducting and normal states of tin as a function of frequency.[88]

state.

Electromagnetic absorption experiments also give support to the idea of an energy gap in superconductors.[88] It is observed that the absorption of AC radiation is identical in normal and superconducting materials for radiation in the optical frequencies. However, in the infrared region, superconducting materials start to exhibit different response to electromagnetic radiation. At microwave frequencies there is no absorption of electromagnetic radiation in superconductors. The microwave radiation is well below the frequency $\Delta/\hbar$ and hence cannot be absorbed by the conduction electrons in the superconducting state. Figure 2.5 shows one of the earliest attempts at measuring the superconducting energy gaps of tin. It shows the difference in the power reaching the detector between the superconducting and normal states of tin as a function of frequency of electromagnetic radiation.

A similar situation occurs with sound waves. Sound waves can be attenuated as they pass through materials by contributing some of their energy to the electrons near the Fermi level. It is observed that this attenuation of sound waves is considerably smaller in superconducting materials than in normal materials at frequencies $h\omega < 2\Delta$.[106]

2.5 London Equations

London brothers first developed a simple description of superconductivity.[57] Lorentz force law specifies the motion of the superconducting electrons in response to a uniform electric field inside a perfect conductor:

$$m\mathbf{a_s} = m\frac{d\mathbf{v_s}}{dt} = -e\mathbf{E} \tag{2.4}$$

The mean velocity of the electrons $\mathbf{v_s}$ is related to the current density $\mathbf{j_s}$ by:

$$\mathbf{j_s} = -e\mathbf{v_s}n_s \tag{2.5}$$

where n_s is the number of superconducting electrons. Substituting this expression into equation 2.4:

$$\frac{d\mathbf{j_s}}{dt} = \frac{n_s e^2}{m}\mathbf{E} \tag{2.6}$$

This equation describes perfect conductivity. In a normal conductor, the electric field is counterbalanced by the resistance due to scattering and the electrons maintain a constant drift velocity. Conversely, in a superconductor, the electrons experience a constant acceleration due to the electric field. In equation 2.6, n_s is the number density of superconducting electrons. The model assumes that n_s is a fraction of the total density of conduction electrons n and that it varies continuously at temperatures $T < T_c$. At $T \ll T_c$, n_s approaches the limiting value of n. Similarly, when $T = T_c$, $n_s = 0$. The superconducting electrons n_s are able to move freely with no resistance while the "normal" electrons $n - n_s$ move usually as in any normal conductor. Therefore, the superconducting electrons n_s are responsible for all of the current caused by any electric field (ie. $\mathbf{j} = \mathbf{j_c}$).

Using equation 2.6 and Faraday's law of induction 2.1, we can obtain the relationship between current density and magnetic field:

$$\frac{\partial}{\partial t}\left(\nabla \times \mathbf{j} + \frac{n_s e^2}{mc}\mathbf{B}\right) = 0 \tag{2.7}$$

The above equation states that any static magnetic field $\mathbf{B}$ and static current density $\mathbf{j}$ are possible solutions for a perfect conductor. However, this contradicts the behaviour detected in superconductors. As stated earlier, no magnetic field exists inside superconducting material. In order to describe the superconducting phenomenon, we have to be restrictive and limit the possible solutions such that the the term inside the brackets in equation 2.7 is not only time-independent, but more specifically equal to zero:

$$\nabla \times \mathbf{j} = -\frac{n_s e^2}{mc}\mathbf{B} \tag{2.8}$$

Combining the above equation with the Maxwell equation:

$$\nabla \times \mathbf{B} = -\frac{4\pi}{c}\mathbf{j} \tag{2.9}$$

leads to the equation:

$$\nabla^2 \mathbf{B} = -\frac{4\pi n_s e^2}{mc^2}\mathbf{B} \tag{2.10}$$

$$\nabla^2 \mathbf{j} = -\frac{4\pi n_s e^2}{mc^2}\mathbf{j} \tag{2.11}$$

This equation implies that any magnetic field that penetrates into a superconductor is exponentially screened from the interior by electric currents. This is precisely the Meissner effect. The magnetic fields penetrate into the sample a distance referred to as London penetration depth and defined as:

$$\lambda_L = \left(\frac{mc^2}{4\pi n_s e^2}\right)^{\frac{1}{2}} \tag{2.12}$$

2.6 The BCS Theory

Bardeen, Cooper, and Schrieffer put together a microscopic theory of superconductivity in 1957 which has become to be known simply as the BCS theory.[10] In this section we will briefly and qualitatively describe some of the more pertinent aspects of the theory, and present few notable theoretical results.

The basic underlying principle behind the theory of superconductivity is that there exists a net attractive force between pairs of electrons. Given this assumption, Cooper showed that there exists a bound state for pairs of electrons with energy that is negative relative to the Fermi energy.[20] His approach was to examine the problem of two electrons in a simple attractive potential with additional constraint that the effect of other electrons limits the possible momenta of the two interacting electrons to those with wave vectors $k > k_F$. His calculations showed that, even though the electrons have kinetic energies higher then Fermi energy, the negative contribution due to the attractive potential offsets this excess energy and results in formation of a bound-pair state. In other words, in the presence of any attractive interaction, regardless of how small it may be, two electrons will form bound pairs called Cooper pairs. The electrons that constitute a Cooper pair have equal and opposite momenta and spin, and have spherical symmetry, ie. they form an S state. Cooper's results also showed that only electrons with energies $E' \sim k_B T_c \ll \hbar\omega_D$[2] above

[2] ω_D is a measure of the maximum phonon frequency and defined by $\hbar\omega_D = k_B\Theta_D$

the Fermi energy are involved in the binding process. Thus, the transition temperature is insignificant in relation to the other characteristic temperatures of the material and the distribution of energy states pertinent to superconductivity is very narrow. Another crucial result is that the size of the Cooper pairs, called the coherence length, is $\xi_0 \sim \hbar v_F / k_B T_c$. The importance of this is that the coherence length is much larger than the interparticle distance. This means that Cooper pairs overlap; between two electrons forming a Cooper pair, there are many other Cooper pairs.

The attractive interaction between electrons that is necessary for superconductivity originates from the complex influence that the electrons and the motion of the ions have on each other. Electrons experience mutual repulsion due to the electrostatic Coulomb force. However, in a more complete analysis that considers atomic structure, it is possible for the motion of ions to screen the Coulomb repulsion between the electrons. The result is a net attractive interaction. An intuitive argument as to how this may happen is described by Tinkham:[106]

> The physical idea is that the first electron polarizes the medium by attracting positive ions; these excess positive ions, in turn, attract the second electron, giving an effective attractive interaction between the electrons. If this attraction is strong enough to override the repulsive screened Coulomb interaction, it gives rise to a net attractive interaction, and superconductivity results.

A more realistic picture that takes into account the effects of ionic motion on the electrons can be approximated by an effective potential:[110]

$$V^{eff}(\mathbf{q},\omega) = \frac{4\pi e^2}{q^2 + k_0^2}\left[1 + \frac{\omega(\mathbf{q})^2}{\omega^2 - \omega(\mathbf{q})^2}\right] \tag{2.13}$$

where

$$\mathbf{q} = \mathbf{k} - \mathbf{k}'; \quad \omega = \frac{\varepsilon_{\mathbf{k}} - \varepsilon_{\mathbf{k}'}}{\hbar}$$

and k_0 is the Thomas-Fermi wave vector which is on the order of k_F.[110]

Equation 2.13 describes the effective interaction between two electrons with wave vectors $\mathbf{k}$ and $\mathbf{k}'$ and energies $\varepsilon_{\mathbf{k}}$ and $\varepsilon_{\mathbf{k}'}$. The first term is the repulsive Coulomb force altered to include the screening effects of the dielectric constant of the medium. This accounts for the screening effect of the conduction electrons. The second term describes the effect of the phonons on the interaction between a pair of electrons. The wave vector $\mathbf{q} = \mathbf{k} - \mathbf{k}'$ represents the momentum of a phonon that scatters an electron with momentum wave vector $\mathbf{k}$ to an electron with momentum wave vector $\mathbf{k}'$. It is a statement of momentum conservation. $\omega(\mathbf{q})$ is therefore the characteristic frequency of the phonons involved in the scattering process. If the pair of electrons are separated by energy substantially higher

than $\hbar\omega(\mathbf{q})$, the second term in equation 2.13 becomes negligible and the interaction is repulsive. Since $\omega(\mathbf{q})$ is on the order of ω_D, and the differences in electron energies are generally orders of magnitude higher than $\hbar\omega_D$, only electrons with very similar energies are considerably influenced by the phonon interaction. When the two electrons have energies very close together, then the denominator in the phonon contribution in equation 2.13 has a negative sign and larger magnitude. The result is that the effective interaction becomes attractive, and the electrons form a bound pair.

The complete BCS theory extends the idea of bound pair formation to all electrons. Each electron limits possible wave vectors of *other* electrons involved in the pair formation process (as discussed earlier), and concurrently, it is involved in the formation of a bound pair. Additionally, as stated earlier, the size of Cooper pairs is large compared to typical spacing between electrons and hence there is large overlap between pairs. Hence, Cooper pairs are not independent particles, but interact mutually in a very elaborate arrangement. Thus, when a material undergoes a superconducting transition, the electrons 'condense' into the BCS ground state where electrons are bound, in pairs, into identical two-electron states. Identical pair wave functions are essential to stability of superconducting state and in explaining the phenomenon of persistent currents and the absence of thermal currents.

The BCS theory of superconductivity requires only that there is some attractive interaction between electrons, and is not specifically concerned with the origin of that attraction. To this effect, the electron-electron interaction is reduced to a very basic form:

$$V_{\mathbf{k}\mathbf{k}'} = \begin{cases} -V & \text{if } |\varepsilon_{\mathbf{k}}| \text{ and } |\varepsilon_{\mathbf{k}'}| \leq \hbar\omega_D \\ 0 & \text{otherwise} \end{cases} \tag{2.14}$$

Even with this oversimplification, the BCS theory is able to make some important theoretical predictions.

2.6.1 Critical Temperature

When no magnetic field is present, the superconducting transition occurs at the critical temperature given by:

$$k_B T_c = 1.13\hbar\omega_c e^{-1/N(0)V} \tag{2.15}$$

$N(0)$ designates the electronic level density at the Fermi level of electrons with one spin orientation, and ω_c is the phonon cutoff frequency and is on the order of ω_D. For typical superconductors $N(0)V \ll 1$, and hence the transition temperature is orders of magnitude below the Debye temperature Θ_D even though $\hbar\omega_c$ is on the order of $k_B\Theta_D$. Also note that the theory predicts existence of a transition temperature as long as there exists an attractive interaction with no consideration as to how weak the coupling potential V may be.

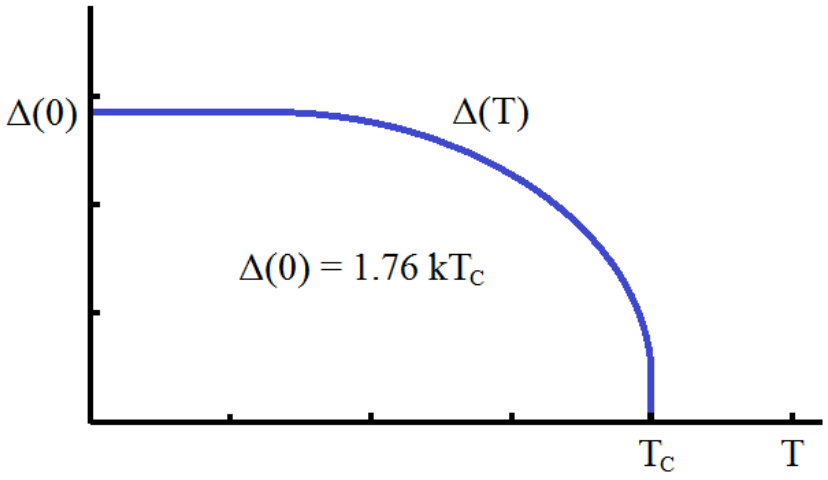

Figure 2.6: Temperature dependence of the energy gap in the BCS theory.

2.6.2 Energy Gap

The BCS theory also predicts a similar equation for the superconductivity energy gap at zero-temperature in zero magnetic field:

$$\Delta(0) = 2\hbar\omega_c e^{-1/N(0)V} \tag{2.16}$$

Combining this equation with equation 2.15, one obtains a very useful relation:

$$\frac{\Delta(0)}{k_B T_c} = \frac{2}{1.13} = 1.76 \tag{2.17}$$

The above relation is generally is good agreement with experimental results for a multitude of superconductors.

Temperature dependence of the energy gap is illustrated in Figure 2.6. At very low temperatures, the energy gap can be approximated by its zero-temperature value and it does not vary much with temperature, ie. $\Delta(T) \approx \Delta(0)$. As the temperature approaches the critical temperature, the energy gap drops promptly to zero. This means that the energy gap is nearly constant until a significant number of Cooper pairs become broken due to thermal excitations. Temperature dependence of the energy gap at temperatures near the critical temperature is describe by the formula:

$$\frac{\Delta(T)}{\Delta(0)} \approx 1.74 \left(1 - \frac{T}{T_c}\right)^{1/2} \quad T \approx T_c \tag{2.18}$$

2.6.3 Specific Heat

The zero-field specific heat of electrons in the superconducting state is described by the relation:

$$\frac{C_{en}}{\gamma T_c} = 1.34 \left(\frac{\Delta(0)}{T} \right)^{3/2} e^{-\Delta(0)/T} \tag{2.19}$$

where γ is the coefficient of the linear term in the normal state specific heat of metals. The above equation correctly describes the exponential behaviour in the specific heat that was experimentally observed.

The BCS theory also shows that the specific heat should exhibit a discontinuity in the electronic specific heat at the critical temperature in zero field:

$$\frac{\Delta C}{C_{en}} = 1.43 \quad T = T_c \tag{2.20}$$

This relation is generally in fair agreement with the experimental measurements for most superconductors.

2.6.4 Flux Quantization

One of the most crucial and extraordinary predictions of the theory of superconductivity is the phenomenon of flux quantization. Any closed loop of superconducting current must enclose a quantized amount of magnetic flux such that the total flux through the ring is $\Phi = n\Phi_0$ where

$$\Phi_0 = \frac{hc}{2e} = 2.0689 \times 10^{-7} gauss - cm2 \tag{2.21}$$

is a quantum of flux, or the fluxoid. This surprising property has been confirmed experimentally.[24, 25]

The idea of flux quantization has many important consequences. It plays a crucial role in explaining the stability of the superconducting state and persistent currents as described eloquently by Tinkham:[106]

> This concept forms the basis for understaning the quantum nature of persistent currents in a ring. The current cannot decrease by infinitesimal amounts, but only in quantum jumps in which the fluxoid quantum number decreases by one or more units. Such a quantum jump could occur readily if only a single electron were involved, as in an atomic transition. However, in the superconductor such a quantum jump for the macroscopic wavefunction ψ requires a collective transition of all the pairs involved. The extremely long life of persistent currents

results from the extreme improbability of such a simultaneous quantum jump by $\sim 10^{20}$ particles. Until a quantum jump occurs, there is no decay whatsoever of the persistent current.

Flux quantization has consequences for type II superconductors. In a type II superconductor that is in the mixed state, each vortex encloses a single quantum of magnetic flux.

The quantization of magnetic flux has practical implications as well. It is a crucial idea in operation of superconducting quantum interference devices (SQUIDs) used for sensitive measurements of very weak magnetic fields.

2.7 Unconventional Superconductors

Superconducting material that can be described by the BCS theory are called conventional superconductors. However, there are many materials that exhibit superconductivity and properties that do not agree with the standard model of the BCS theory. These materials are called unconventional superconductors.

The BCS model of superconductivity assumes that the attractive potential can be described by a simple effective potential in equation 2.14. This framework works very well for a large number of superconductors called "weak coupling" superconductors. However, for some materials, this effective potential is a gross oversimplification and does not yield correct description of the superconducting properties. Lead and mercury are just a couple of example of these "strong coupling" superconductors. Even equation 2.13 is too crude to be of practical relevance. A more accurate treatment of the electron-phonon interaction must be employed to correctly describe strong coupling superconductors.

Cooper pairs in the BCS theory are bound in a singlet S state. Some unconventional superconductors show anisotropy in the pairing (ie. there are nodes in the energy gap). The energy gap can have different magnitudes along different crystallographic directions. This concept is illustrated in Figure 2.7. An example of material with d-wave pairing is the superconductor $YBa_2Cu_3O_7$. Other superconductors may have Cooper pairs that form a triplet state. This leads to a different pairing function, and hence unconventional energy gap.

Some unconventional superconductors have unique properties because the source of the attractive force between electrons is not due to interaction with the phonons. For example, UPt_3 is a superconductor with a magnetically mediated attractive interaction between the electrons.[72]

High temperature superconductors is a class of materials that manifest superconductivity at unusually high temperatures. The transition temperatures of high temperature

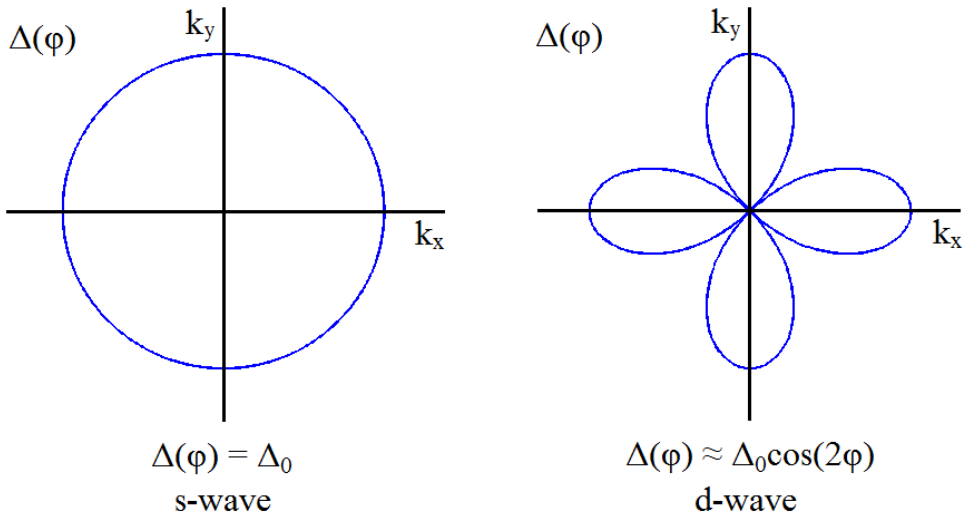

Figure 2.7: Comparison of a s-wave gap function and a d-wave gap function.

superconductors are usually above 30 K, and can even be above 100 K. These materials exhibit many of the unusual properties mentioned above, such as anisotropy in the energy gap. Their superconductivity and properties do not conform to the standard BCS theory, and a new theory of superconductivity is required.

Chapter 3

Specific Heat

In this chapter, we will make some general remarks about specific heat. Then, we will briefly and succinctly describe various contributions to the specific heat of crystals. Expressions for the contribution to the specific heat due to ionic vibrations at various temperature ranges will be described in section on lattice specific heat. Next, the specific heat of electrons will be quickly described. This is followed by a section on the specific heat contribution due to magnetic moments. For completion, we will restate the specific heat of superconductors in the final section.

The quantity of heat Q required to increase the temperature of a mass m of a certain material from T_1 to T_2 is proportional to the temperature change $\Delta T = T_2 - T_1$. Heating two cups of water for coffee requires twice as much heat as heating one cup; ie. the heat required is proportional to the mass of the material. Finally, the amount of heat also depends on the material being heated. Putting everything together, the amount of heat required to change the temperature of a material is:

$$Q = mc\Delta T \tag{3.1}$$

where m is the mass of the material, ΔT is the temperature change, and c is the material dependent proportionality constant called the specific heat of the material.

The state of a macroscopic system can be specified by its absolute temperature T and some other macroscopic parameter y, such as the volume or the mean pressure of the system. Suppose that the system is at some temperature T and the macroscopic parameter y is held fixed. Then a more accurate or precise definition of heat capacity is given as the ratio:

$$C_y = \lim_{dT \to 0} \frac{đQ}{dT}\bigg|_y \tag{3.2}$$

where $đQ$ is an infinitesimal amount of heat added to the system. The resulting change in temperature dT depends on the nature of the system and on the particular macrostate of the system, ie. $C_y = C_y(T, y)$.

The heat capacity C_y depends on the amount of material. Therefore, it is customary to define specific heat as a quantity that does not depend on the amount of material present, but only on the nature of the system. Hence, specific heat per gram is:

$$c_y = \frac{1}{m}\frac{đQ}{dT}\bigg|_y \tag{3.3}$$

where m is the mass of the substance. Likewise, molar heat capacity is:

$$c_y = \frac{1}{n}\frac{đQ}{dT}\bigg|_y \tag{3.4}$$

where n is the number of moles of the substance, and hence has units of $J/molK$.

The second law of thermodynamics relates the heat $đQ$ that a system absorbs during a quasi-static infinitesimal process to the change of entropy of the system:

$$dS = \frac{đQ}{T} \tag{3.5}$$

This means that we can relate the change in entropy of two macroscopic states (a and b) of the system to the heat capacity of the system:

$$S(T_b) - S(T_a) = \int_a^b \frac{đQ}{T} = \int_{T_a}^{T_b} \frac{C_y(T')dT'}{T'} \tag{3.6}$$

The above equation is important because it explicitly connects two different types of information about the system. The left hand side involves entropy which is related to a microscopic knowledge of the quantum states of the system under consideration. The right hand side of equation 3.6 involves the heat capacity which is a macroscopic characteristic of the system. In other words, a macroscopic measurement of absorbed heat, which in turn provides us with heat capacity, supplies us with information about microscopic nature of the energy levels of the system.

If the external parameter being held fixed is the volume, then the system does no macroscopic work, ie. $đW = 0$. Thus, the first law of thermodynamics[1] allows us to equate

[1] A system's equilibrium state is characterized by its internal energy $\bar{E}$. If the system changes from one macrostate to another, the resulting change in internal energy of the system is $d\bar{E} = đQ + đW$, where $đQ$ is the heat absorbed by the system and $đW$ is the work done by the system as a result of the system's change in external parameters.

the heat absorbed by the system to the change in the average internal energy of the system: $đQ = d\bar{E}$. The heat capacity at constant volume then becomes:

$$C_V = \left.\frac{\partial \bar{E}}{\partial T}\right|_V \tag{3.7}$$

As stated earlier, heat capacity depends on the macroscopic parameter y that is being held constant. Most commonly, it is convenient to keep either the volume constant or the atmospheric pressure. This results in heat capacity at constant volume C_V and heat capacity at constant pressure C_p, respectively. These two quantities are related to each other:

$$c_p - c_v = VT\frac{\alpha^2}{\kappa} \tag{3.8}$$

where V is the molar volume of the substance, and α and κ are the thermal expansion coefficient and the compressibility, respectively. In gases, the quantities c_p and c_V may be substantially different. However, for liquids and solids, the right hand side is usually small, and the two quantities differ negligibly. For solids, the difference may be a few percent at room temperature and at atmospheric pressure.

For example, lead at room temperature and atmospheric pressure has the specific heat at constant pressure $c_p = 26.4 J/molK$. The density of lead is $11.34 g/cm^3$ and its atomic weight is 207.2. Therefore, the molar volume of lead is $V = 207.2/11.34 = 18.27 cm^3/mol$. The coefficient of expansion of lead is $\alpha = 87 \times 10^{-6} deg^{-1}$, and the Bulk modulus is $46 GPa$ resulting in $\kappa = 2.17 \times 10^{-11} cm^2/N$. From equation 3.8, we compute $c_p - c_V = 1.9 J/molK$. Thus, the specific heat capacity at constant volume $c_V = 24.5 J/molK$ and $\gamma = c_p/c_V = 1.078$. This means that for solids at low temperatures, there is no necessity to make any distinction between the specific heats at constant pressure and constant volume.

3.1 Lattice Specific Heat

The atoms making up the lattice of crystalline materials are not static, but rather experience constant motion. It is the mean equilibrium position that determines their position in the crystal structure. This motion of atoms contributes to the specific heat of the material. When describing the kinetics of the atoms, it is useful to employ the Harmonic approximation. The atoms are considered as simple harmonic oscillators experiencing small displacements from their mean equilibrium position. The excitations of vibrational modes of these simple harmonic oscillators, so called phonons, play a crucial role when one considers the specific heat of solids.

3.1.1 High Temperature Specific Heat: Dulong-Petit Law

At sufficiently high temperatures (room temperature is normally high enough), all of the vibrational modes of the atoms are excited. The atoms experience small oscillations about their equilibrium positions. The atoms can be approximated as classical independent simple harmonic oscillators. Each atom can therefore be specified by three position and three momentum coordinates. Thus the total energy of N_a (Avagadro's number) of atoms is the same as that of $3N_a$ independent one-dimensional harmonic oscillators:

$$E = \sum_{i=1}^{3N_a} \left(\frac{p_i^2}{2m} + \frac{1}{2} k_i q_i^2 \right) \tag{3.9}$$

where p_i are the momenta of the atoms, q_i are the position coordinates, and k_i are positive constants. The first term in the above equation is the total kinetic energy and the second term is the total potential energy of N_a atoms in three dimensions. The equipartition theorem states that each degree of freedom that has quadratic form in the energy contributes on average an amount equal to $\frac{1}{2}k_BT$. Therefore, lattice vibrations have the total average energy per mole:

$$\bar{E} = 3N_a \times \frac{1}{2} k_B T \times 2 = 3N_a k_B T = 3RT \tag{3.10}$$

where R is the gas constant. The molar specific heat (at constant volume) of a material is:

$$c_V = 3R = 24.94 J/molK \tag{3.11}$$

The above result is known as the Dulong-Petit law. It states that at high temperatures, the specific heat due to lattice vibrations of all solids approaches a constant value. The Dulong-Petit law provides generally a fair approximation at temperatures of the order of $100K$ and above. However, it has its limitations.

The harmonic approximation uses the Taylor expansion[2] to approximate the potential energy $\phi(\mathbf{r})$[3] of the vibrating atoms about their equilibrium position. It is assumed that the atoms do not deviate considerably from their equilibrium positions, and hence only the quadratic term is considered significant (the linear term being zero[4]). However, at sufficiently high temperatures, the atoms are energetic enough to drift far enough from their equilibrium positions that the small displacement approximation becomes invalid. The higher order terms in the Taylor expansion become considerable and cannot be ignored.

[2] $f(\mathbf{r}+\mathbf{a}) = f(\mathbf{r}) + \mathbf{a}\cdot\nabla f(\mathbf{r}) + \frac{1}{2}(\mathbf{a}\cdot\nabla)^2 f(\mathbf{r}) + \frac{1}{3!}(\mathbf{a}\cdot\nabla)^3 f(\mathbf{r}) + \cdots$

[3] $\phi(\mathbf{r})$ can be the Lennard-Jones potential for example, with $\mathbf{r}$ being the separation between a pair of atoms.

[4] The linear term $\nabla\phi$ is equal to the negative of the force exerted on a atom by other atoms. At equilibrium, the net force is zero, and hence this term must vanish.

The Dulong-Petit law fails even more catastrophically at lower temperatures. As the temperature decreases, the specific heat of materials does not stay constant, but rather it decreases towards zero as the temperature approaches zero. This breakdown occurs because as temperature decreases, not all of the lattice vibrations will be excited. At low temperatures, classical theory fails, and the quantum theory must be utilized in order to explain the specific heat of lattice vibrations.

3.1.2 Low Temperature Specific Heat

The crystal is described by N-ion crystal with 3N independent oscillators. Energy eigenvalues E_i of the harmonic crystal contribute to the total energy, and depend on the frequencies of the 3N classical normal modes of the oscillators. In a "ladder operators" procedure analogous to the quantum theory solution of the single one dimensional harmonic oscillator, the discrete possible energy values of a particular normal mode can be computed to be:

$$(n_s(\mathbf{k}) + \frac{1}{2})\hbar\omega_s(\mathbf{k}) \tag{3.12}$$

where $\omega_s(\mathbf{k})$ is the angular frequency of the normal mode, and $n_s(\mathbf{k})$ is the excitation number of the normal mode. In one dimension, the dispersion relation has two possible solutions for the angular frequency giving rise to two "branches", the optical branch at higher frequencies, and the acoustic branch at lower frequency. In three dimensions, this solution is extended to three optical branches, and three acoustic branches. Thus, s specifies the branch, and $\mathbf{k}$ specifies the wave number of the particular normal mode. The excitation number specifies that the normal mode of a particular branch s with wave vector $\mathbf{k}$ is in its $n_s(\mathbf{k})$th excited state, ie. the number of phonons in the particular branch s with wave vector $\mathbf{k}$. The total energy is thus the sum of the energies due to all of the excited phonons in the crystal:

$$E = \sum_{\mathbf{k}s}(n_s(\mathbf{k}) + \frac{1}{2})\hbar\omega_s(\mathbf{k}) \tag{3.13}$$

where the mean number of phonons of branch s with wave vector $\mathbf{k}$, $n_s(\mathbf{k})$ is given by

$$n_s(\mathbf{k}) = \frac{1}{e^{\beta\hbar\omega_s(\mathbf{k})} - 1} \tag{3.14}$$

Therefore, the energy density is given by

$$u = u_{eq} + \frac{1}{V}\sum_{\mathbf{k}s}\frac{1}{2}\hbar\omega_s((k)) + \frac{1}{V}\sum_{\mathbf{k}s}\frac{\hbar\omega_s(\mathbf{k})}{e^{\beta\hbar\omega_s(\mathbf{k})} - 1} \tag{3.15}$$

where the first term u_{eq} is the equilibrium energy of a static lattice, and the second term is the zero-point energy of the ground state of the ionic oscillators. The specific heat of the crystal is given by the temperature dependent third term:

$$c_V = \frac{1}{V} \sum_{\mathbf{k}s} \frac{\partial}{\partial T} \frac{\hbar\omega_s(\mathbf{k})}{e^{\beta\hbar\omega_s(\mathbf{k})} - 1} \tag{3.16}$$

The above equation may be rewritten in an integral form in the limit of large crystals

$$c_V = \frac{\partial}{\partial T} \sum_{s} \int \frac{d\mathbf{k}}{(2\pi)^3} \frac{\hbar\omega_s(\mathbf{k})}{e^{\beta\hbar\omega_s(\mathbf{k})} - 1} \tag{3.17}$$

where the integral is over the first Brillouin zone.

In order to get a result applicable at low temperature, we can make few simplifications. Since normal modes with $\hbar\omega_s(\mathbf{k}) >> k_B T$ will not contribute considerably to the specific heat, the optical branches may be ignored from the integral. Near $\mathbf{k} = \mathbf{0}$, the dispersion relation can be approximated by the linear form

$$\omega = c_s(\hat{\mathbf{k}})k \tag{3.18}$$

The above approximations are illustrated in Figure 3.1.

Doing the integral in equation 3.17 with the above simplifications, one gets the result for the lattice specific heat at low temperatures:

$$c_V = \frac{2\pi^2}{5} k_B \left(\frac{k_B T}{\hbar c} \right)^3 \tag{3.19}$$

where c is the average phase velocity of the three acoustic normal modes. The above result is only valid at very low temperatures, while the Dulong-Petit law is valid at high temperatures. Another model is required to describe the lattice contribution to the specific heat in the intermediate temperature.

3.1.3 Intermediate Temperature Specific Heat: Debye model

The Debye model of lattice vibrations is an interpolation scheme that approximates the acoustic branch and the optical branch by a single branch that is described by a linear dispersion relation:

$$\omega = ck \tag{3.20}$$

In three dimensions, there are three dispersion relations all having the same wave propagation velocities. Further simplification is made in equation 3.17 by doing the integral

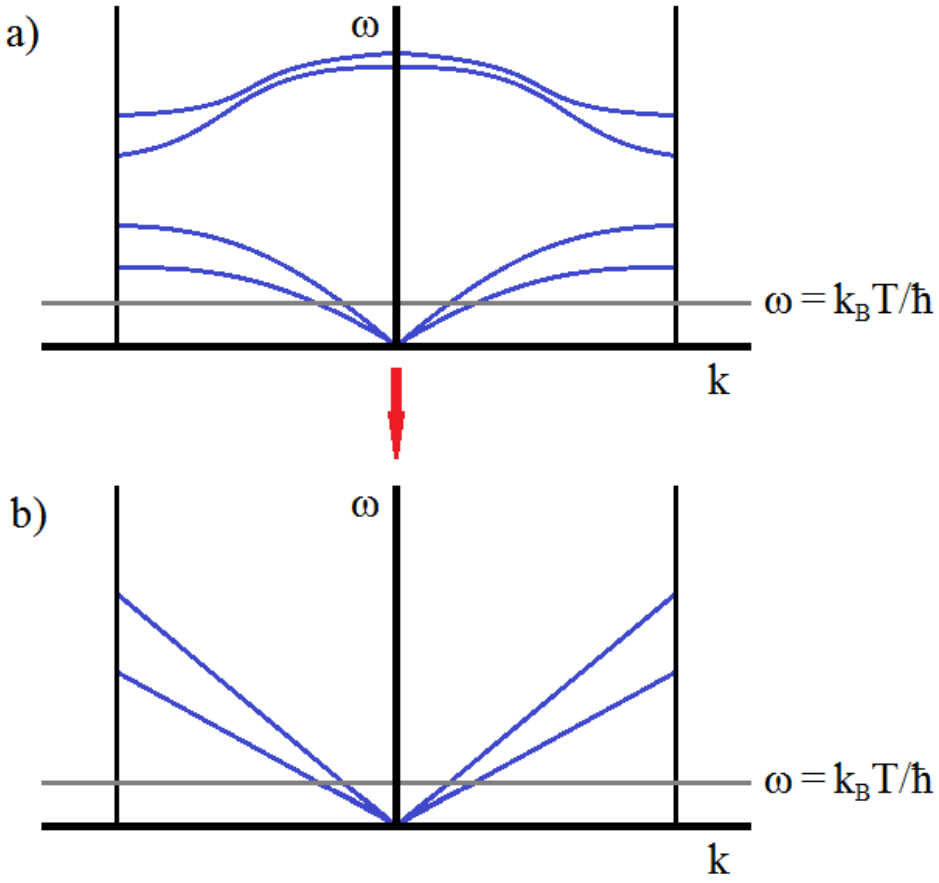

Figure 3.1: The simplifications made in evaluating the low temperature specific heat of a harmonic crystal. a)Typical normal-mode dispersion relations including the optical modes (top) and acoustic modes (bottom). b) The approximation that replaces a). Frequencies above $k_B T/\hbar$ don't contribute significantly to the specific heat. The optical branches are ignored. The acoustic branches are replaces by linear branches.

over a sphere in k-space. The size of the sphere is chosen so that it contains the number of wave vectors equal to the number of ions in the crystal. Therefore, the sphere radius k_D is determined by the relation:

$$\frac{4}{3}\pi k_D^3 = \frac{(2\pi)^3}{V} \times N \tag{3.21}$$

The left side of the above equation is the volume of a sphere with radius k_D. The right hand side is the single wave vector volume in k-space multiplied by N wave vectors that must be enclosed by the whole sphere. Simplifying the equation, density of ions can be related to k_D:

$$n = \frac{k_D^3}{6\pi^2} \tag{3.22}$$

k_D is therefore a measure of inverse interparticle spacing. In addition, it is customary to define the Debye frequency ω_D which is a measure of the maximum phonon frequency in the model:

$$\omega_D = k_D c \tag{3.23}$$

and the Debye temperature Θ_D:

$$k_B \Theta_D = \hbar \omega_D \tag{3.24}$$

The Debye temperature is a measure of the temperature below which phonons begin to "freeze out". In other words, at low temperatures only oscillators with low frequencies are thermally excited substantial amount and are important to the specific heat considerations. At temperatures above Θ_D, even high frequency vibrations start to become significant. Θ_D may also be regarded as a representation of the "stiffness" of the crystal. Materials made up of light and strongly bound atoms have very high Debye temperatures, whereas weakly bound heavy atoms result in materials with low Debye temperatures. Qualitatively, it signals the crossover temperature where high temperature classical statistical mechanics become unsatisfactory and low temperature quantum mechanics must be applied.

In the Debye model, equation 3.17 simplifies to:

$$c_V = 9nk_B \left(\frac{T}{\Theta_D}\right)^3 \int_0^{\Theta_D/T} \frac{e^x}{(e^x-1)^2} x^4 dx \tag{3.25}$$

The Debye temperature Θ_D is material dependent parameter that is empirically determined by fitting the above equation to the measured low temperature specific heat. Debye temperature values for some materials are listed in table 3.1.[110]

In the limit of low temperatures ($T \ll \Theta_D$), the upper limit in the above integral may be set to infinity, and the specific heat reduces to a T^3 dependent form:

$$c_V = \frac{12\pi^4}{5} nk_B \left(\frac{T}{\Theta_D}\right)^3 \tag{3.26}$$

Table 3.1: Debye Temperatures For Few Elements

Element	$\Theta_D(K)$	Element	$\Theta_D(K)$
Li	400	Ne	63
Au	170	Sb	200
Na	150	Zn	234
Be	1000	Fe	420
Al	394	Ni	375
In	129	Co	385
C (diamond)	1860	Au	170
Pb	88	Pr	74

In the limit of high temperatures ($T \gg \Theta_D$), $e^x \approx 1 + x$ in the integrand in equation 3.25, and the specific heat reduces to the Dulong-Petit law.

3.2 Electronic Specific Heat

The most basic model used to describe electrons in metals is that of electron gas. It is assumed that the nucleus of the atoms and core electrons form positive ions that are stationary. The valence electrons are detached from the ions and are free to move throughout the metal forming an electron gas. The model then applied the kinetic theory of gas to this electron gas, replacing the role of gas molecules with electrons. Any interactions between the electrons making up the gas are ignored in the independent electron approximation. Additionally, any electron-ion electromagnetic interaction are also neglected in the free electron approximation. The model assumes that, in place of collisions, there exists some scattering mechanism, without concern for the exact source of the scattering.

The ground state of an electron is a plane wave:

$$\Psi_{\mathbf{k}}(\mathbf{r}) \approx e^{i\mathbf{k}\cdot\mathbf{r}} \tag{3.27}$$

with energy eigenvalue:

$$\varepsilon(\mathbf{k}) = \frac{\hbar^2 k^2}{2m} \tag{3.28}$$

Electrons are fermions. Therefore, they are subject to the Pauli exclusion principle. This means that, with each wave vector $\mathbf{k}$, we can pair up two electrons with opposite spins. Therefore, a N-electron system ground state is built by placing two electrons in the lowest possible energy level: $\varepsilon = 0$ with the corresponding wave vector $\mathbf{k} = 0$. We then sequentially insert electron pairs into higher levels with increasing energy values and wave vectors.

This process continues until all N electrons are accounted for. In k-space, these electrons form a sphere called the Fermi sphere, with the radius defined by:

$$n = \frac{k_F^3}{3\pi^2} \tag{3.29}$$

where $n = N/V$ is the electronic density. All energy levels with $k < k_F$ in the Fermi sphere are occupied, and all energy levels with $k > k_F$ are unoccupied. The energy of the highest occupied level is the Fermi energy given by:

$$\varepsilon_F = \frac{\hbar^2 k_F^2}{2m} \tag{3.30}$$

The total energy of the ground state of the N-electron system is given my adding up the energies of all the occupied levels. The energy density is then given by:

$$u = 2 \times \frac{1}{(2\pi)^3} \int_{k<k_F} \frac{\hbar^2 k^2}{2m} d\mathbf{k} = \frac{1}{\pi^2} \frac{\hbar^2 k_F^2}{10m} \tag{3.31}$$

Combining the above equation with equation 3.29, we get a formula for the energy per electron:

$$\frac{E}{N} = \frac{3}{5}\varepsilon_F \tag{3.32}$$

It is useful to define the Fermi temperature T_F such that:

$$\varepsilon_F = k_B T_F \tag{3.33}$$

Fermi temperatures are on the order of 10^4 K.

Electrons, being fermions, obey Fermi-Dirac statistics. Therefore, the mean number of electrons in the energy level with the energy $\varepsilon(\mathbf{k})$ is determined by the Fermi function:

$$f(\varepsilon) = \frac{1}{e^{(\varepsilon-\mu)/k_B T} + 1} \tag{3.34}$$

where μ is the chemical potential of the material. At $T = 0$, the electron ground state requires that electron levels with $\varepsilon(\mathbf{k}) < \varepsilon_F$ be occupied, and all electron levels with $\varepsilon(\mathbf{k}) > \varepsilon_F$ be unoccupied, as shown in Figure 3.2. This requirement implies that in the low-temperature limit ($T = 0$), the chemical potential is equal to the Fermi energy, ie. $\mu = \varepsilon_F$. At temperatures $T \ll T_F$, which includes room temperature, the chemical potential μ is shifted from ε_F by an amount on the order of $(T/T_F)^2$.[110]This implies that for most temperatures, $\mu \approx \varepsilon_F$ and the Fermi function differs from its zero temperature shape only slightly, as illustrated in Figure 3.2. At finite temperatures ($T > 0$), electrons with energies on the order of $k_B T$ lower then the Fermi energy are able to be thermally

excited to a higher energy on the order of k_BT above the Fermi energy. In other words, the transition region in which the fermi function goes from a value close to 1 to a value close to zero corresponds to an energy interval of order of k_BT about μ. This implies that the excitation energy of the electrons that become thermally excited at $T > 0$ is on the order of k_BT. Since the energy interval of excited electrons is on the order of k_BT, the total number of excited electron per unit volume is $g(\varepsilon_F) \times k_BT$, where $g(\varepsilon_F)$ is the energy level density about the fermi energy:

$$g(\varepsilon_F) = \frac{3}{2}\frac{n}{\varepsilon_F} \tag{3.35}$$

That means that the total change in energy due to the thermally excited electrons is $\Delta E \approx g(\varepsilon_F)k_B^2T^2$. Hence the electronic specific heat is $c_e \approx 2g(\varepsilon_F)k_B^2T$. A more rigorous mathematical approach reveals that the correct result contains a factor of $\pi^2/6$, giving the electronic specific heat:[110]

$$c_e(T) = \frac{\pi^2}{2}nk_B\left(\frac{T}{T_F}\right) \tag{3.36}$$

3.3 Magnetic Specific Heat

Atoms with magnetic moments have a number of degenerate levels associated with the different orientations of the magnetic moments. In particular, there are $2l + 1$ energy levels, where l is the quantum number corresponding to the magnetic moment. In the presence of a magnetic field, this degeneracy is removed. The degenerate levels are split into $2l + 1$ distinct energy levels. This increases the degree of freedom of the system resulting in additional contribution to the specific heat of the material. In cases when the lowest energy levels are modestly separated from the other levels and the temperature is low enough, the system may be treated as a simple two energy level system. It is useful to define the characteristic temperature Θ associated with the energy difference ΔE of the two energy levels using the relation:

$$\Delta E = k_B\Theta \tag{3.37}$$

At low temperatures ($T \ll \Theta$), the system will be in the lower energy state. As the temperature increases, some magnetic moments may be thermally excited to the higher energy state. The specific heat associated with this transition is:[82]

$$c_m = N_0k_B\left(\frac{\Theta}{T}\right)^2\frac{e^{\Theta/T}}{(1+e^{\Theta/T})^2} \tag{3.38}$$

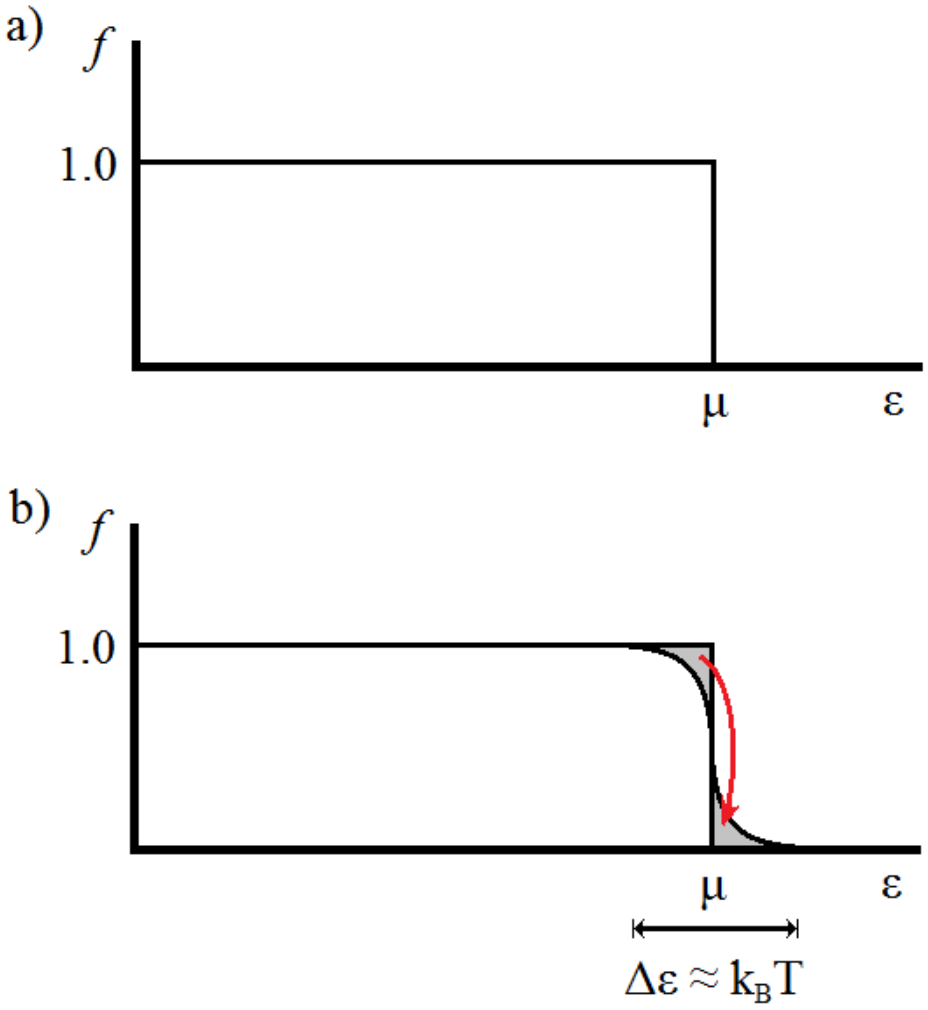

Figure 3.2: The Fermi function versus ε at a) $T = 0$ and b) $T > 0$. The two curves differ only in the region of order $k_B T$ about μ because some electrons just below ε_F have been thermally excited to levels just above ε_F.

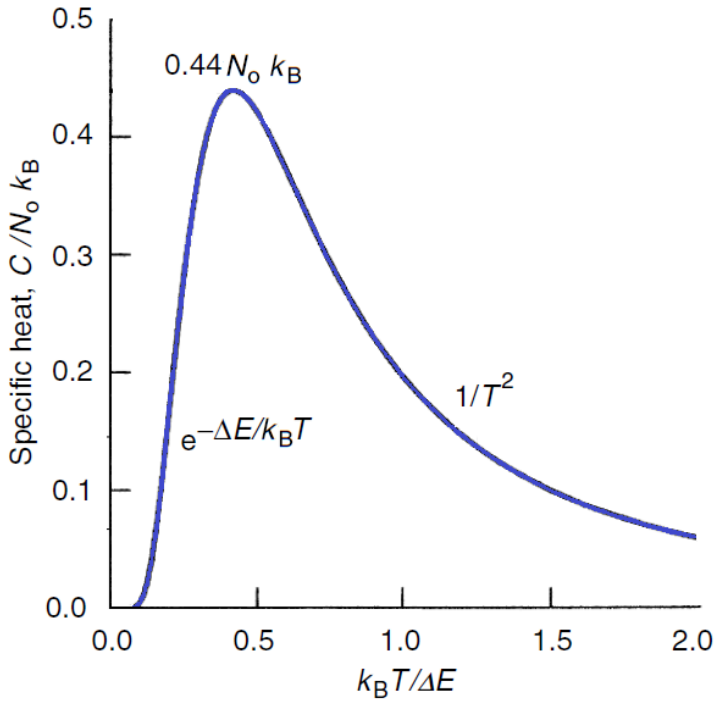

Figure 3.3: Specific heat of a two level system with energy separation ΔE.

where N_0 is the total number of atoms. The heat capacity of a two energy level system is illustrated in Figure 3.3. At lower temperatures, the specific heat falls exponentially to zero:

$$c_m = N_0 k_B \left(\frac{\Theta}{T}\right)^2 e^{\Theta/T}; \quad T \ll \Theta \tag{3.39}$$

At high temperatures, the specific heat can be approximates as:

$$c_m = N_0 k_B \frac{1}{4} \left(\frac{\Theta}{T}\right)^2; \quad T \gg \Theta \tag{3.40}$$

The maximum in the specific heat occurs at $T = 0.42\Theta$ and its height is given by $0.44 N_0 k_B$. The temperature at which the maximum in the magnetic specific heat occurs is a function of the energy splitting ΔE. Since the nuclear magneton is about 1000 times smaller then the Bohr magneton, nuclear magnetic moments are considerably smaller than the electronic magnetic moments. This implies that the maximum in specific heat due to nuclear magnetic moments occurs at much lower temperature then the maximum in specific heat due to electronic magnetic moments.

In the absence of a magnetic field, the crystalline field of a material can lift the degeneracy of the lowest electronic levels of ions. At low temperatures, the specific heat

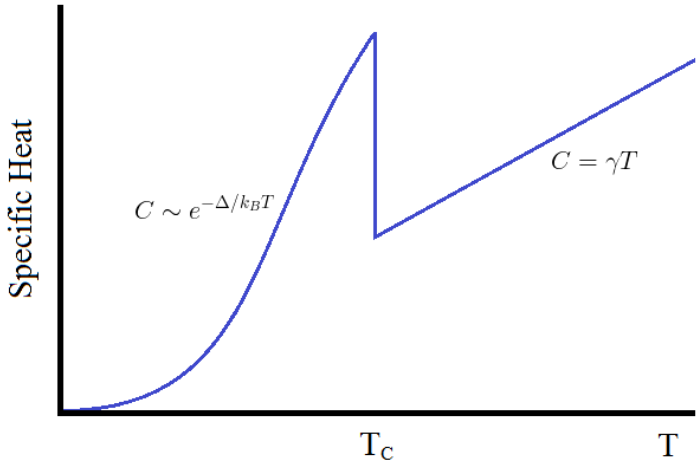

Figure 3.4: Electronic specific heat of a superconductor. At the transition temperature T_c, the specific heat changes from linear behaviour in the normal state to exponential behaviour in the superconducting state.

associated with this splitting of the energy levels can be large relative to the electronic and lattice specific heat. The result is an increase in the specific heat. This feature is termed a Schottky anomaly.

3.4 Specific Heat of Superconductors

When a material undergoes the transition into the superconducting state, the state of the electrons is changed. This alters the behaviour of the electronic specific heat. As specified earlier, the electronic specific heat of superconducting electrons is described by the exponential formula:

$$C_{en} = 1.34\gamma T_c \left(\frac{\Delta(0)}{T}\right)^{3/2} e^{-\Delta(0)/T} \tag{3.41}$$

Figure 3.4 illustrates the change in electronic specific heat of a superconductor from linear behaviour to exponential behaviour. As stated earlier, the jump in the electronic specific heat at the transition temperature is $\Delta C/C_{en} = 1.43$ where C_{en} is the electronic specific heat in the normal state.

The above holds true for conventional superconductors. According to "Anderson theorem", non-magnetic impurities have no effect on the energy gap and transition temperature

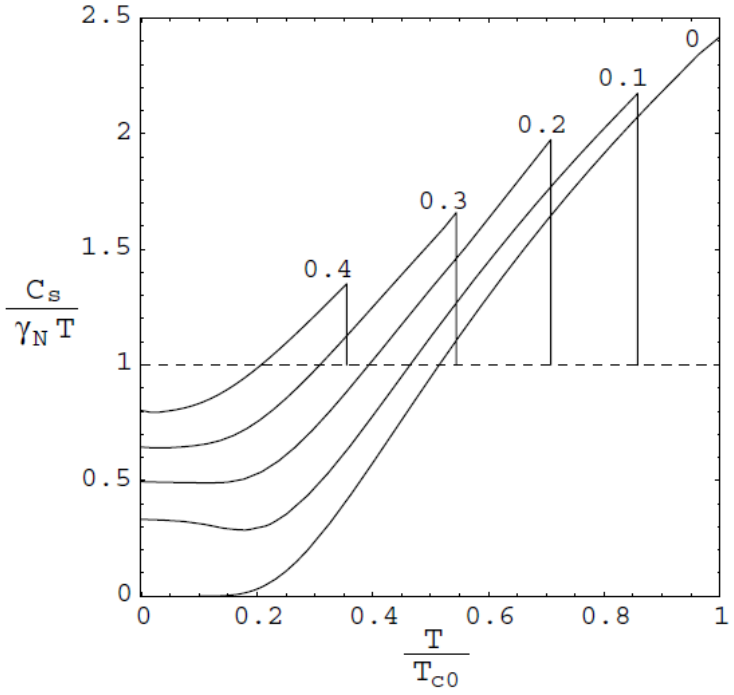

Figure 3.5: Normalized specific heat for a p-wave superconductor for several impurity levels.[62] With increasing impurity, the specific heat jump becomes smaller, the transition temperature shifts to lower temperatures, and there is a non-zero residual heat capacity.

of conventional (s-wave) superconductors.[9] However, this is not the case for unconventional (for example, d-wave or p-wave) superconductors. In unconventional superconductors, potential scattering impurities act as pairbreakers preventing formation of Cooper pairs. The net effect of this is suppression of superconductivity, ie. the superconducting transition occurs at lower temperatures. Additionally, due to reduction in Cooper pair formation, there will be a change in the density of states in the superconducting state, and hence the heat capacity.[40, 92] Instead of the usual exponential behaviour in the specific heat, unconventional superconductors exhibit power law behaviour, such as T^2 or T^3.[35, 74]. Thus, observation of a power law behaviour in the specific heat below the superconducting transition is indicative of unconventional superconductivity, anisotropy in the energy gap, and presence of point or line nodes. Also, if there are point of line nodes in the energy gap, there will be uncondensed electrons even at $T = 0K$. This is because electrons located at the point or line nodes will not form Cooper pairs because of presence of impurities (which act as pairbreakers). Therefore, there will be residual heat capacity due to unpaired electrons even at absolute zero. Figure 3.5 illustrates the effects of impurities in a p-wave unconventional superconductor.

The lattice contribution to the specific heat is unaltered by the superconducting transition and is given by the cubic relation in equation 3.19.

3.5 Summary

In this section we will briefly recap the important ideas we have developed thus far and restate some of the more useful equations.

The low temperature total specific heat of a metal is given by:

$$C = \gamma T + \beta T^3 \tag{3.42}$$

where γ and β are numerical proportionality constants. The linear term is the electronic contribution to the specific heat and γ is known as the Sommerfeld constant. The cubic term is the lattice contribution to the specific heat due to vibrations of crystal ions. For electrons, low temperature refers to temperatures far below the Fermi temperature T_F. For phonons, low temperature means temperature negligible compared to the Debye temperature Θ_D.

If we compare the low temperature electronic specific heat (equation 3.36) to the low temperature lattice specific heat (equation 3.26), we get the following relation:[5]

$$\frac{C_{ph}}{C_{el}} = \frac{24\pi^2}{5Z}\frac{T_F}{\Theta_D^3}T^2 \tag{3.43}$$

The phonon specific heat and the electronic specific heat become comparable at temperature:

$$T = 0.145\left(\frac{Z\Theta_D}{T_F}\right)^{1/2}\Theta_D \tag{3.44}$$

The Debye temperatures are of the order of $100K$ while the Fermi temperatures are of the order of $1000K$ to $10000K$. This means that for most of the temperature range the phonons are the dominant contribution to the specific heat, and the electronic specific heat is negligible. However, at low temperatures of $\sim 10K$, the contribution of the electrons to the specific heat becomes significant. At even lower temperatures of few degrees Kelvin, the electronic specific heat becomes the prevalent term.

When a material undergoes a transition from the normal state into the superconducting state, there is a discontinuity in the specific heat of the material that manifests itself as

[5] n in the electronic specific heat is number of conduction electrons per unit volume, and n in the lattice specific heat is number of ions per unit volume. They are related by $n_e = Zn_i$ where Z is the valence of the atom.

a jump in the specific heat data. The electronic specific heat changes as the electrons enter the superconducting state. In the normal state, electronic specific heat is a linear function of temperature. In the superconducting state, the electronic specific heat decays exponentially with decreasing temperature (equation 3.41).

In some materials, the crystalline field can cause the splitting of energy levels associated with different orientations of the electronic magnetic moments. This removal of degeneracy introduces extra degrees of freedom and results in a bump in the specific heat called the Schottky anomaly (see Figure 3.3).

Nuclear magnetic moments are orders of magnitude smaller than electronic magnetic moments. This means that the removal of the degeneracy in the nuclear magnetic moments occurs at much lower temperatures, and the energy splitting is usually very small compared to the thermal energy. Therefore, the specific heat due to nuclear magnetic moments becomes significant only at very low temperatures. Hence, the specific heat due to nuclear magnetic moments usually can be approximated by the high temperature portion of the Schottky anomaly (refer to Figure 3.3). The specific heat due to nuclear magnetic moments has the form:

$$C_m = \delta T^{-2} \tag{3.45}$$

where δ is a proportionality constant.

Chapter 4

$PrOs_4Sb_{12}$

$PrOs_4Sb_{12}$ belongs to a group of compounds called filled skutterudites. The chemical composition of the lanthanide filled skutterudites is given by RM_4X_{12}, where R is a rare earth element or U ; M is Fe, Ru, or Os; and X is P, As, or Sb.[90] The crystal structure of filled skutterudite compounds is shown in Figure 4.1. Each rare earth atom is located at the center of a distorted icosahedron formed by twelve pnictogen atoms. Together they form a body-centered cubic (bcc) lattice. In many of the antimonide compounds, the rare earth atoms are poorly bonded to the pnictogen cage and experience displacement about their equilibrium positions. This "rattling" of the atoms in the cage is suspected to play a role in some of the unusual properties of filled skutterdites. The transition metal atoms form a simple cubic lattice.

In obtaining the electronic specific heat equation 3.36, we used the free-electron model; electron-ion interactions were ignored. However, in real metals, we have to account for the effect of lattice ions on the electrons and we have to take the complicated band structure of the crystal into consideration. We can treat the electrons as quasi-particles with an effective mass m^* that accounts for these additional interactions. Materials with large effective mass of $50 - 1000$ times greater than the electron mass are called heavy fermion systems. The same equations for specific heat still apply; the only alternation is that the electron mass is exchanged with the effective mass m^*. The linear term γ in the electronic specific heat depends on the electron mass through equations 3.33 and 3.29. Thus, for heavy fermions, the linear term in the electronic specific heat is considerably larger than in normal metals. For normal metals, γ is of the order $1mJ/molK^2$. In heavy fermion systems, γ is generally greater than $400mJ/molK^2$.[72] Other than the large effective mass, heavy fermion systems do not share many common characteristics and exhibit a wide range of physical properties. Due to the large effective mass of the charge carriers, the electron-phonon interaction is not very effective as the pairing mechanism for the heavy-fermion superconductors. In contrast to the conventional superconductors, a heavy electron is un-

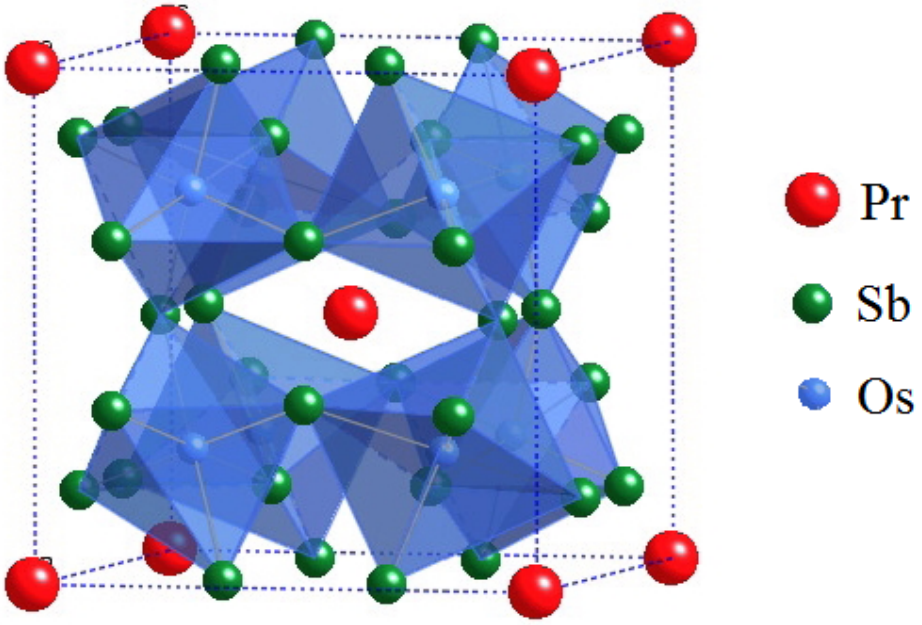

Figure 4.1: Crystal structure of $PrOs_4Sb_{12}$ from [90].

able to escape fast enough from a location where it has caused a lattice distortion in order to reduce the Coulomb repulsion of its partner. Therefore, heavy-fermion superconductors are usually unconventional. In the usual BCS superconductors, the presence of magnetic interactions destroys superconductivity. However, superconductivity in heavy-fermion systems commonly coexists along with magnetic order and the electron pairing is magnetically mediated.[72]

4.1 Review of Previous Experimental Results

$PrOs_4Sb_{12}$ is a heavy fermion system. While there are other Pr based heavy fermion systems ($PrFe_4P_{12}$ being another example[7]), $PrOs_4Sb_{12}$ is the first known heavy fermion superconductor containing Pr. Evidence for heavy fermion behaviour comes from the specific heat measurements.[66] Figure 4.2 shows the results of specific heat measurements on a sample of $PrOs_4Sb_{12}$. From the specific heat measurements and the specific heat jump at T_c, it is estimated that $\gamma \sim 500 mJ/molK^2$ and that the effective mass of the electrons is $m^* \sim 50 m_e$. Other specific heat measurements provide comparable results measuring $\gamma \sim 350 - 600 mJ/molK^2$.[12, 64, 85] The other interesting feature in the specific heat measurements is the existence of two specific heat jumps as shown more clearly in the insert of Figure 4.2. The first specific heat discontinuity occurs at $T \approx 1.89K$ and the second at

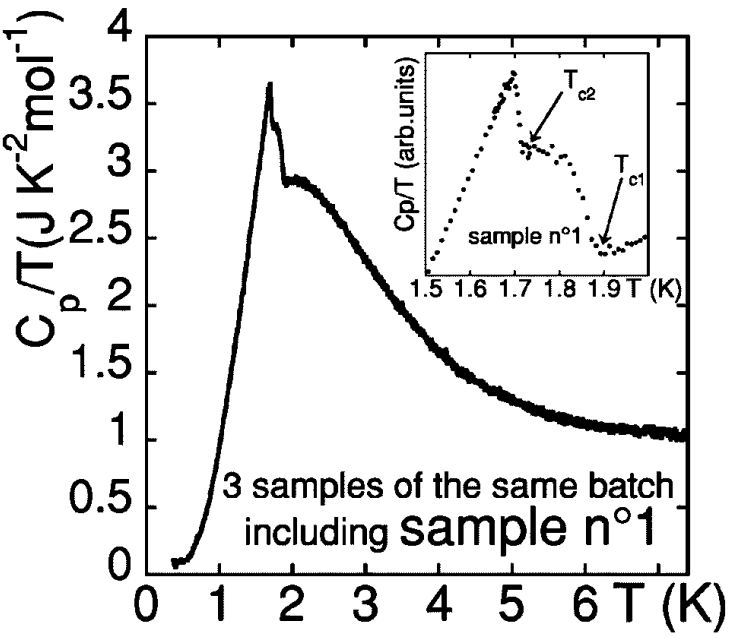

Figure 4.2: Specific heat of $PrOs_4Sb_{12}$ from [66].

$T \approx 1.72K$. The two jumps raise the possibility that two superconducting transitions exist in $PrOs_4Sb_{12}$. It also provides evidence for unconventional superconductivity in $PrOs_4Sb_{12}$ and that it is a strongly correlated system. Other experiments also confirm heavy fermion behaviour.[98]

The broad bump feature with a peak at $T \sim 2.2K$ in the specific heat data is a Schottky anomaly arising from a two level system. The exact crystal electric field (CEF) level scheme is still a matter of debate and controversy. Inelastic neutron scattering (INS) experiments, along with an analysis of magnetic susceptibility $\chi(T)$ and specific-heat C(T) data suggest that the Pr^{3+} energy scheme comprises of a nonmagnetic Γ_3 doublet ground state, a Γ_5 triplet first exited state ($\sim 8K$), and higher energy Γ_4 triplet ($\sim 133K$) and Γ_1 singlet ($\sim 320K$) excited states.[64] Electrical resistivity and magnetization experiments performed by Ho provided additional support for this picture.[41]. Bauer[12] and Vollmer[85] analyzed the magnetic field dependence of the specific heat. Their results also suggest that the ground state is a Γ_3 doublet. However, other experiments do not agree with these findings. Goremychkin[34] and Kuwahara[52] also performed INS experiments on samples of $PrOs_4Sb_{12}$. From their results, they concluded that the ground state is a Γ_1 singlet. Neutron diffraction experiments[49] and dc magnetization experiments[104] also show results consistent with this energy level scheme. Although the exact ground state is still up to debate, all experiments agree that the ground state must be non-magnetic and that the first excited state is the Γ_5 triplet.

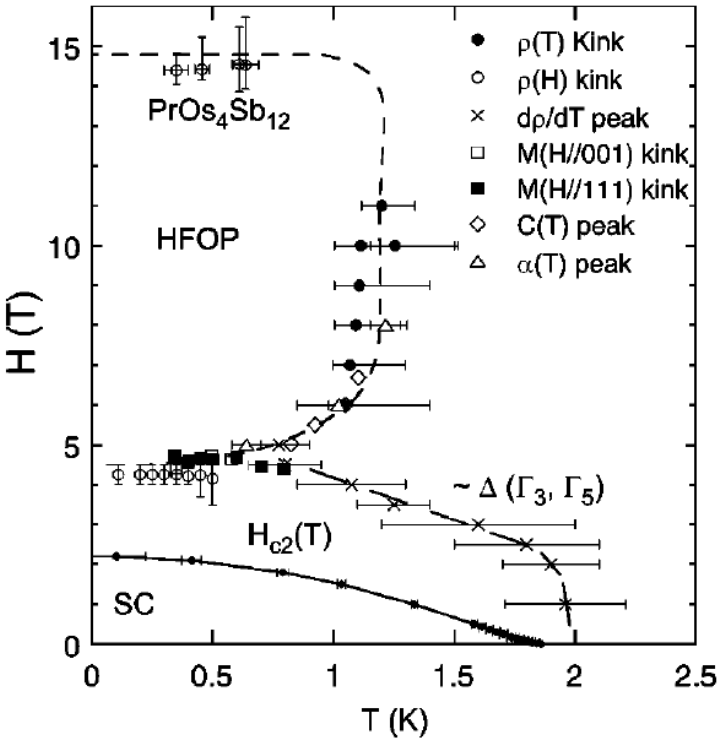

Figure 4.3: H-T phase diagram for $PrOs_4Sb_{12}$[41]. The superconducting state phase boundary is determined from the electrical resistivity measurements. The HFOP is obtained from the features observed in electrical resistivity, specific heat, magnetization, and thermal expansion coefficient data. See paper for original references.

The case of Γ_3 doublet ground state leads to a possibility of a new mechanism for heavy fermion superconductivity called "quadrupolar Kondo effect"[30]. In other heavy fermion systems, such as UPt_3, the heavy fermion superconductivity behaviour is magnetically mediated. The material consists of a lattice of magnetic ions. At low temperatures, these systems experience magnetic ordering. The magnetic moments interact with the spins of the conduction electrons resulting in a screening effect. The heavy fermion behaviour and superconductivity results from this magnetically mediated screening developing coherently throughout the lattice. In the quadrupolar Kondo effect, the role of ionic magnetic moments is replaced by the quadrupole moments. The Pr^{3+} Γ_3 doublet ground state has the electric quadrupole moment. The interaction between the Pr^{3+} quadrupole moments and the charges of conduction electrons results in the observed heavy fermion behaviour and superconductive pairing. Thus $PrOs_4Sb_{12}$ could exhibit a novel mechanism for the origin of superconductivity that is neither electron-phonon mediated nor magnetically mediated.

Figure 4.3 shows the H-T phase diagram for $PrOs_4Sb_{12}$ derived from a number of

measurements. The superconducting state phase boundary is derived from the electrical resistivity[12, 41]. An interesting feature of the H-T phase diagram is the ordered phase that occurs at high fields when superconductivity is extinguished. This high field ordered phase (HFOP) is deduced from the features observed in number of experiments: electrical resistivity[41] and specific heat[85], magnetization[64] and thermal expansion[79]. The dashed line is a measure of the energy difference between the Pr^{3+} Γ_3 ground and Γ_5 first excited state[63, 85]. The measurements indicate that the ordered phase occurs at temperatures below $1.3K$ in fields above $4.5T$ and below the maximum field of $14T$. Neutron diffraction experiments suggest that the HFOP exhibits antiferro-quadrupolar order.[49] It is suggested that the HFOP may be due to the mixing of the ground state and the first excited state caused by the increase in magnetic field as illustrated in Figure 4.4.[85] One crossing of the upper level of the Γ_3 doublet and the lowest level of the Γ_5 triplet states occurs at magnetic field of $\sim 4.5T$. At fields $\sim 10T$, the lowest levels of the Γ_3 triplet states cross with the lowest states of the Γ_5 tripled resulting in a new ground state. These crossing may induce the HFOP.

The double jump in the specific heat data of $PrOs_4Sb_{12}$ suggests unconventional superconductivity. Further evidence for unconventional superconductivity comes from the uncharacteristic value of the specific heat jump at the transition temperature. A measured value of $\Delta C_{SC}/\gamma T_C \approx 3$[85] is higher than the weak coupling BCS value of 1.43 suggesting strong coupling superconductivity. Values for $\Delta/k_B T_C$ have been determined to be 2.6 by nuclear quadrupole resonance measurements[51], 2.1 by muon spin relaxation experiments[61], and 3.7 by specific heat measurements[36]. These are higher than the BCS prediction of 1.76 further suggesting strong coupling.

In order to try and resolve this issue, it is useful to experimentally determine the symmetry of the energy gap and whether it exhibits any nodes on the Fermi surface. Once the Schottky anomaly and the lattice contributions are eliminated from the specific heat data, specific heat measurements suggest that superconducting specific heat has a power law dependence $C_S(T) \sim T^n$ with $n = 2.5$[63].[1] If the gap function has nodes at the Fermi surface, then there is a considerable number of unpaired electrons that contribute to the specific heat. Therefore, a power law dependance in the superconducting specific heat implies that the energy gap vanishes along some directions in k-space.[15]Experiment measuring magnetic field orientation dependence of specific heat suggest that there are nodes in the energy gap.[23] Thermal transport measurements performed by Izawa et al. also point to existence of nodes in the gap function.[44] Nuclear quadrupole resonance measurements also suggest presence of gap nodes.[75] Fits to the data of magnetic penetration depth in various magnetic field orientations also suggest that the energy gap has nodes.[18] However, other experiments have contradictory results. Measurements of the magnetic

[1] A value of $n = 3.9$ is obtained when the Schottky anomaly contribution is not subtracted from the specific heat data.[64]

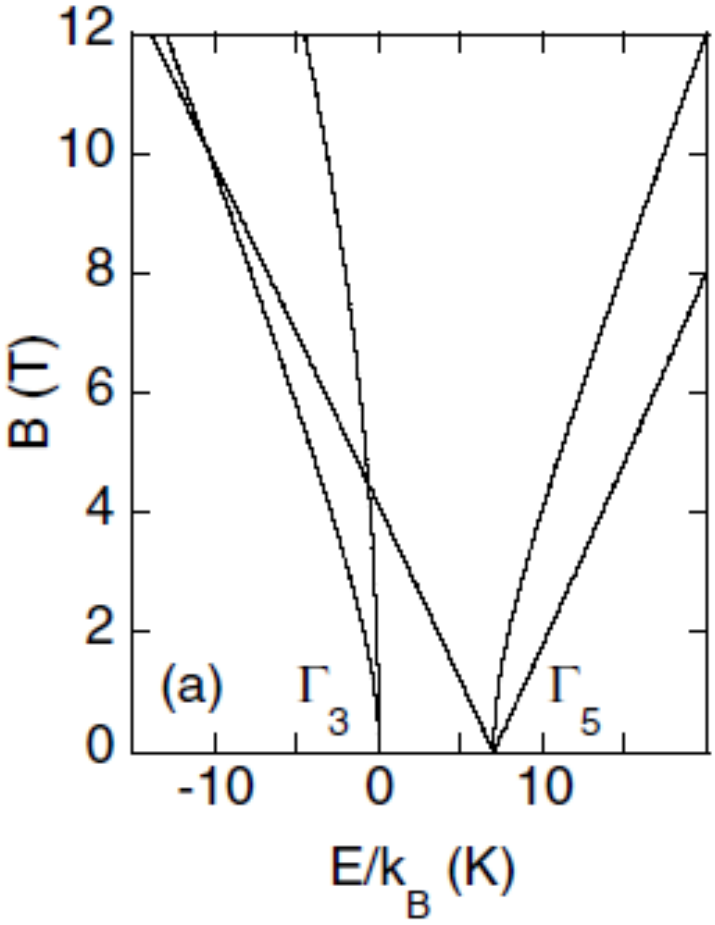

Figure 4.4: Zeeman splitting of the Γ_3 doublet and Γ_5 triplet CEF levels. The doublet and triplet cross at $\sim 4T$ and $\sim 10T$, suggesting a stabilization of a different ground state in this regime.[85]

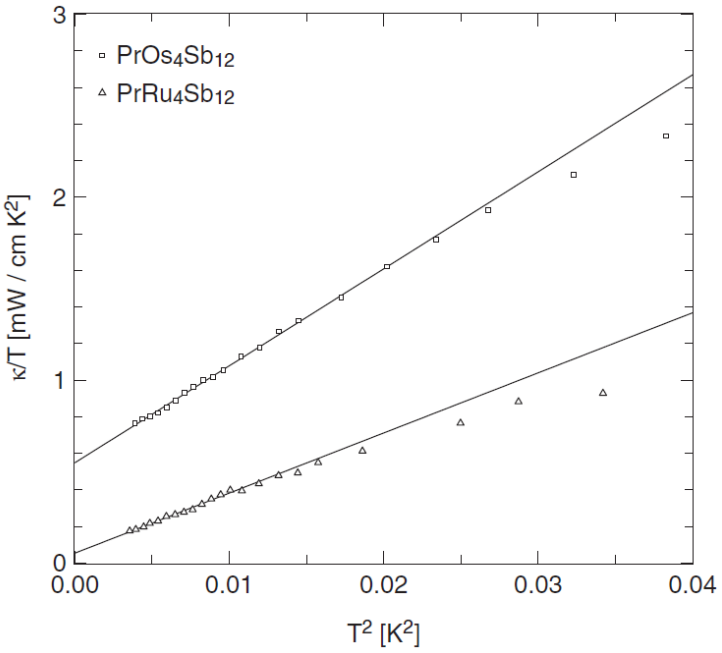

Figure 4.5: Thermal conductivity divided by temperature T versus T^2 for $PrOs_4Sb_{12}$ and $PrRu_4Sb_{12}$. The lines represent linear fits to the low temperature data with an extrapolation to T = 0 K.[38]

penetration depth using muon spin relaxation technique concluded that the energy gap is isotropic.[61] Analysis done by an Sb nuclear quadrupole study found that $PrOs_4Sb_{12}$ has an isotropic gap.[51] Scanning tunneling spectroscopy measurements conclude that the superconducting gap is fully open over entire Fermi surface.[97] Low temperature thermal conductivity under magnetic field experiments suggest that $PrOs_4Sb_{12}$ may exhibit multiband superconductivity with isotropic gaps; there are two types of electrons at the Fermi level with different energy gaps.[95, 94] Another study of thermal conductivity under various magnetic fields found evidence for multiband superconductivity in $PrOs_4Sb_{12}$.[38, 86] Their data suggests that, in the limit of zero temperature, $PrOs_4Sb_{12}$ has a finite and significant residual electronic conduction as shown in Figure 4.5. This property is indicative of nodes present in the energy gap. Field dependence of the thermal conductivity shows that it increases quickly at low fields before reaching a plateau at higher fields and then increasing rapidly up to the normal state value at H_{c2} (Figure 4.6). The authors state that this behaviour is consistent and suggestive of multiband superconductivity. They argue that $PrOs_4Sb_{12}$ has one band with a nodal order parameter and another distinct anisotropic band that is fully gapped. Andreev spectroscopy study also shows evidence in support of this proposed multiband and multisymmetry scenario for $PrOs_4Sb_{12}$.[89]

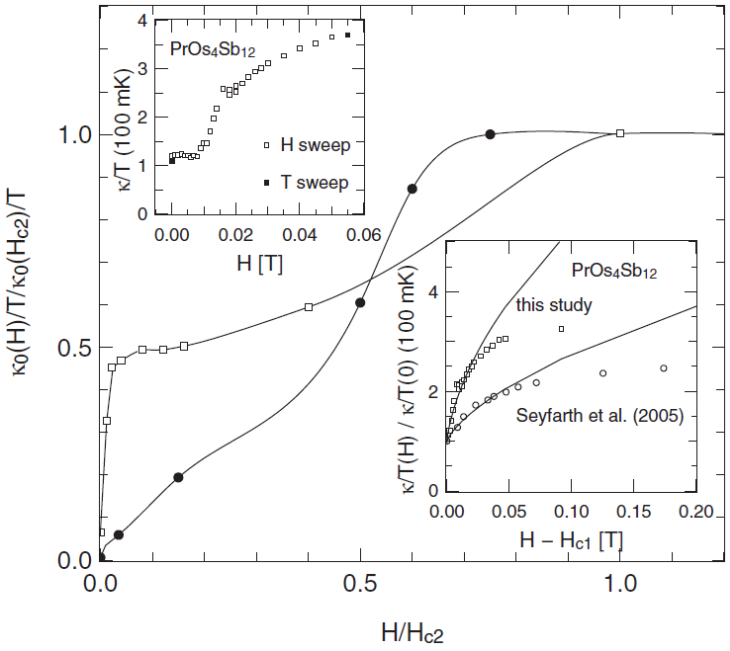

Figure 4.6: Magnetic field dependence of the extrapolated $T = 0K$ thermal conductivity of $PrOs_4Sb_{12}$ and $PrRu_4Sb_{12}$. The lines are guides to the eye in each case. Lower inset: Field dependence of the conductivity normalized to the zero-field value for $PrOs_4Sb_{12}$ both from this study and from earlier work[95]. Upper inset: Low-field dependence of the thermal conductivity divided by temperature for $PrOs_4Sb_{12}$ at $T = 0.1K$. Open symbols are for sweeping the magnetic field, closed symbols are from temperature sweeps at fixed magnetic field.[38]

Another important question concerns the nature of the two superconducting transitions observed in experiments. The fundamental issue is whether the two transitions are intrinsic to the system, ie. are the two transitions associated with two distinct superconducting phases. The other option is that the system has only one superconducting phase with different transition temperatures in segregated regions due to sample inhomogeneity. In order to shed light on this problem, Grube et al. performed specific heat measurements and ac susceptibility measurements in various magnetic fields.[36] The resulting H-T phase diagram is shown in Figure 4.7. With decreasing temperature, the onset of superconductivity first occurs at the transition temperature $T_{c1} = 1.86K$ with an upper critical field $B_{c2}(T)$. The maximum value of the upper critical field is $B_{c2}(0) = 2.3T$. The second transition $B^*_{c2}(T)$ starts at $T^*_c = 1.75K$, follows $B_{c2}(T)$, increasing to the maximum value $B^*_{c2}(0) = 2.1T$. Magnetic field dependence of both transitions is proportionate; ie. they can be scaled to one another with approximately the same scaling factors for the B and T axis $B^*_{c2}(0)/B_{c2}(0) \approx T^*_c(0)/T_c(0)$. This suggests that the two transitions are not intrinsic. Instead, they are due to sample inhomogeneity.

Magnetic dependence of the specific heat measurements conducted by Measson et al. produce an H-T phase diagram shown in Figure 4.8.[70] Their results also show that T_{c2} has the same magnetic field dependence as T_{c1} (up to a scaling factor). This asserts that the superconducting transition at the lower temperature is not intrinsic.

Low temperature dc magnetization measurements of $PrOs_4Sb_{12}$ also show that the magnetic field dependence of the second superconducting transition is similar to that of the first superconducting transition.[104] This provides further evidence that the second transition is due to sample inhomogeneity.

Izawa et al. carried out thermal transport measurements in various magnetic field orientations relative to the $PrOs_4Sb_{12}$ sample crystal axes.[44] Their data analysis produced another H-T phase diagram depicted in Figure 4.9. Their results indicate that the two transitions do not scale, and hance are intrinsic to the system. In other words, there exist two superconducting phases with different energy gaps. The second transition is due to the change of symmetry of the order parameter. Their results also indicate that there are nodes at the Fermi surface in the energy gap.

Measson et al. performed specific heat measurements at low temperature and under high pressure.[69] They investigated the double superconducting transition behaviour at various pressure values up to maximum pressure of $4.3GPa$. Above $1GPa$ the behaviour of the two transitions becomes similar, and $T_{c1} - T_{c2}$ stabilizes to a constant value. They argue the two superconducting transitions are extrinsic in nature with the lower transition being intrinsic to the system. They suggest that the double transition behaviour is caused by Pr vacancies.

In order to further clarify this issue, experimentalists investigated the effects of sample quality on superconducting properties of $PrOs_4Sb_{12}$. Seyfarth et al. found that when

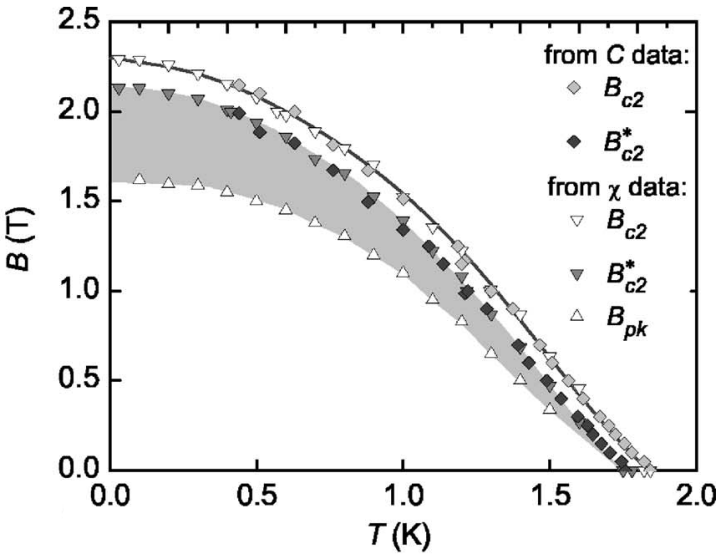

Figure 4.7: H-T phase diagram for $PrOs_4Sb_{12}$ obtained specific heat measurements and ac susceptibility measurements in various magnetic fields.[36]

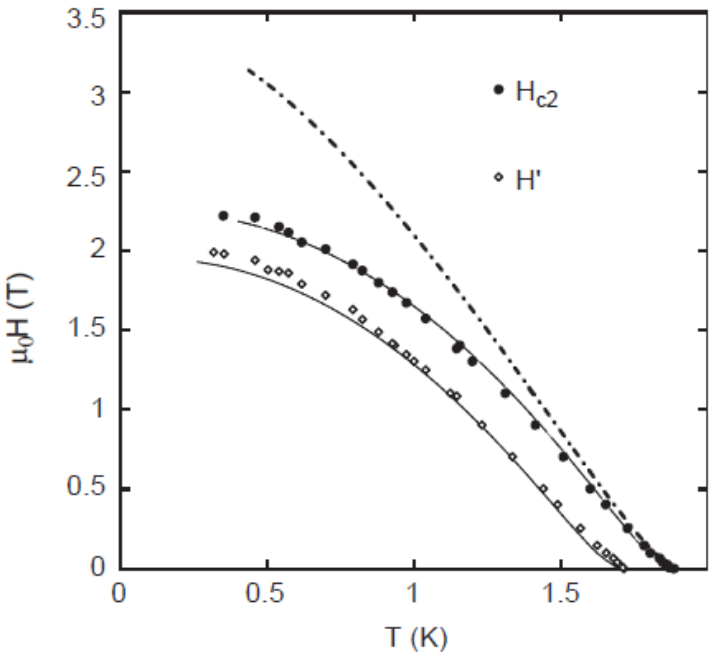

Figure 4.8: H-T phase diagram for $PrOs_4Sb_{12}$ obtained specific heat measurements in various magnetic fields.[70]

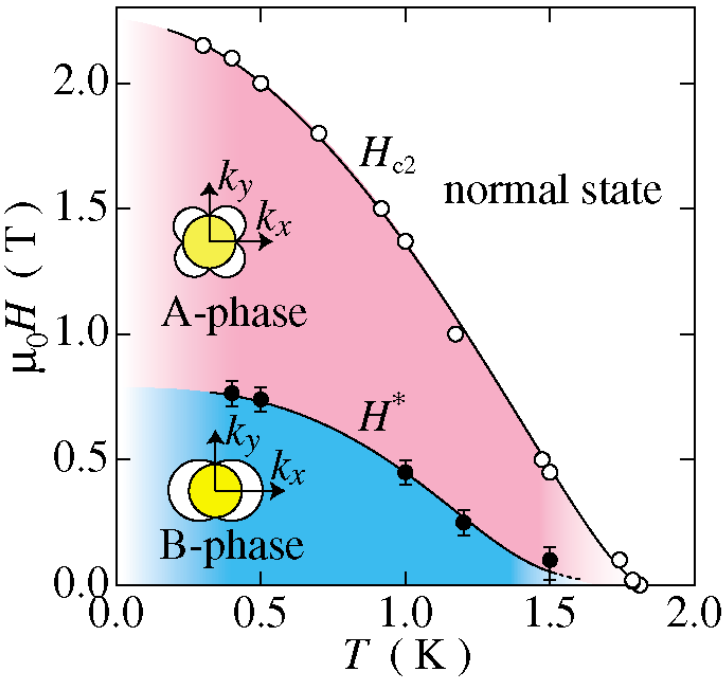

Figure 4.9: $PrOs_4Sb_{12}$ phase diagram obtained by thermal transport measurements in various magnetic field orientations.[44] The results indicate that the energy gap has nodes, and that two transitions are due to the change of symmetry of the order parameter.

they reduced the size of a sample crystal, specific heat measurements produced a single superconducting transition at T_{c2}.[94] This result indicates that the two superconducting transitions manifest because of sample inhomogeneity.

McBriarty et al. compared the properties of single crystal samples and powder samples.[65] In particular, they were interested whether the upper transition may be caused by Pr ion deficiency in regions near the sample surface. In specific heat measurements, the single crystal sample displayed standard double transition behaviour with a sharp upper transition at $1.85K$ and a broad lower transition at $1.7K$. One of the interpretations of the broad characteristic of the upper transition is that it is due to a distributions of T_{c1}'s. This suggests that the upper transition is due to inhomogeneous superconductivity. The powder sample exhibited a single broad transition at approximate temperature $1.75K$. Comparison of the two results is shown in Figure 4.10. They also found that single crystal sample had much higher $\Delta C/T$ ($1000mJ/molK^2$) than the powder sample ($140mJ/molK^2$). The results also indicated that the powder sample had much lower and broader Schottky anomaly. They also found that annealing the powder sample increased the specific heat jump. Their findings led them to three conclusions:

> First, it is unlikely that the anomaly at T_{c1} is due to a minority phase. Powdering has the advantage over polishing or slicing that does not discard any material. Thus, if the secondary phase was present in the crystal it should also exist in the powdered sample. Second, the results disagree with the possibility of the anomaly at T_{c1} due to Pr vacancies. Again, powdering is not likely to improve the quality of material and reduce the concentration of vacancies. Third, the anomaly at T_{c1} does not seem to be related to any kind of defects near the surface. Powdering strongly increases the ratio of surface to volume and thus would rather promote such defects.

Specific heat measurements on a number of $PrOs_4Sb_{12}$ samples from various batches suggested that sample quality has great effect on the double transition behaviour.[68] The results exhibit a broad scatter of values of the ratio of the two specific heat jumps $\Delta C(T_{c1})/\Delta C(T_{c2})$ on crystals from different batches and even within the same batch. Furthermore, there was a single sample with a sharp superconducting transition with T_c of $1.73K$. These findings argue against the double superconducting transition being intrinsic in nature.

Measson et al. performed a comprehensive characterization of numerous $PrOs_4Sb_{12}$ samples and examined the relationship between sample quality as defined by the residual resistivity ratio (RRR) and their superconducting properties.[67] Figure 4.11 shows the specific heat data for a number of samples surveyed in the study. There does not appear to be any substantial dependance between the upper superconducting transition and sample

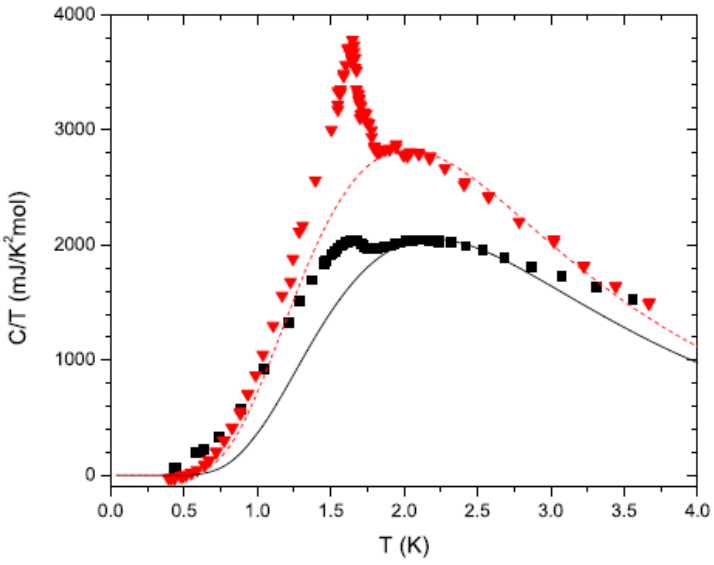

Figure 4.10: Comparison of specific heat measurements of single crystal and powder sample from [65].

quality. T_{c1} increases slightly from a minimum value of $1.805K$ to a maximum value of $1.897K$ with increasing RRR. However, the lower superconducting transition seems to be highly sample dependent. While a number of samples have T_{c2} values in the range between $1.716K$ and $1.761K$, there are three samples with much lower values of T_{c2}: $1.53K$, $1.535K$ and $1.685K$. Samples with a single broad transition seem to be of poorer quality as their RRR values are small. However, it is interesting that some samples with a single broad transition have higher RRR values than some samples that exhibit two superconducting transitions. There are also few samples with single sharp transition that seems to occur at similar temperatures as T_{c2} in double transition samples. These samples may be characterized as being high quality as they have high RRR values. There also seems to be correlation between RRR values of samples and their specific heat data. Samples with high RRR seem to have higher specific heat at $2K$ and their superconducting jump at the transition temperature is higher. In summary, high quality samples are characterized by having large RRR, a large C/T at $2K$ and a large specific heat jump at T_c, as indicated in Figure 4.12. It seems that all double transition samples meet this criteria, and hence may be considered to be of high quality.

All samples with single sharp superconducting transition are very small. Furthermore, they seem to have higher normalized specific heat jumps than samples showing two transitions. Additionally, the width of the superconducting transition in these samples is considerably narrower than the width of the second transition in double transition sam-

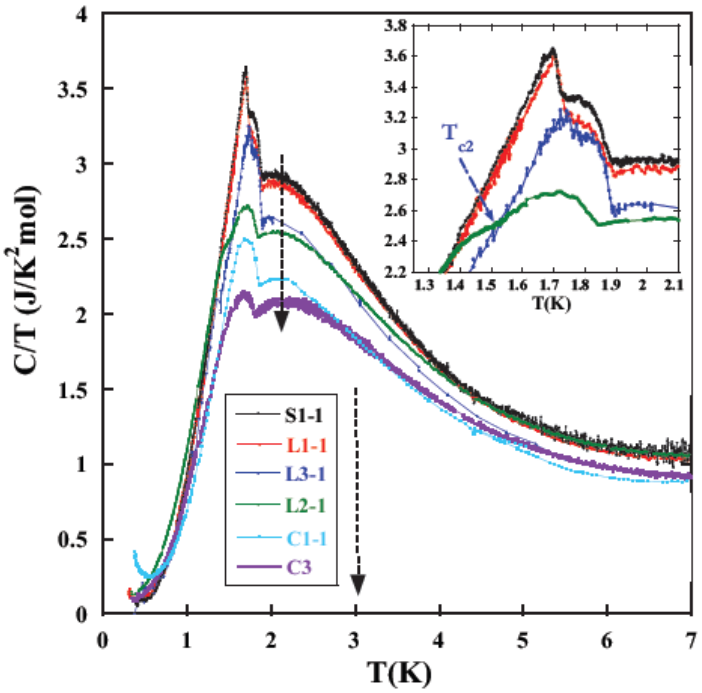

Figure 4.11: Specific heat as for selected samples of PrOs4Sb12 from [67]. The insert gives a zoom around the superconducting transition for the samples with a double superconducting transition. The absolute value of C clearly depends on the sample. A double superconducting transition appears in samples S1-1, L1-1, L3-1, L2-1 while samples C1-1, C3 exhibit a broad single transition.

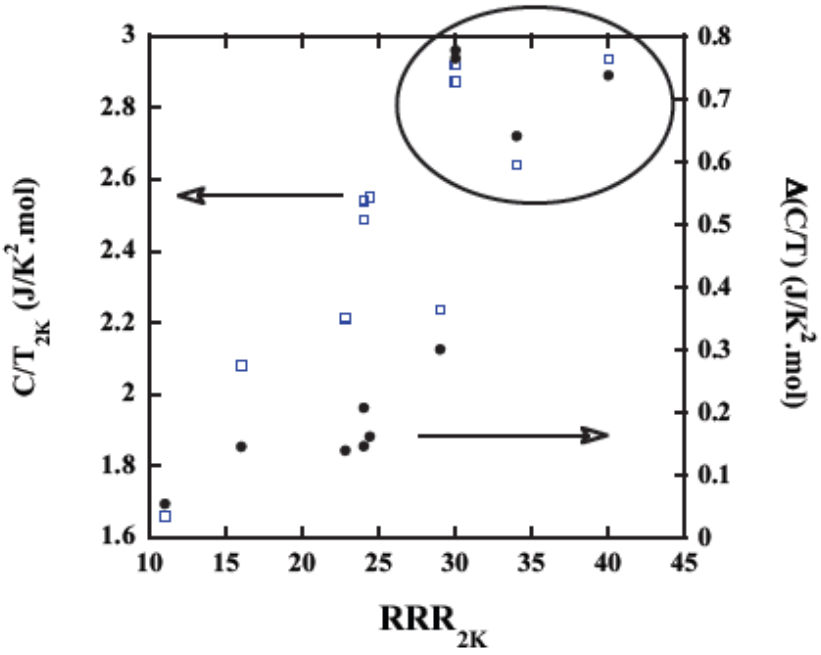

Figure 4.12: C/T at $2K$ and the total specific heat jump $\Delta(C/T)$ versus RRR2K from [67]. There is apparently a positive correlation between the three quantities. All the samples exhibiting clear double superconducting transitions (batches S1, L1 and L3) are within the large circle. They are of high quality: they are characterized by a large RRR2K, a large C/T at $2K$ and a large specific heat jump at the superconducting transition.

ples. Measson et al. argue that these results suggest that single sharp transition samples are of higher quality than samples displaying two transitions.

Their studies also showed that the upper transition at T_{c1} disappears after crystal samples have been polished. This suggests that the two transitions occur due to macroscopic segregation of the samples. The authors argue that the broad transition at T_{c1} and the sharp transition at T_{c2} indicate two domains in the samples. One part of the sample has a distribution of T_c's below T_{c1} and the other part has a single sharp transition at T_{c2}. The transition at T_{c1} is always broader than the transition at T_{c2}. Additionally, all single transition samples become superconducting at $T_c \sim T_{c2}$. These observations suggest that the T_{c2} superconducting transition is intrinsic to the system. The authors dismiss the argument that the upper transition may be intrinsic but disappears due to poor sample quality. They argue that this would broaden the lower transition, and point out the existence of samples with single and very sharp transition. One perplexing issue is why do some samples exhibit much lower T_{c2}; ie. why does T_{c2} seem to be so sensitive to the sample quality while T_{c1} is relatively stable in all samples.

Table 4.1 summarizes some of the major results obtained from various experiments. It is obvious that there does not seem to be a consensus on many of the crucial properties describing the superconducting state of $PrOs_4Sb_{12}$. Data from many and various experiments seems to lead to contradictory interpretations. Even same experiments performed by different groups result in dissimilar conclusions. This cannot be accounted for by irregularity in sample quality as samples with same sources have results that disagree. Perhaps, there is inconsistency in sample quality from different batches even if the source is the same. It is also likely that various experiments are challenging to perform on this material and data is ambiguous and difficult to interpret.

In conclusion, some of the questions concerning $PrOs_4Sb_{12}$ that still have no clear consensus are:

- What is the exact energy level scheme of $PrOs_4Sb_{12}$?
- Is the observed superconductivity conventional or unconventional in nature? What is the source of superconductivity in $PrOs_4Sb_{12}$?
- Does the energy gap have nodes at the Fermi surface? Is the energy gap isotropic or anisotropic?
- Are the two superconducting transitions intrinsic or extrinsic? Are they just a manifestation caused by sample quality?

Table 4.1: Summary of Experimental Results

Result	Experiment	Sample Source
Γ_3 doublet ground state	Inelastic neutron scattering (INS) experiments, magnetic susceptibility, and specific heat[64]	Maple
	Electrical resistivity and magnetization[41]	Maple
	Magnetic field dependence of the specific heat[12, 85]	Maple
Γ_1 singlet ground state	INS experiments[34]	Maple
	INS experiments[52]	Sugawara
	Neutron diffraction experiments[49]	Sugawara
	dc magnetization experiments[104]	Sugawara
Nodes in energy gap	Power law dependence of low T specific heat[63]	Maple
	Magnetic field orientation dependence of specific heat[23]	Sugawara
	Thermal transport in various magnetic fields[44]	Sugawara
	Nuclear quadrupole resonance[75]	Sugawara
	Magnetic penetration depth[18]	Sugawara
Multiband and multisymmetry	Thermal conductivity in various magnetic fields[38, 86]	Maple
	Andreev spectroscopy[89]	Maple
Isotropic energy gap	Magnetic penetration depth using muon spin relaxation technique[61]	Maple
	Sb nuclear quadrupole study[51]	Sugawara
	Scanning tunneling spectroscopy[97]	Canfield
	Low T thermal conductivity in various magnetic field[95]	Lapertot
	Low T thermal conductivity in various magnetic field[94]	Sugawara
Transitions due to sample inhomogeneity	Specific heat measurements and ac susceptibility measurements in various magnetic fields[36]	Maple
	Specific heat at low T under high pressure[69]	Lapertot
	Magnetic field dependence of specific heat[70]	Sugawara
	Low temperature dc magnetization[104]	Sugawara
	Specific heat[94]	Lapertot
	Specific heat[65]	Andraka
Transitions are intrinsic	Thermal transport in magnetic fields[44]	Sugawara
	Thermal transport in magnetic fields[38, 86]	Maple
	Andreev spectroscopy[89]	Maple

Chapter 5

Specific Heat of $PrOs_4Sb_{12}$: Experimental Procedure

The goal of this experiment was to measure the specific heat of a $PrOs_4Sb_{12}$ sample in two temperature ranges: high temperature range ($\sim 1.4 - 2.8K$) and low temperature range ($\sim 0.3 - 1.2K$). The high temperature range is interesting because the double transition behaviour occurs at these temperatures. The low temperature range is useful for studying the low temperature behaviour of the superconductor's specific heat. The sample studied had approximate dimensions $1mm \times 0.5mm \times 0.5mm$ and mass of $5.6mg$. The single crystals of $PrOs_4Sb_{12}$ studied in this work were grown using an Sb flux method[30, 29] by Brian Maple at UC San Diego. This chapter will describe the equipment and experimental procedure utilized in performing the specific heat measurements.

5.1 Dilution Refrigerator

Figure 5.1 shows the phase diagram for mixtures of ^{3}He and ^{4}He for various temperatures and ^{3}He concentrations. Pure ^{4}He liquid will undergo a transition into the superfluid state at $2.177K$. The temperature at which this transition occurs decreases as the concentration of ^{3}He increases. When the ^{3}He concentration reaches 67.5% and temperature becomes $0.867K$, the superfluid transition disappears. At ^{3}He concentrations above 6.6%, and temperatures below $0.867K$, ^{3}He/^{4}He mixtures separate into two distinct phases, much like water and oil. This region is noted as the shaded region in Figure 5.1. One phase contains mostly ^{4}He . The other phase contains mostly ^{3}He and floats on top of the ^{4}He-rich phase due to its smaller density. As the temperature approaches absolute zero, ^{3}He-rich phase (also known as the concentrated phase) becomes a pure ^{3}He liquid. However, ^{4}He-rich phase (also called the dilute phase) never becomes a pure ^{4}He liquid. Instead

it contains 6.6% ^{3}He even at absolute zero. The idea that a ^{3}He/^{4}He mixture does not separate into pure ^{3}He and pure ^{4}He , but exhibits a finite solubility of ^{3}He in ^{4}He is critical to the operation of a dilution refrigerator. The specific heat of ^{3}He in the dilute phase is greater than the specific heat of ^{3}He in the concentrated phase. This implies that the enthalpy of ^{3}He in the dilute phase is larger than the enthalpy of ^{3}He in the concentrated phase. Therefore, if one can force ^{3}He atoms in the concentrated phase to cross the phase boundary and enter the dilute phase, it is possible to use the heat of mixing to provide cooling power. This process is analogous to evaporation; in order to evaporate a liquid into a gas, heat must be put into the system from its surroundings. Due to the quantum mechanical properties of ^{3}He and ^{4}He , a ^{3}He/^{4}He mixture is inclined to maintain a finite concentration of ^{3}He . Another crucial fact is that if one pumps on a ^{3}He/^{4}He mixture, ^{3}He evaporates preferentially. Hence, it is possible to pump on the dilute phase removing ^{3}He atoms from it. This process then forces ^{3}He atoms to cross the phase boundary from the concentrated phase into the dilute phase in order to maintain the preferred ratio. This process provides cooling power and is the basic principle behind the cryogenic properties of dilution refrigerators.

A schematic illustration of various components of a dilution refrigerator is depicted in Figure 5.2. The 1K pot acts as a usual ^{4}He refrigerator. Dilution refrigerators contain a helium bath that surrounds the interior contents and also acts as a source of liquid helium for the 1K pot. A mechanical pump is used to pump on the helium bath in the 1K pot and lower its temperature to approximately $1.5K$ through evaporative cooling. The ^{3}He gas comes from ^{3}He/^{4}He mixture gas handling system sitting at room temperature. It is initially cooled to $4.2K$ by passing through the ^{4}He bath. It then passes through the 1K pot helium bath where it is condensed and precooled to $\sim 1.5K$. The condensation of ^{3}He occurs through the use of a flow impedance that creates pressure large enough to condense the ^{3}He gas into liquid. Liquid ^{3}He passes through heat exchangers that are thermally connected to the still. This brings the temperature of ^{3}He down to $\sim 0.7K$. Next, the ^{3}He liquid passes through another flow impedance and a set of heat exchangers that bring its temperature low enough so that it may enter the mixing chamber. The mixing chamber is a critical part of a dilution refrigerator. The ^{3}He/^{4}He phase separation occurs in the mixing chamber. This is where ^{3}He crosses the boundary from the concentrated phase to the dilute phase. Hence, the cooling power and the base temperature of a dilution refrigerator are provided by the mixing chamber. Inside the mixing chamber, the ^{3}He concentrated phase floats on top of the dilute phase. A small pipe is located in the lower dilute phase inside the mixing chamber. It leaves the mixing chamber and passes through the heat exchangers used to precool the incoming ^{3}He . The tube ends inside the still. A heat exchanger attached to the still keeps the temperature of the still at approximately $0.6 - 0.7K$. This temperature maintains the ratio of ^{3}He to ^{4}He in the vapour phase of the still as large as possible. Mechanical pumps are used to pump on the dilute phase liquid bath in the still. Since ^{3}He evaporates preferentially, its concentration will decrease. This develops an

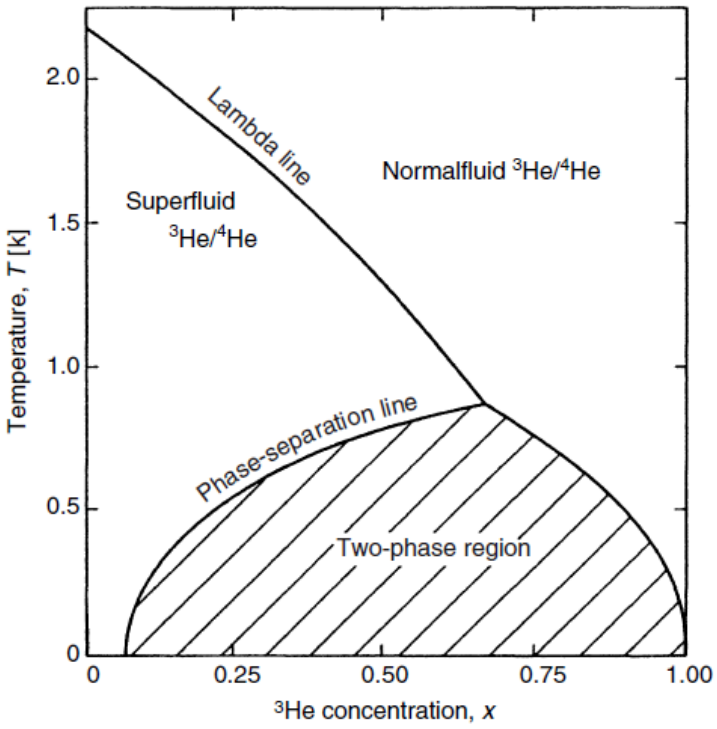

Figure 5.1: Phase diagram of liquid ^{3}He/^{4}He mixtures at saturated vapour pressure. Lambda line shows the superfluid phase transition of ^{4}He . The shaded region shows the phase separation region where the mixture separates into two distinct phases: a dilute phase containing mostly ^{4}He and a concentrated phase containing mostly ^{3}He .[82]

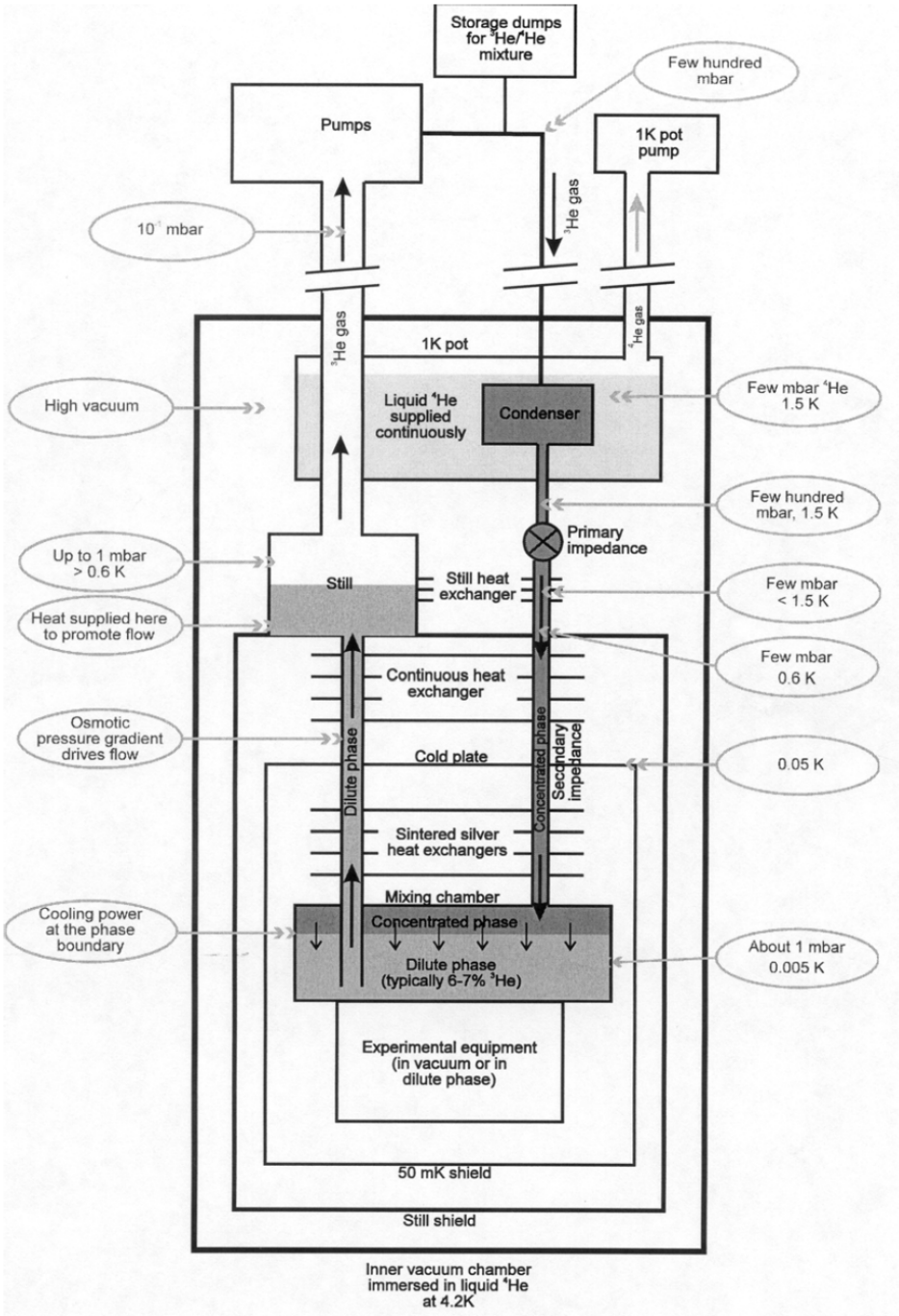

Figure 5.2: Illustration of a typical dilution refrigerator.[21]

osmotic pressure difference that drives ^{3}He from the dilute phase in the mixing chamber up the pipe and into the still. This leads to a decrease in concentration of ^{3}He in the dilute phase inside the mixing chamber. To maintain the desired concentration of ^{3}He in the dilute phase, ^{3}He atoms must then cross the phase boundary from the concentrated phase. ^{3}He pumped away from the still is sent into a closed gas handling system. This system, then feeds the ^{3}He gas back into the dilution refrigerator where it is again condensed, liquified, precooled and routed into the mixing chamber. This continuous cycle provides the cooling power of a dilution refrigerator.

In order to keep the efficiency and base temperature of a dilution refrigerator as optimal as possible, radiation shields are usually attached at various temperature stages. These shields surround the inside components protecting the fridge and any experiments from unwanted radiative heating. Electrical leads coming into the dilution refrigerator need to be thermally anchored at various points for heat sinking purposes. This is usually done at multiple stages, such as at the 1K pot, at the still, and at the mixing chamber.

5.2 Specific Heat Measurements

Low temperature specific heat measurements are essential in developing an understanding about lattice and electronic properties of materials. They are especially useful in studying the characteristics of the superconducting transitions. There are a few different methodologies available in performing experiments to measure a sample's specific heat.

5.2.1 The Quasi-adiabatic Method

The definition of the specific heat, equation 3.2, is the inspiration for the quasi-adiabatic method of measuring the heat capacity of a material. A current is passed through a heater resistor delivering a heat pulse $đQ$ to the sample. A thermometer is used to measure the change in temperature dT of the sample. It's impossible to have the sample perfectly isolated thermally since it is must be connected to the dilution refrigerator stage. Therefore, it is desirable that the thermal connection between the sample and the stage is such that the relaxation time constant is adequately long. During data analysis, it is necessary to account for any possible heat loss that occurs during the application of the heat pulse.

5.2.2 The ac Method

In the ac specific heat measurement, ac current is passed through a heater resistor coupled to the sample. The result is an oscillating heating current of frequency $\frac{1}{2}\omega$ that causes a

temperature response at frequency ω[99]:

$$T_{ac} = \frac{\dot{Q}}{2\omega C}\left[1 + \frac{1}{\omega^2\tau_1^2} + \omega^2\tau_2^2 + \frac{2K_b}{3K_s}\right]^{-1/2} \tag{5.1}$$

where τ_1 is the relaxation time of the sample to the stage, τ_2 is the response time of the sample, heater, and thermometer to the heat input, K_b is the thermal conductivity between the sample and the stage, K_s is the sample thermal conductivity, and C is the total heat capacity of the sample, wire support, the heater, and the thermometer. If the internal response time τ_2 can be made insignificant compared to $1/\omega$, the sample-to-stage relaxation time τ_1 can be made much larger with respect to $1/\omega$, and the sample thermal conductivity K_s can be made considerable greater than the sample-to-stage thermal conductivity K_b, then equation 5.1 becomes a very simple measure of the total heat capacity:

$$C = \frac{\dot{Q}}{2\omega T_{ac}} \tag{5.2}$$

One of the advantages of the ac specific heat measurements is its sensitivity to small changes in heat capacity.

5.2.3 The Relaxation Method

The relaxation method is based on the relation between the heat capacity C of a sample (and the addendum) and the thermal conductivity K of the contact wires and the relaxation time constant τ_1 between the sample and the stage:[8]

$$C = K\tau_1 \tag{5.3}$$

In this technique, the sample is heated (by a resistance heater) a small ΔT above the reference temperature of the stage. The temperature of the sample is described by:

$$T(t) = T_0 + \Delta T e^{-t/\tau_1} \tag{5.4}$$

Therefore, after the sample has been heated, its temperature exponentially decays to the steady state temperature of the stage T_0. If the thermal conductivity K of the supporting wires is known, then by measuring the relaxation time τ_1 taken by the sample to reach the equilibrium temperature T_0, one can calculate the total heat capacity. Signal averaging numerous decays at a given T_0 allows the relaxation method to improve the signal-to-noise ratio of results. The thermal conductance and the addenda heat capacity have to be determined independently. It is possible to adjust thermal conductivity K by selecting a particular type of wire contact and by choosing the wire diameter. If K is too large, then

the internal conductivity of the sample must be large. Otherwise, internal time constant τ_2 might be long and thermal lag between the sample and the stage may cause problems. If the relaxation time τ_1 is not considerably larger compared to all internal relaxation times of the system, the temperature dependence may not be a simple exponential function. In the limit of low thermal conductivity, the relaxation method becomes the quasi-adiabatic method. A disadvantage of this method is the difficulty in analyzing the data to determine the relaxation time correctly. The base temperature of the stage T_0 must be accurately accounted for by subtracting it from the exponential decay. Then the logarithm of the measurement data is taken, and a least-squares fit of the resulting line provides a value for the time constant.

In this work, measurements were performed using the quasi-adiabatic method.

In order to measure the heat capacity of a particular material, we have to cool it to the initial temperature T_I. Then, a known amount of heat Q is applied to the sample. The sample attains the final temperature T_F. The specific heat at the intermediate temperature $T = (T_F + T_I)/2$ may be calculated as

$$C = \frac{Q}{T_F - T_I} \tag{5.5}$$

There are a number of problems and considerations that need to be taken into account when performing heat capacity measurements. Inherently, in determining the heat capacity, it is not the absolute temperature that is important, but instead it is the difference in temperature that is of significance. This means that great amount of experimental precision is required. Properties of the thermometers, such as calibration, stability, sensitivity, and accuracy, need to be well known and are of utmost importance for obtaining high precision and high resolution heat capacity data. The sample needs to be supported in some sort of holder, and it needs to be connected to a cryostat/refrigirator stage that provides the necessary temperature control. This gives rise to a number of issues that have to be considered. Since the sample needs to be thermally anchored to the stage in some way, the heat pulse is not genuinely adiabatic. Any heat loss through the thermal links has to be properly accounted for in order to acquire precise data. The electronic leads to the sample heater and thermometer need to be of very low thermal conductivity (ideally superconducting if possible) and need to be heat sunk at nearly the same temperature as the sample temperature. These precautions are necessary in order to minimize any heat flow into/out of the sample. A heater and a thermometer need to be on the sample. Therefore, their heat capacities and the heat capacities of any additional addenda (such as the wires providing electrical connections) need to be insignificant relative to the heat capacity of the sample. Alternatively, they need to be accurately measured and subtracted from the data in order to calculate correct specific heat of the sample. Thermal contacts between the sample and the heater and the thermometer need to be very good in order to minimize time

constants needed for thermal equilibrium between these components. Also, time needed for the entire sample to thermally equilibrate needs to be fast, or carefully accounted for. It is important that the power used to measure the thermometer is insignificant so that it does not input any considerable heat into the sample. Furthermore, any other sources of heat (such as radiation) need to be minimized and considered for accurate measurements. Great care must be taken to avoid any interference from outside sources of electromagnetic radiation. Dilution refrigerators may be contained inside shielded rooms to keep radio frequency interference away from the electrical leads and from the thermometers to avoid unintended heating. Electrical leads and the thermometer should be shielded from RF as they may be prone to absorb stray RF energy. Electrical leads should be twisted in pairs to minimize the total flux through the loop and reduce any induced currents. Another consideration with electrical wires and devices is grounding. A circuit with multiple ground references gives rise to a possibility of current flow from one ground point to another that may interfere with the signal.

5.3 Experimental Apparatus

Figure 5.3 illustrates the custom machined copper sample holder used to secure and mount the sample onto the dilution refrigerator. No substrate was used in assembling the components. Elimination of the substrate minimizes addendum that needs to be considered in performing heat capacity measurements. Instead, the sample heater and thermometer were coupled directly to the sample itself. This was done in order to maximize the thermal conductivity (ie. minimize the thermal equilibrium time constant) between the sample and the heater/thermometer. The sample heater was a $20k\Omega$ metal-film resistor. The sample thermometer was a RuO_2 resistor with room temperature resistance of $\sim 1k\Omega$. Both chips had their substrates polished away. This was done with two purposes in mind. Firstly, it reduces the masses of the chips, and hence their specific heat. This further minimizes the specific heat of the addendum. Secondly, polishing of the substrate improves the thermal contact between the chips and the sample reducing the time necessary for all of the components to reach thermal equilibrium. The sample thermometer and the sample heater were affixed to the sample using a small amount of GE varnish. The sample itself was held in place by very thin nylon strands. It was attached to the the nylon threads using GE varnish. The very thin nylon strands were used in order to minimize any parasitic heat leaks into or out of the sample.

The electrical leads to the sample heater/thermometer were six NbTi wires with $6\mu m$ diameter and length of approximately $5mm$. The individual wires were obtained by dissolving the copper-nickel cladding of multifilamentary NbTi wires using a solution of nitric acid. Four of the wires were connected to the thermometer in order to read the temperature

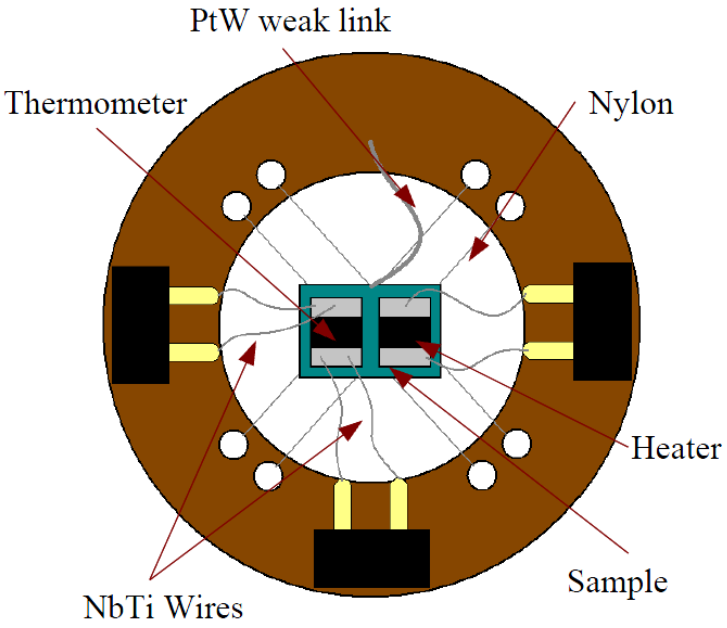

Figure 5.3: Illustration of the sample holder used in this experiment.

by measuring its resistance using the 4-terminal technique (described below in section 5.5). Two remaining wires were connected to the heater resistor in order to apply the heating current. The connections were made using silver epoxy. The rationale for selecting these wires is to minimize the thermal conductivity of the electrical leads. Heat transported by a thermal link connecting two objects at temperatures T_1 and T_2 is determined by:[82]

$$\dot{Q} = \frac{A}{L}\int_{T_1}^{T_2} \kappa(T)dT \tag{5.6}$$

where A, L, and $\kappa(T)$ are the cross-section area, length, and thermal conductivity of the thermal link. The superconducting transition temperature of NbTi is $\sim 9.2K$. This means that in the temperature range of importance in these measurements, the electrical leads will be superconducting. The thermal conductivity of normal electrons is a linear function of temperature ($\kappa_{e,n} \propto T$[110]). In a superconducting metal, electrons that are condensed into Cooper pairs carry no entropy. Therefore, they do not transport any heat. So, thermal transport properties of a superconducting metal are determined by the number of unpaired electrons which decreases exponentially with temperature. Hence, thermal conductivity of electrons in a superconductor is $\kappa_{e,s} \propto Te^{-\Delta E/k_B T}$. This means that at low temperatures ($T \ll T_C$), the thermal conductivity of a superconductor becomes miniscule[1]. To further

[1]Thermal energy may be transported by phonons. However, this contribution is insignificant compared to heat transport due to electrons.

Table 5.1: Table of thermal conductivities and specific heats of various experimental components

	Thermal Conductance (W/K)	Specific Heat (J/K)
Sample	8.75×10^{-3}	1×10^{-5}
Weak Link (PtW)	2×10^{-9}	1×10^{-9}
Thermometer	$> 5 \times 10^{-8}$	1×10^{-8}
Heater	$> 5 \times 10^{-8}$	1×10^{-8}
Electrical Leads (NbTi)	$< 1 \times 10^{-10}$	Negligible
Nylon Threads	$< 1 \times 10^{-10}$	Negligible

decrease the heat transported by the electrical leads, the diameter of the wires used is chosen to be very small.

In the high temperature range $(1.4 - 2.8K)$, the thermal transport between the sample and the sample holder is governed by the thermal weak link which is a PtW wire with diameter of $25\mu m$. Silver epoxy was used to join the ends of the wire to the sample and the sample holder. We wanted the time constant of relaxation to be long ($\tau \sim 1$ hour). This in turn determined our requirement for the thermal conductance of the weak link ($K_{WL} = C/\tau$). Thermal conductance depends on the thermal conductivity of PtW ($\kappa \propto T$), cross-section area A of the wire, and the length l of the wire. Thus, the desired length of the PtW wire $l = \kappa A/K_{WL}$ was determined to be approximately $1.5cm$.

In the low temperature range $(0.3mk - 1.2K)$, the heat capacity C of $PrOs_4Sb_{12}$ decreases quickly due to the Schottky anomaly. This means that the PtW weak link becomes inadequate in providing the necessary time constant of approximately one hour. For measurements in this temperature range, the PtW weak link was removed. Hence, all thermal transport was through the superconducting wires acting as electrical leads. At these low temperatures, the thermal conductance of the superconducting NbTi wires is very small providing the necessary long time constant.

Table 5.1 shows approximate values for thermal conductivity and specific heat of various components. Sample thermal conductivity is estimated from [86] and specific heat from [66]. Thermometer and heater (alumina substrates) heat capacities are estimated using data from [11]. All other values are estimated using data from [82]. All estimates are at $T = 1.5K$.

The sample holder in Figure 5.3 was contained in a small box machined out of copper. The box enclosed the entire sample holder to provide shielding from any radiation that might cause parasitic heating of the sample. All electrical leads were heat sunk to this box before reaching the sample holder. Thermal anchoring of the leads was performed by gluing them on a Cu rod. A layer of cigarette paper was glued around the rod with

GE varnish to separate the electrical leads from the rod. This was done as a preventive measure in case there are any sharp edges or burrs on the metal post which might damage the wire insulation. The thermometer and heater resistor used for temperature control were also affixed onto this casing. The heater was a $1.3k\Omega$ metal film resistor. In the high temperature range ($1.4-2.8K$), the container was connected to the mixing chamber using a stainless steel screw. At low temperatures, stainless steel has very low thermal conductivity ($\kappa \sim 0.1W/cmK$). Thus, it enabled us to raise the temperature of the casing (and hence the sample holder) to the desired level while the dilution refrigerator was still operating at its base temperature ($\sim 5 - 10mK$). For the low temperature range ($0.3 - 1.2mK$), the casing was coupled directly to the mixing chamber of the dilution refrigerator.

In the high temperature range, the thermometer used for temperature control and as a reference for calibration of the sample thermometer was the thin film ceramic zirconium oxynitride (CERNOX) resistor. CERNOX resistors are manufactured commercially and the thermometer used in this experiment was purchased calibrated. These thermometers are stable, have good sensitivity, and have fast response times (time constant is about $1 - 1.5ms$)[2]. At $4.2K$, the CERNOX model (CX-1030) used in our measurements has typical values for resistance: 574.20Ω, dR/dT: $-97.344\Omega/K$, $(T/R) \cdot (dR/dT)$: -0.71.[2] At $\sim 1.5K$, the resistance of the thermometer used in our measurements is $\sim 3k\Omega$.

In the low temperature range, the temperature control and reference thermometer was a calibrated germanium resistance thermometer (GRT). GRT thermometers consist of Ge sensing element encapsulated in a gold plated copper casing with helium gas used as an exchange gas for thermal coupling. GRT thermometers have good sensitivity and show great stability. Typical resistance values of the GRT thermometer used in our experiments were $\sim 60 - 250\Omega$ in the low temperature range.

5.4 Temperature Control

Temperature control of the experimental system was performed by Lakeshore Model 370 AC resistance bridge using the proportional-integral-derivative (PID) control loop feedback method. The Lakeshore temperature controller measures the resistance of the reference thermometer used for temperature control (CERNOX or GRT) using the 4-terminal technique (see below section 5.5). It then calculates the error from the current resistance reading (representing the current temperature of the system) and the desired resistance (ie. the desired temperature called the setpoint). The feedback control circuit tries to minimize this error by adjusting the dc power output to the temperature control heater. The PID control algorithm depends on three parameters: the proportional (P), the integral (I), and the derivative (D).

5.4.1 Proportional

In order to maintain the temperature of our heat capacity cell that is above the base temperature of the mixing chamber, the temperature controller must apply power across the heater resistor in order to combat the cooling power of the dilution refrigerator. This output is determined by the proportional parameter P (also called gain):

$$HeaterOutput(P) = Pe(t) \tag{5.7}$$

where $e(t)$ is the error between the current temperature reading and the setpoint. In this case, the proportional parameter has to be non-zero for any output, and the output is proportional to the error. A high P value results in large heater output for small error. A too high value of P can result in the temperature of the system to oscillate about the setpoint and become unstable as shown in Figure 5.4. A small P value results in a insensitive temperature controller since the controller may not apply enough power to correct the error.

In a steady state, the temperature controller operating only with the P parameter will not settle at the desired temperature. The output is proportional to the error. Therefore, at some point, the output produced by the heater will exactly cancel the cooling power of the dilution refrigerator, and the system will settle at some temperature below the setpoint (see Figure 5.4). This error is called the droop.

The proportional parameter depends on the characteristics of the experimental setup, heater range output, and cooling power of the dilution refrigerator. It is usually determined through trial and error.

5.4.2 Integral

In order to correct for the offset in the proportional setting, integral parameter is utilized. The output due to the integral parameter depends on the magnitude of the error, and the duration of the error. Accumulated error is calculated by integrating the instantaneous error over time. The accumulated error is multiplied by the I parameter to determine the contribution to the heater output:

$$HeaterOutput(I) = PI \int e(t)dt \tag{5.8}$$

If the system temperature is extremely different from the setpoint, then the integral contribution accelerates the heating to increase the temperature of the system to the desired level faster. Too high of a value for I can cause the system to overshoot the setpoint, and create oscillations. The integral parameter may also eliminate the droop. At this point,

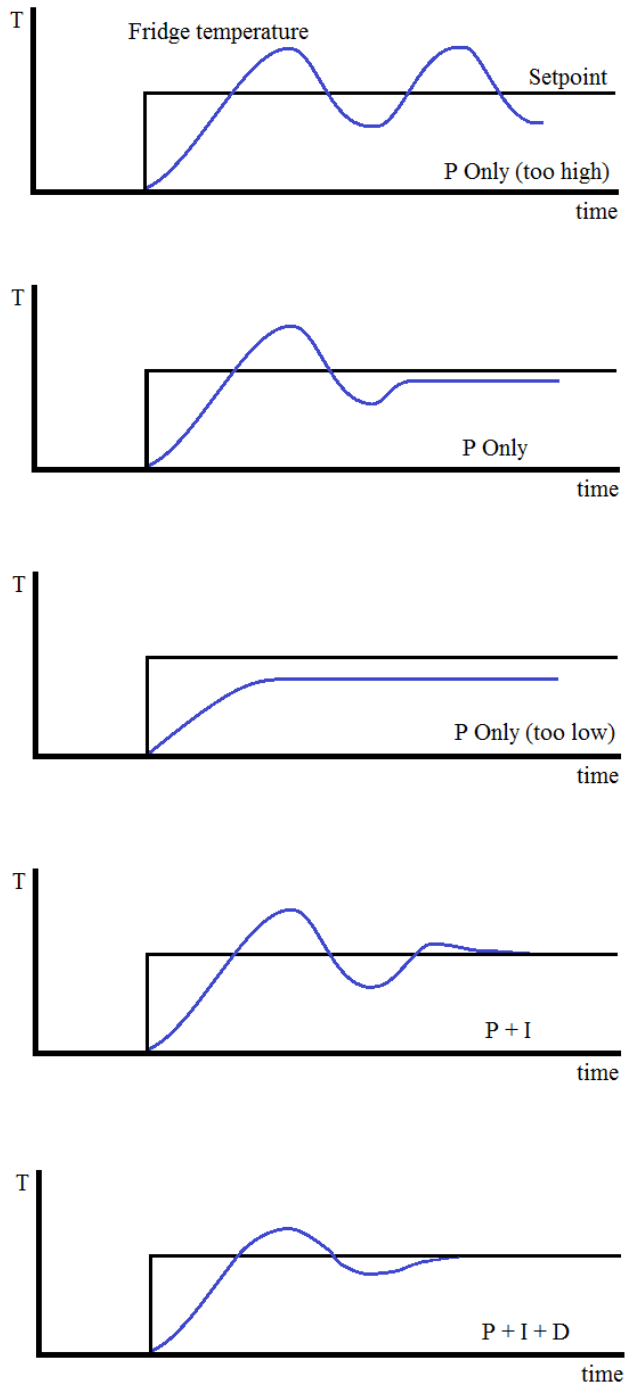

Figure 5.4: Illustration of examples of PID temperature control.

the error is zero and the output due to the proportional parameter is zero. The steady state is therefore maintained by the integral parameter. However, if the value of the I parameter is too low, the droop may not be entirely eliminated. The integral parameter depends on the time constant of the experiment load.

5.4.3 Derivative

If the use of integral setting causes overshoot in the temperature control, derivative parameter may be used to minimize this effect. The rate of change of the temperature is calculated by determining the slope of the error over time. Multiplying this rate of change by the derivative gain D gives the contribution to the heater ouput:

$$HeaterOutput(D) = PD\frac{d}{dt}e(t) \tag{5.9}$$

The derivative term slows the rate of change of the controller output. This effect is most noticeable when the temperature approaches the controller setpoint. The derivative parameter is used to reduce the magnitude of the overshoot produced by the integral component. It should be noted that differentiation of the error amplifies noise in the error. Therefore, if the noise and the derivative gain are large, this can cause the temperature to become unstable.

The total heater output is calculated by combining the total contributions of the three parameters:

$$HeaterOutput = P\left[e(t) + I\int e(t)dt + D\frac{d}{dt}e(t)\right] \tag{5.10}$$

5.5 Resistance Measurement: 4 terminal technique

In low temperature experiments, resistance thermometry has to be performed at very low powers. Therefore, it is necessary to have the ability to measure very small voltages in order to measure thermometer resistances. For this reason, conventional direct current voltage measurements are not satisfactory as they cause unacceptable heating. Alternating current has to be utilized in order to avoid these problems and to achieve higher sensitivities. Furthermore, very accurate resistance measurements are essential for obtaining precise temperature readings. This means that lead resistances of electrical connections to the thermometer resistors inside the dilution refrigerator must be eliminated. The solution to these issues is to use an AC bridge to measure thermometer resistance using the 4 terminal measurement. The essential idea of a 4 terminal measurement is illustrated in the circuit diagram in Figure 5.5. The resistance of the thermometer R_T needs to be

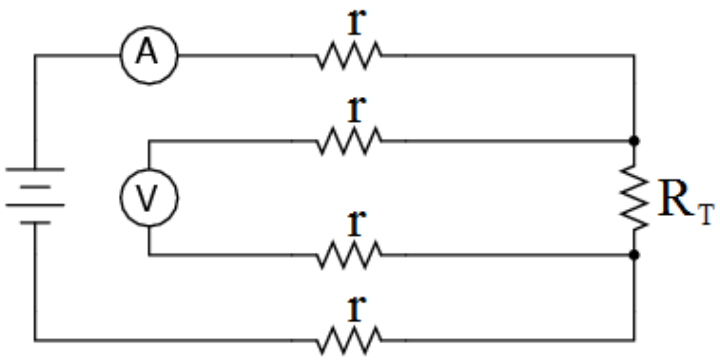

Figure 5.5: Circuit illustrating the basic idea behind a 4 terminal measurement.

accurately measured, while eliminating the resistances r of the leads. A power supply provides a current to the thermometer resistor that is measured by the ammeter. The voltmeter measures the voltage drop across the thermometer resistor. The resistance R_T may be calculated using Ohm's law. The main idea is that the leads to the voltmeter carry minimal current and therefore drop insignificant amount of voltage.

5.6 Experimental Procedure

The sample was placed in the sample holder, which was then enclosed in the copper casing as described above. This arrangement was then affixed to the mixing chamber of a dilution refrigerator. Thermal coupling of the system to the mixing chamber was through a stainless steel in the high temperature range, or by direct contact in the low temperature range. Dilution refrigerator was cooled down to its base temperature. Lakeshore Model 370 AC resistance bridge was used to provide temperature control of the experimental system by monitoring the resistance of the reference thermometer, and applying current to the heater resistor necessary to maintain the specified temperature setpoint. To obtain the heat capacity measurements of the sample, a known heat pulse was applied to the sample, and the resulting change in temperature was measured. The heat pulse was administered by applying voltage across a large current limiting resistor ($600k\Omega$) in series with the sample heater. The analog output channel of a National Instruments DAQ-card was used as the power source for the heat pulse. The duration of the heat pulses was approximately $20-30s$ in the high temperature range, and about $12-20s$ in the low temperature range. The relatively short duration of the heat pulses minimizes the heat loss that occurs during the application of the heat pulse. The sample thermometer resistance data was obtained using a Linear Research LR700 ac resistance bridge by performing the 4 terminal measurement. The excitation level used to measure the resistance was set such

that self heating was insignificant while still maintaining a low level of data noise. Temperature control, experimental procedure, and data acquisition were all automated through the use of a computer running custom written LabVIEW software. In order to acquire the specific heat measurement, following steps were performed. Firstly, the temperature of the experiment stage was set to the desired level. To accomplish this, the program used the known calibration for the reference temperature control thermometer to calculate the equivalent resistance value. This resistance value was set as the setpoint on the Lakeshore temperature controlled. Enough time was allowed so that the temperature controller stabilized at the desired temperature, and for the sample to reach thermal equilibrium. The program then applied the heat pulse to the sample, and waited for the sample temperature to fall back down to the equilibrium temperature. This completes the data acquisition for a single specific heat data point. A new setpoint was determined, and the whole routine is repeated at a different temperature. The temperature steps between adjacent data points ranged from $15mK$ to $25mK$. All of the data was recorded in a data file to be analyzed later.

5.7 Data Analysis

5.7.1 Specific Heat Calculation

Figure 5.6 shows a typical single data point for the measurement of the heat capacity of $PrOs_4Sb_{12}$. Before the heat pulse is applied, the heat capacity stage and the sample are allowed enough time to come to thermal equilibrium. This part of the data is used for calibration of the sample thermometer. Average resistance of a flat portion of the sample thermometer data is correlated with the temperature measured from the reference thermometer used for temperature control. This calibration is carried out at every heat capacity data point. To obtain the resistance-temperature relationship between calibration points, a linear interpolation is performed. A linear fit is calculated for the sample temperature data before the heat pulse, and an exponential fit is calculated for the data after the heat pulse. The lower temperature T_L is determined by using the linear fit to calculate the temperature half way through the heat pulse. Likewise, the upper temperature T_U is obtained by using the exponential fit to calculate the temperature of the sample at the midpoint of the heat pulse. The change in temperature is given by $\Delta T = T_U - T_L$. This method compensates for the heat loss that occurs during the application of the heat pulse. The heat Q applied to the sample is calculated by multiplying the power applied to the heater by the duration of the pulse. Therefore, the specific heat is obtained by $C = Q/\Delta T$. This specific heat value corresponds to the average temperature during the heat pulse $T = (T_U + T_L)/2$.

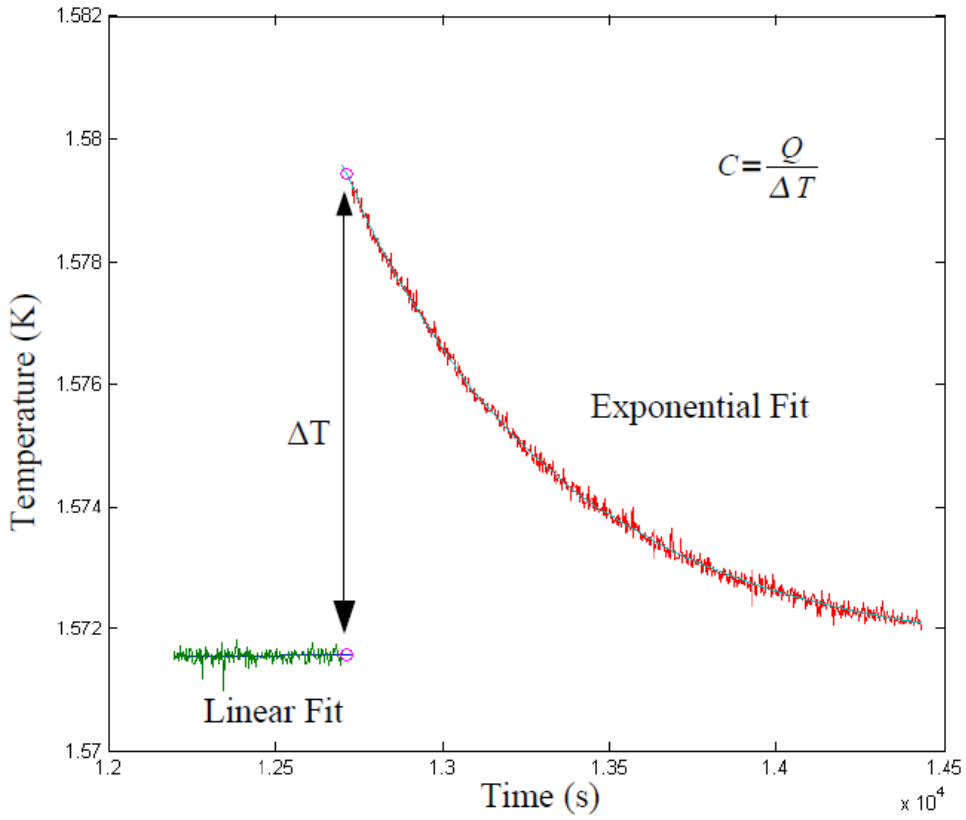

Figure 5.6: Typical data for a single specific heat data point. Linear fit is performed for the data before the heat pulse. Exponential fit is performed for the data after the heat pulse. The change in temperature is calculated by extrapolating these fits to the midpoint of the heat pulse.

5.7.2 Error Analysis

In order to calculate the errors in the values for T_U and T_L, the 66% prediction interval for each extrapolated value of the fit function was determined. The propagation of error in T_U and T_L into calculations of specific heat were tracked using formulas:

$$f = aA \pm bB; \quad \sigma_f^2 = a^2\sigma_A^2 + b^2\sigma_B^2 \tag{5.11}$$

$$f = \frac{A}{B}; \quad \left(\frac{\sigma_f}{f}\right)^2 = \left(\frac{\sigma_A}{A}\right)^2 + \left(\frac{\sigma_B}{B}\right)^2 \tag{5.12}$$

In other words, the error in ΔT and average temperature were calculated using equation 5.11, and the error in specific heat was calculated using equation 5.12.

Chapter 6

Specific Heat of $PrOs_4Sb_{12}$: Results and Discussion

The results of specific heat measurements of $PrOs_4Sb_{12}$ for the temperature range between $1.4K$ and $2.8K$ are shown in Figure 6.1. These results were derived from an aggregation of multiple specific heat experiments on $PrOs_4Sb_{12}$ shown in Figure 6.2. The broad feature in the data is the Schottky anomaly discussed in chapter 4. The data clearly exhibit the double superconducting transition behaviour. In order to analyze our data and compare it with other previous reports, transition temperatures, ΔT_c, and $\Delta(C/T)$ are defined according to Figure 6.5.

The upper transition is a broad transition at approximate temperature $T_{c1} = 1.871K$ and the lower transition is very sharp at temperature $T_{c2} = 1.63K$. The upper transition occurs at temperature comparable to previous results ($T_{c1} \approx 1.85K - 1.89K$). The lower transition occurs at temperature that is lower then most previous results ($T_{c2} \approx 1.72K - 1.76K$). However there have been previous reports of $PrOs_4Sb_{12}$ samples with T_{c2} transition temperatures occurring at lower temperatures ($1.53K - 1.68K$)[67]. The specific heat amplitude at the second transition is $3.353J/molK^2$ which is comparable to values usually reported in other works. Figures 6.3 and 6.4 show the results from these measurements alongside some of the previously published data. As is easily seen in the figure, the upper transition is sample independent and is extremely stable among all of the samples. On the other hand, the lower transition is very sample sensitive as its critical temperature varies between many samples. One possible explanation for such behaviour is that the two transitions are due to two different superconducting phases. It seems that the upper transition is not sensitive to impurities in the sample. This implies that it exhibits s-wave superconductivity.[9] Conversely, the lower transition seems to be affected by impurities suggesting that its order parameter is asymmetric. This interpretation is consistent with the results and the multiband scenario proposed in [38, 86, 89]. However, one puzzling

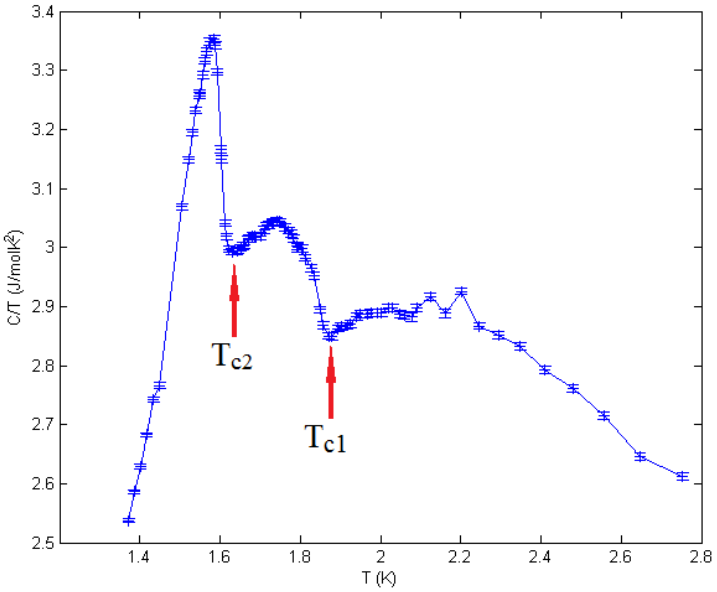

Figure 6.1: Average of all $PrOs_4Sb_{12}$ specific heat measurement results for the temperature range $1.4K$ and $2.8K$. The two transition temperatures are at $1.871K$ and $1.63K$.

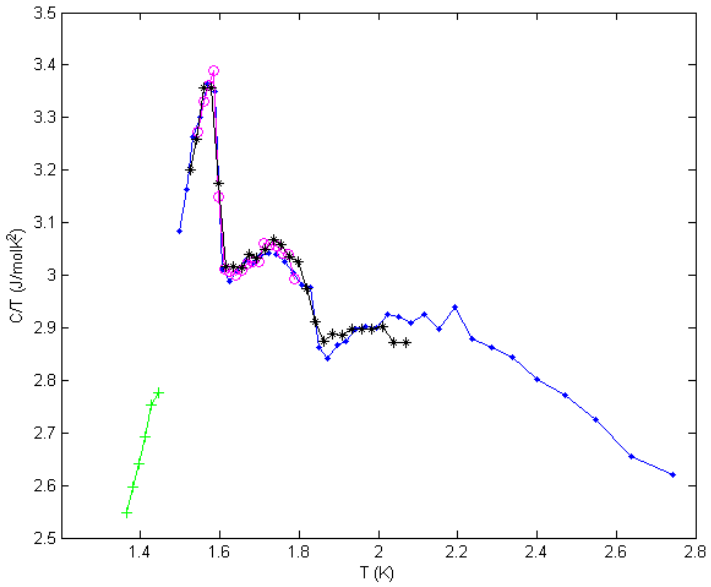

Figure 6.2: $PrOs_4Sb_{12}$ specific heat measurement results for the temperature range $1.4K$ and $2.8K$.

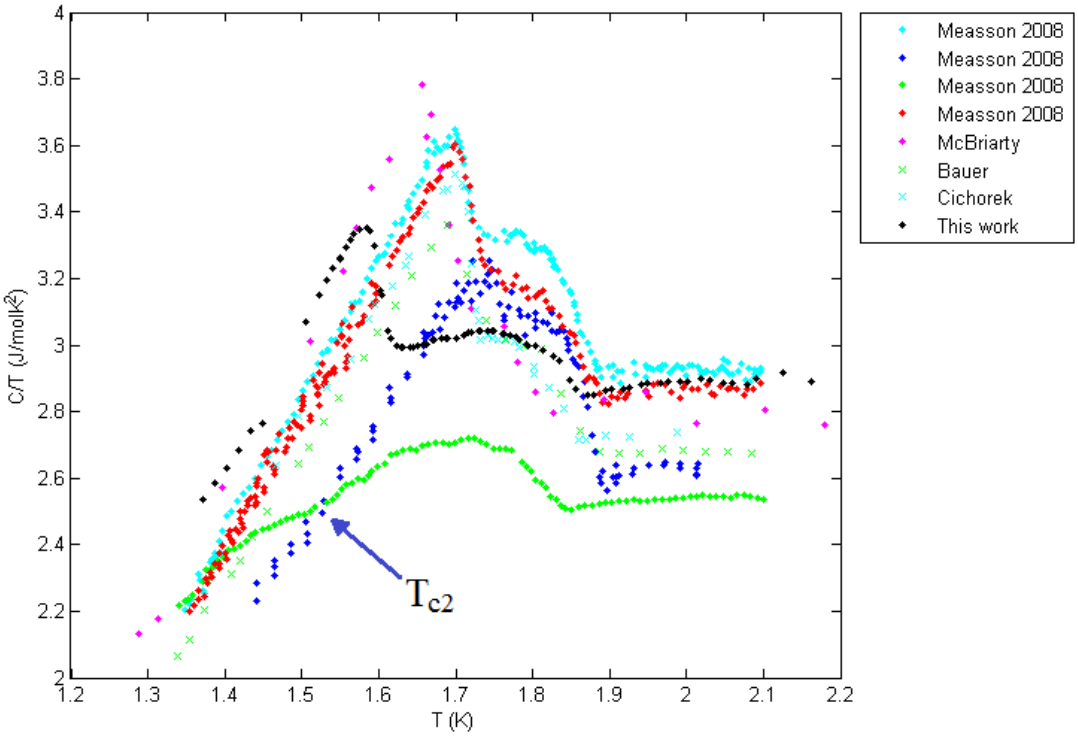

Figure 6.3: Heat capacity data from our results (black) and from [67] (cyan, blue, green, red), [65] (magenta), [63] (green crosses), and [19] (cyan crosses). The upper transition temperature is sample independent while the lower transition temperature varies among samples.

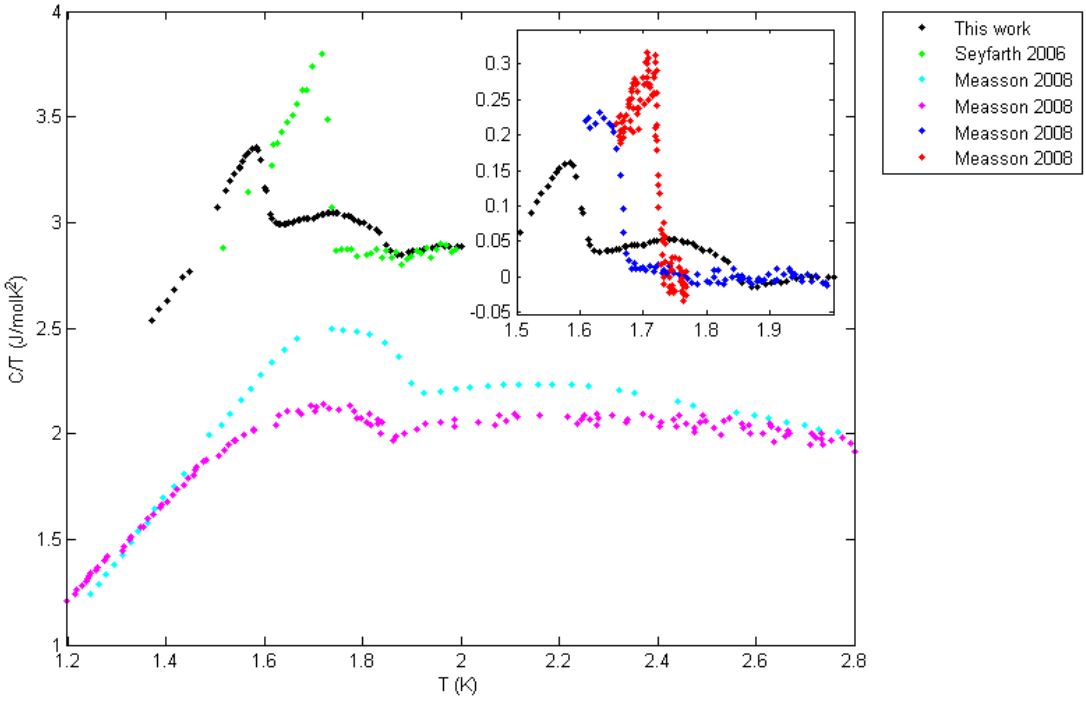

Figure 6.4: Heat capacity data from our results (black) and from [67] (cyan, blue, magenta, red), and [94] (green). The main plot shows our results along with one sample with a single sharp transition and two samples with single broad transitions. The inset shows our results along with two samples with single sharp transitions. Samples with a single broad transition have a T_c that coincides with the upper transition. Samples with single sharp transitions have T_c's that coincide with the lower transition and the transition temperature varies between samples.

question is the existence of samples with single transitions. As seen in Figure 6.4, samples with a single broad transition have a T_c that coincides with the upper transition. On the other hand, samples with a single sharp transition have a T_c that is in the temperature range of the lower transition of samples with two superconducting transitions. Additionally, this transition temperature varies between samples.

In order to characterize the sample, we can examine certain aspects of the superconducting transition data and compare them to other samples reported in [67]. The C/T at $2K$ for our sample is approximately $2.89J/molK^2$. This value is quite high. All of the "high quality" samples in the referenced paper have values for C/T at $2K$ in the range between $2.6J/molK^2$ and $3J/molK^2$. The total specific heat jump $\Delta(C/T)$ in our data is $0.503J/molK^2$. The "high quality" samples exhibit $0.6J/molK^2 - 0.8J/molK^2$ for the total specific heat jump. This is slightly higher than the value obtained for our sample. The width of the first superconducting transition is $\Delta T_{c1} = 121mK$. This is slightly larger than most other reported values. However, given the broad and ill-defined nature of this transition, it is expected that there will be large range of values for its width. The width of the second superconducting transition is $\Delta T_{c2} = 47mK$ and is comparable to other published results. The height of the first superconducting transition is approximately half of the height of the second superconducting transition. If the two transitions are due to inhomogeneity, then this suggests that large and comparable fractions of the sample are undergoing superconducting transitions at two different temperatures.[65]

If we assume the BCS model weak coupling prediction:

$$\frac{\Delta C}{\gamma T_C} = 1.43 \tag{6.1}$$

we can get the estimate for the Sommerfeld constant $\gamma \approx 350mJ/molK^2$. This value is in agreement with other results and confirms the heavy fermion behaviour of $PrOs_4Sb_{12}$. If we follow the calculations and approximations performed in [12], this Sommerfeld constant corresponds to effective electron mass $m^* = 50m_e$.

Figure 6.6 shows the results of specific heat measurements from approximately $150mK$ to approximately $1.2K$. The upturn in the specific heat data that occurs below $T \approx 450mK$ is due to nuclear magnetic moments (see section 3.3). The low temperature range is interesting because unconventional superconductors with nodes in the energy gap exhibit a power law ($C_S \propto T^n$) dependance in the superconducting specific heat instead of the usual exponential behaviour. In order to obtain a power law fit to the specific heat data, two different methods were used. First, a general power law function ($f(x) = ax^b + c$) was fit to the specific heat data. Second, a linear function ($f(x) = bx + c$) was fit to the logarithm of the specific heat data. Temperature range used for the fitting was from $450mK$ to $1.2K$. Below this temperature range, the nuclear magnetic moments contribution to the specific heat starts to become significant. From the two methods, we obtained two values for the

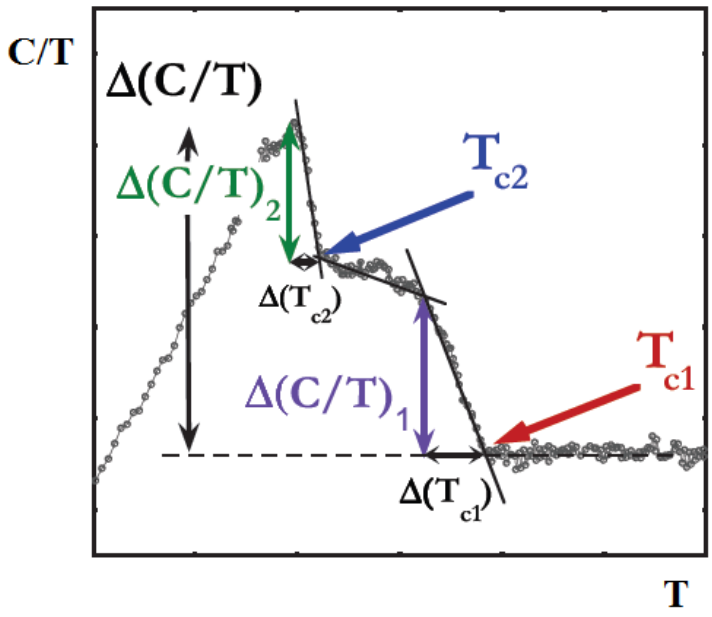

Figure 6.5: Definition of transition temperatures, ΔT_c, and $\Delta(C/T)$.[67]

exponent in the power law behaviour. Using the first fit model, we calculated exponent value $n_1 = 4.168$. Using the second method, the power law behaviour is described by the exponent $n_2 = 3.703$. Figure 6.7 shows the two fits (n_1 is red and n_2 is green) as they compare to the specific heat data and Figure 6.8 shows the two fits as they compare to the C/T data. For completeness, Figure 6.9 shows the two fits and the specific heat data on a logarithmic scale. It can be deduced from the plots that $n = 3.703$ exponent provides generally a better fit to the specific heat data. This exponent value is in very good agreement with $n = 3.9$ obtained in previous measurements[64]. The power law behaviour of the low temperature specific heat in the superconducting state suggests the the order parameter is anisotropic. This is in direct agreement with the results obtained by Andreev spectroscopy study done on crystal samples from the same batch as our sample.[89]

One way to improve on our analysis would be to measure the specific heat of $PrOs_4Sb_{12}$ at higher temperatures to approximately $8K$. Unfortunately, the RuO_2 resistor used as the thermometer in this study loses the sensitivity necessary for accurate temperature measurements at temperatures above $5K$.[71] With the data for the specific heat up to $8K$, it could be possible to model the Schottky anomaly in the specific heat. By subtracting the Schottky anomaly from the total specific heat, a more accurate calculation of the electronic specific heat could be obtained. A similar procedure was performed on the specific heat data from [64]. This changed the value of the power law exponent from $n = 3.9$ to $n = 2.5$.[63] The power law dependance of the electronic specific heat in the superconduct-

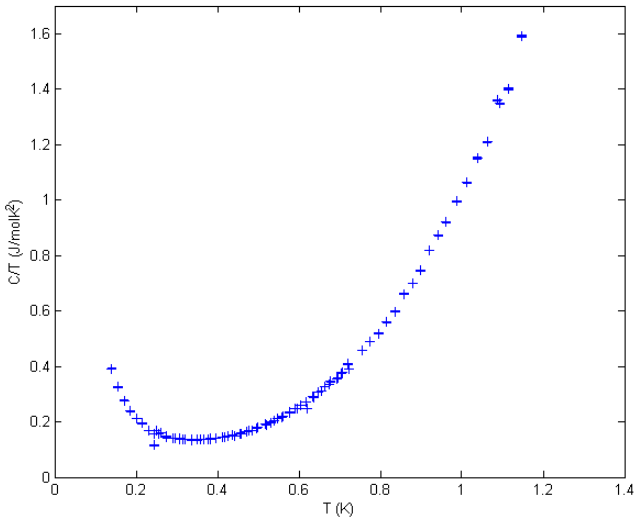

Figure 6.6: $PrOs_4Sb_{12}$ specific heat measurement results for the temperature range $150mK$ and $1.2K$.

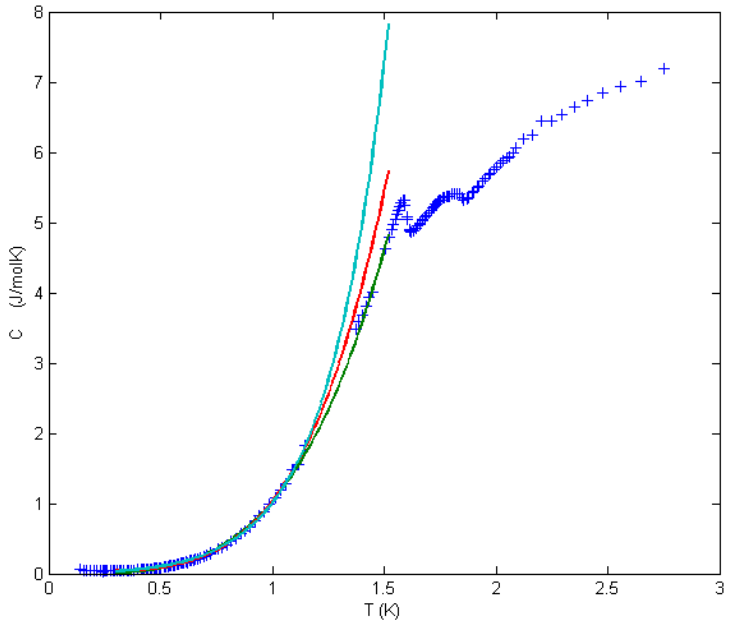

Figure 6.7: Power law and exponential fits to the specific heat data. $n_1 = 4.168$ is red, $n_2 = 3.703$ is green, and exponential fit is cyan. n_2 makes the best fit.

ing state implies anisotropic energy gap and unconventional superconductivity. Further enhancements are possible by measuring the specific heat to even lower temperatures. It would be useful to model the nuclear magnetic contribution to the specific heat by fitting a T^{-2} function to this low temperature data. Accuracy of the results could be improved by subtracting this term.

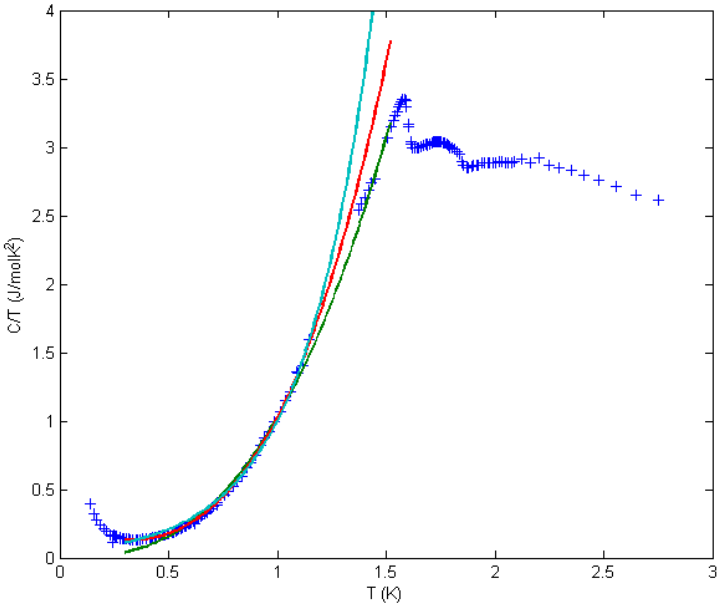

Figure 6.8: Power law and exponential fits to the C/T data. $n_1 = 4.168$ is red, $n_2 = 3.703$ is green, and exponential fit is cyan. n_2 makes the best fit.

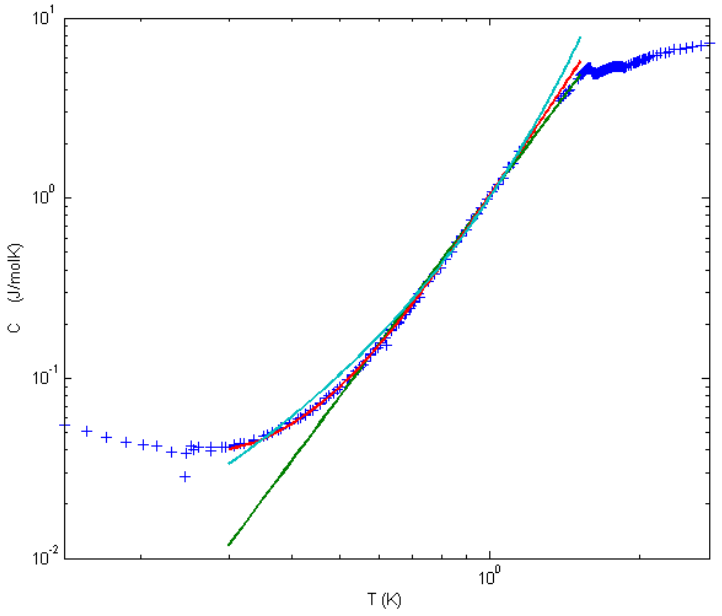

Figure 6.9: Power law and exponential fits to the specific heat data on a logarithmic scale. $n_1 = 4.168$ is red, $n_2 = 3.703$ is green, and exponential fit is cyan. n_2 makes the best fit.

Chapter 7

Cuprates and YBCO

7.1 General Remarks

The discovery of superconductivity of mercury at liquid helium temperature in 1911[106] stimulated a search for materials with higher transition temperatures. In 1973, superconductivity in Nb_3Ge was observed to occur at a critical temperature of approximately $23K$.[32] In about sixty years the transition temperature of superconductors was raised from $\approx 4K$ of liquid helium to $\approx 23K$. Nb_3Ge remained the highest-T_c superconductor for next thirteen years. In 1986, Bednorz and Muller found that the cuprate compound $La_{2-x}Ba_xCuO_4$ becomes superconducting at approximate temperature of $30K$.[13] This finding sparked a revolution in research of superconducting materials. The next pivotal breakthrough was the creation of superconducting cuprate $YBa_2Cu_3O_7$ (YBCO) by Wu et al.[113] The transition temperature of YBCO was found to be as high as $90K$, above the boiling point of liquid nitrogen at temperature of $77K$. Further research led to development of other cuprates with even higher critical temperatures, such as $HgBa_2Ca_2Cu_3O_{8+\delta}$ with the transition temperature of $133K$.[14]

The crystal structure of cuprates is relatively simple. Most cuprates consist of CuO_2 planes separated by a spacer layer. The crystal structure of YBCO is shown in Figure 7.1. It is made up of CuO_2 planes and CuO_4 ribbons perpendicular to these planes. The yttrium atoms are located between the CuO_2 planes, and the barium atoms are located between the CuO_4 ribbons and the CuO_2 planes. Most superconducting properties of cuprates are determined by the electronic structure of the CuO_2 planes.

Cuprates belong to a category of materials called Mott insulators. Conventional band theory predicts that these materials should be conductors. This is because the standard tight-binding theory predicts that the energy band associated with the 3d orbitals of the Cu ions is half filled due to the presence of odd number of electrons. However, this is in

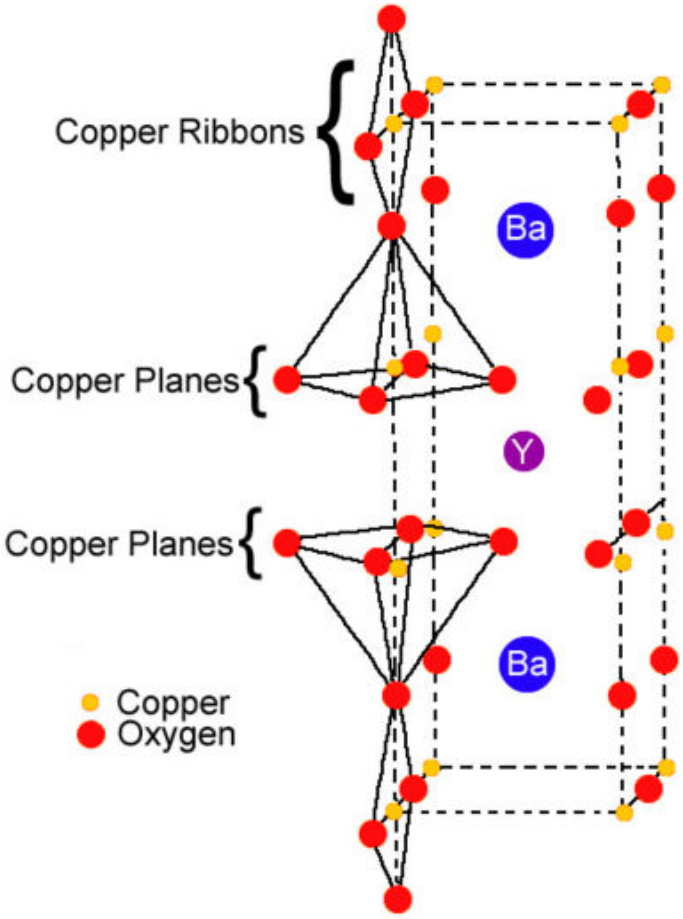

Figure 7.1: Crystal structure of YBCO.[1]

contradiction to experimental results which show that cuprates are insulators. The discrepancy arises because the tight-binding method used in conventional band theory assumes the independent electron approximation. However, for a proper description of cuprates, electron-electron interactions must be considered. The Hubbard model was developed as an extension to the tight-binding approximation to include the electron-electron interactions. The Hubbard model contains two terms. It contains the term t associated with kinetic energy of electrons hopping from one atom to one of its neighboring atoms. The second term is known as the Hubbard U and accounts for the electron-electron interactions. It represents the potential energy associated with the Coulomb repulsion arising when one electron hops from one Cu site to a neighboring atom. If this intersite Coulomb repulsion is greater than the gain in kinetic energy due to electron hopping ($U \gg t$), the electrons become localized. Due to the Pauli exclusion principle, two parallel spins are forbidden to reside at the same Cu site, but antiparallel spins are not. In this case and at low temperatures[1], virtual hopping of antiparallel spins between Cu ions causes the formation of antiferromagnetic order between the Cu ion spins. This superexchange interaction is established by the separating O atoms and has the exchange energy $J = 4t^2/U$.[110] The actual situation in cuprates is more elaborate due to the hybridization of Cu 3d and O 2p orbitals[78], but the crucial idea remains the same.

If the cuprates are chemically hole doped, different physical behaviour emerges. Hole doping can be achieved by removing cations from the spacer layer or replacing them with atoms that have lower valence. In order to sustain charge neutrality, electrons from the CuO_2 planes transfer into the spacer layer leaving behind holes. The removal of electrons from the CuO_2 planes severs the magnetic interaction between the adjacent Cu ions. Thus, introducing holes into cuprate CuO_2 planes tends to destroy the antiferromagnetic order. As the hole doping is increased, cuprate materials seize to be antiferromagnetic, and instead become superconductors. The critical temperature forms a "dome" as a function of hole doping. The transition temperature increases with increasing hole doping, reaching a maximum when doping is approximately 15%. As doping is increased beyond this value, the transition temperature decreases. At approximately 25% hole doping, cuprates lose their superconducting properties and become ordinary metals. This behaviour is illustrated in the phase diagram of cuprates shown in Figure 7.2.

The superconducting state in cuprates exhibits many properties characteristic of conventional BCS superconductors.[77] It has zero electrical resistance and possesses the Meissner effect characteristic of Type-II superconductors. The electrons condense forming Cooper pairs. One unusual property is that cuprates have very short coherence length. For usual superconductors, the coherence length is of the order 10^3Å. In cuprates, the coherence length is of order 20Å in CuO_2 planes and 2Å between the CuO_2 planes.[2] A

[1] At temperature below the Néel temperature, T_N.

[2] The coherence length between the planes is so short that cuprate materials behave like a stack of

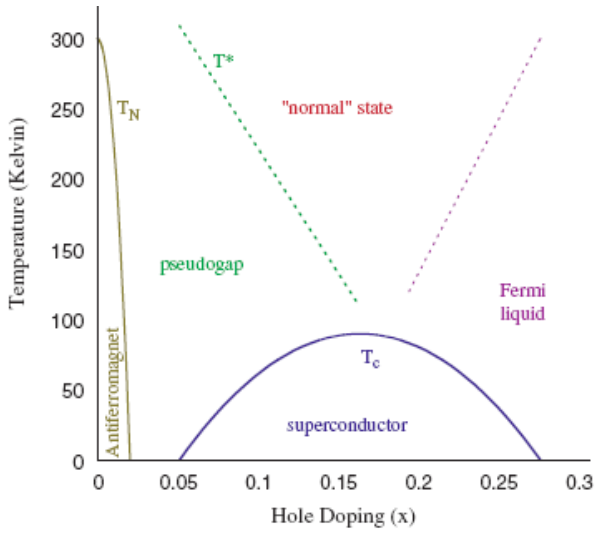

Figure 7.2: Cuprate phase diagram from [77]

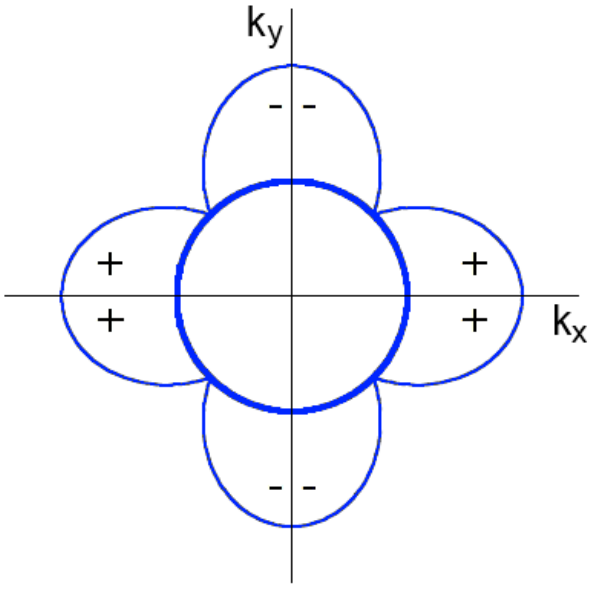

Figure 7.3: Variation of the energy gap around the Fermi surface in a d-wave superconductor.

more significant and atypical characteristic is that the symmetry of the superconducting energy gap is not spherical as is the case in the conventional BCS superconductors. Instead of the usual s-wave symmetry, the order parameter in cuprates shows evidence for d-wave symmetry[101] (Figure 7.3). This was directly measured on single crystals of YBCO by Wollman et al.[111] and Tsuei et al.[107]. The anisotropy in the order parameter suggests that the cause of pairing in cuprates is unconventional, ie. the pairing mechanism is not phonon mediated.

The most interesting and controversial feature is the evidence for existence of another phase, the so-called pseudogap, in cuprates with small hole doping level. Early experiments such as NMR measurements[108], Knight shift measurements[4], and magnetic susceptibility measurements[46] showed a reduction in spin response in cuprates. Such reduction occurs in conventional superconductors in the superconducting state when Cooper pairs condense into a spin singlet state. The remarkable finding here is that this effect occurs in cuprates at temperatures above the critical temperature and no anomalous results are detected at the superconducting transition. This indicates the possibility of formation of spin singlet state at temperature T^*, which is above T_c. Experiments also indicate that, unlike the critical temperature, T^* increases with decreasing hole doping (see phase diagram in Figure 7.2). Historically, pivotal data suggesting the presence of the pseudogap came from angle resolved photoemission spectroscopy (ARPES) experiments performed by Loeser et al.[56] and Ding et al.[76] Another crucial indication that there is something strange about the normal state of cuprates came from thermal transport measurements[39] which show the breakdown of the Wiedmann-Franz law[3]. This suggests that the normal state does not behave as a typical metal described by the Fermi-liquid theory; fermions are not responsible for heat transport in cuprates in normal state. Over the years, there have been numerous experiments performed in order to detect and study the pseudogap. Evidence for the existence of another phase above the superconducting state has been observed in various experiments including ARPES, scanning tunneling microscopy, Cu NMR, resistivity, specific heat, infrared conductivity, and inelastic neutron scattering. A review of experimental techniques and results related to investigating the pseudogap has been performed by Timusk and Statt in [105] and in books Handbook of High-Temperature Superconductivity: Theory and Experiment[93] by J.S. Brooks and J. Robert Schrieffer, and Superconductivity: Conventional and Unconventional Superconductors[14] by Karl-Heinz Bennemann and John B. Ketterson.

There are a couple of findings from the ARPES experiments worth mentioning here. First, the experiments show that the anisotropy of the pseudogap is the same as that of the superconducting energy gap, ie. the pseudogap has the same k dependence as the

superconductor-insulator-superconductor Josephson junctions.[48]

[3]The Wiedmann-Franz law states that the ratio of the thermal to the electrical conductivity of metals is directly proportional to the temperature: $\frac{\kappa}{\sigma} \propto T$.[110]

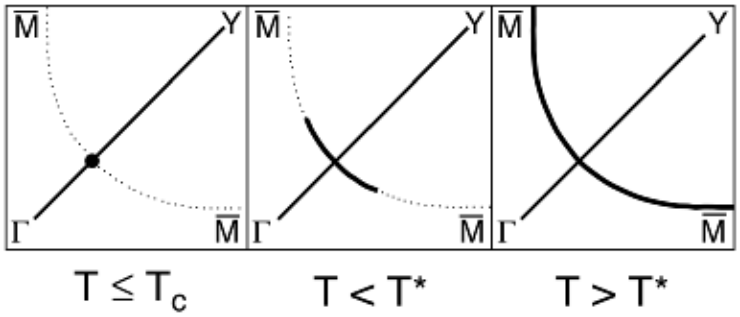

Figure 7.4: Illustration of the temperature dependence of the Fermi surface in underdoped cuprates. The d-wave node below T_c becomes an arc above T_c which expands with increasing T to form the full Fermi surface at T^*.

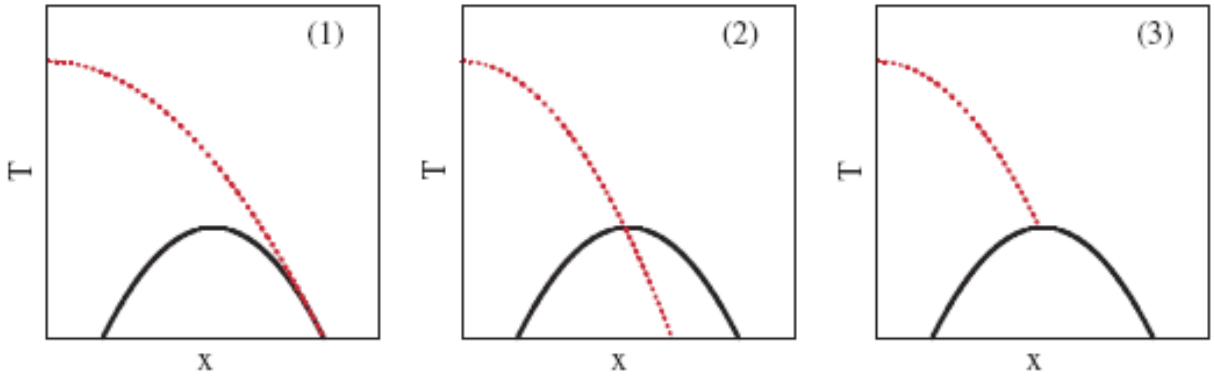

Figure 7.5: Possibilities for the relationship between the pseudogap and the superconducting state in the cuprates. The solid black line is the superconducting transition temperature, and the red dashed line the pseudogap phase line.

superconducting energy gap. Moreover, measurements of the temperature dependence of the pseudogap show that the Fermi surface becomes gapped in different directions of k space at different temperatures. Results show the pseudogap opens at T^* and continuously grows into the superconducting energy gap at T_c. These observations are consistent with data obtained from other experiments, such as thermal conductivity[100]. These ideas are illustrated in Figure 7.4.

A comprehensive review of results and features of the pseudogap obtained from experiments, a detailed survey of theoretical models used to describe the pseudogap, and further references to original papers can be found in the books mentioned above.

The most intriguing, puzzling, and disputed issue concerning cuprates is the nature of the pseudogap and its relationship to the superconducting state. Various possibilities for

how the pseudogap phase may be associated with the superconducting state in cuprates are illustrated in Figure 7.5.

The first scenario is that the pseudogap phase is a precursor to the superconducting state (panel (1) in Figure 7.5). This means that the pseudogap phase represents a state from which antiferromagnetic order arises at low doping levels, or the superconducting state forms at higher doping levels. In this scenario, the pseudogap is not an ordered state and T^* is a crossover line and not a true transition temperature. A possible theory for the pseudogap phase is that of preformed pairs. Cuprates exhibit very short superconducting coherence length, low charge carrier density, and are quasi-two dimensional due to CuO_2 planes. The main idea behind preformed pairs suggests that Cooper pair formation is possible above the critical temperature, but strong phase fluctuations[4] prevent any long range phase coherence. Thus, the pseudogap is associated with the spin gap created by the formation of spin singlet pairs. There are experimental evidence in support of the idea of preformed pairs, such as [100]

A related theory is that of spin liquid state or "resonating valence bond" (RVB) state.[5, 6] The RVB theory suggest that, although increase in hole doping destroys the antiferromagnetic order, it still allows for antiferromagnetic interaction between the spins. It postulates that any one spin can be paired with one of its neighbouring spins to form a spin singlet. However, these spin singlet bonds fluctuate from being paired to not paired, thus forming a "spin liquid". Authors in [78] suggest a useful analogy. They compare the spin liquid fluctuations to the situation of C-C bonds in benzene rings where each bond alters between being a single bond and a double bond. An interesting idea in the RVB model is that of spin-charge separation. The spin is associated with "spinons" which have spin of 1/2 and no charge, while charge of $+e$ is carried by "holons" which have no spin. Spinons form singlet pairs at temperatures below T^* creating the spin gap associated with the pseudogap. Hole doping has a disruptive effect of formation of pairs just as it destroys the antiferromagnetic order, ie. the energy gain associated with pair formation is in opposition with the kinetic energy associated with a hole hopping from one ion to another. This implies that T^* should decrease with increasing hole doping. On the other hand, doped holes, which carry the charge, become phase coherent only below certain temperature T_ϕ that is proportional to hole doping level. There is not much experimental evidence for the coherence transition, and T_ϕ line is ill defined. Below both of these temperatures, it is possible to have spin pairing and long range phase coherence, creating the superconducting state. This idea is illustrated in Figure 7.6 (a). There are additional consequences of RVB model. Spin-charge separation only occurs in the CuO_2 planes. Therefore, experimental measurements detecting spin response (such as NMR) should be able to observe the spin gap associated with pair formation, while experiments associated with charge

[4]The wavefunction of a superconductor is represented by $\psi(x) = |\psi|e^{i\phi(x)}$ where ϕ is the phase of the wavefunction.

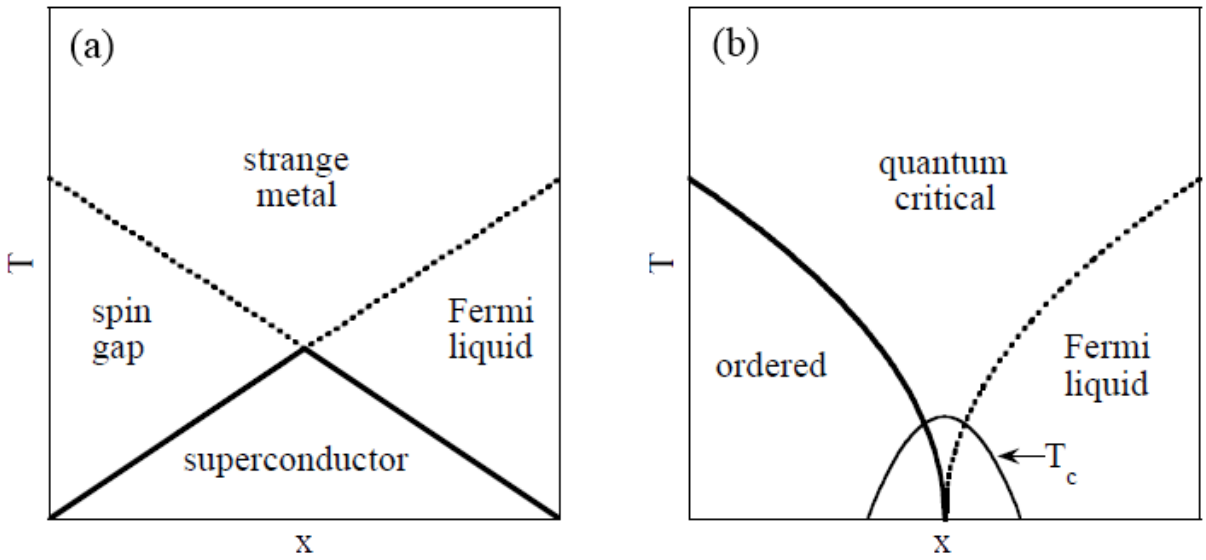

Figure 7.6: Two proposed theoretical phase diagrams for the cuprates. RVB scenario (left panel) and quantum critical scenario (right panel)

transport (such as in plane conductivity) should not be greatly effected. This is observed experimentally.[43] On the other hand, spinons and holons must bind into actual electrons in order to leap between the planes. This should have a significant effect on any measurements performed on the axis perpendicular to the planes. Experimental evidence is also consistent with these predictions.[83]

Another theory proposed for cuprate superconductors is that of stripes. In this model, doped holes form layers of one-dimensional "stripes" which act as mobile charge carriers. In between these stripe layers, spins arrange into magnetic domains that possess antiferromagnetic order. There has been some experimental evidence in support of this model.[31, 27]

A second possibility is that the pseudogap phase and the superconducting state are unrelated. Instead, they are in competition with each other over the Fermi surface, and as one wins the other loses. This idea is illustrated in panel (2) of Figure 7.5. In this scenario, the pseudogap represents an ordered state and T^* represents a well defined transition temperature. Some theoretical ideas for competing order in the pseudogap involve spin density waves or charge density waves[16, 93] and orbital currents[96]. There have been some experimental arguments in support of this scenario[102, 103]. In this scenario, the pseudogap phase is an ordered state at low doping levels, and Fermi liquid is a disordered phase at high doping levels. These two phases meet at a quantum critical point that is surrounded by the superconducting state. This version of the phase diagram is illustrated

in Figure 7.6 (b).

Authors in [77] suggest a third possibility that has not received much consideration in current experimental and theoretical research. As illustrated in panel (3) of Figure 7.5, it is possible that the pseudogap phase represents some order that is replaced by the superconducting phase, and that T^* terminates at the T_c.

The major hurdle in understanding and developing a theory of high-T_c superconductivity in cuprates is inherently linked to our insight of the pseudogap phase and its relation to the superconducting state. The important issue is whether the pseudogap phase exhibits true long range order or whether it is merely a form of a precursor state. The difficulty in answering this question stems from the fact that experimental results have not been able to clearly define the T^* line and there is no consensus on the correct phase diagram for cuprates.

7.2 Specific Heat of YBCO

7.2.1 Evidence for d-wave Pairing

For conventional superconductors with s-wave symmetry in the energy gap, low temperature electronic specific heat is characterized by an exponential function of temperature as described in chapter 2. However, in case of d-wave pairing, low temperature electronic specific heat is proportional T^2[74]. For type-II d-wave superconductors, in the presence of magnetic field, the low temperature specific heat is predicted to be of the form $B^{1/2}T$.[93, 50] At higher temperatures, and at low magnetic fields, the electronic specific heat is represented by both a T^2 term that is independent of the magnetic field, and a temperature independent term that is proportional to the magnetic field. The crossover between these two regions is determined by the parameter $z = B^{-1/2}T$ and occurs when $z_c = B_c^{-1/2}T_c$. Analysis of low temperature specific heat of YBCO is further complicated because additional terms need to be considered and accounted for. These terms include a magnetic term due to paramagnetic centers[5], a term due to nuclear magnetic moments, phonon specific heat term, and a residual linear term associated with impurities. Moler et al. were first to perform measurements and analysis of low temperature specific heat of YBCO samples. Their results exhibited behaviour described above providing evidence for unconventional superconductivity and d-wave pairing in YBCO.[73] There have been other specific heat measurements looking for similar d-wave scaling relations in order to find evidence for unconventional pairing in YBCO.[112, 87, 109]. Figure 7.7 shows the spe-

[5]These are related to chemical impurities, or, in the case of chemical substitutions on the Cu sites, the moments of the substituent ions or moments they induce on neighboring Cu sites.

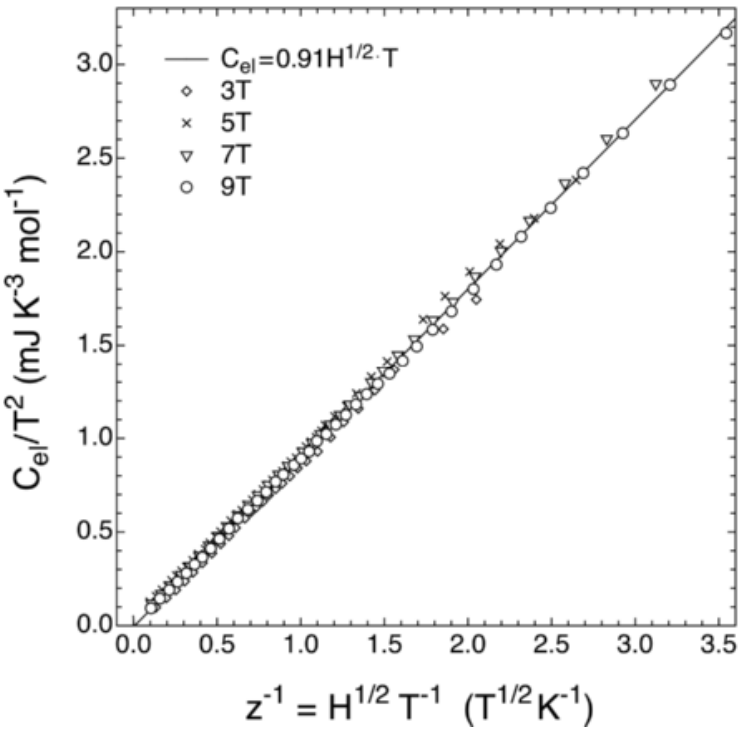

Figure 7.7: A test of the scaling relation for d-wave superconductor specific heat as it relates to magnetic field and temperature.[112] The specific heat data is for a YBCO sample.

cific heat results and scaling from [112]. Similar d-wave behaviour was observed in specific heat measurements of the cuprate compound $(La_{1.85}Sr_{0.15})CuO_4$.[28]

7.2.2 Evidence for the Pseudogap

As stated in chapter 3, a measurement of the specific heat is a direct probe of the quantum states of a system. Therefore, it can be used to study the pseudogap in order to determine the behaviour of electrons in this phase and their density of states. However, cuprates are high temperature superconductors, meaning that their superconducting transition occurs at relatively high temperatures. Additionally, the temperature range of interest in studying the pseudogap is above the critical temperature T_c, when the material is in its normal state. Therefore, the presence of a large phonon term at these temperatures makes the task of determining the electronic specific heat experimentally very challenging. This problem occurs because lattice specific heat is significantly larger then the electronic contribution at these temperatures (see chapter 3).

Loram et al. used a differential technique in order to measure the electronic specific heat

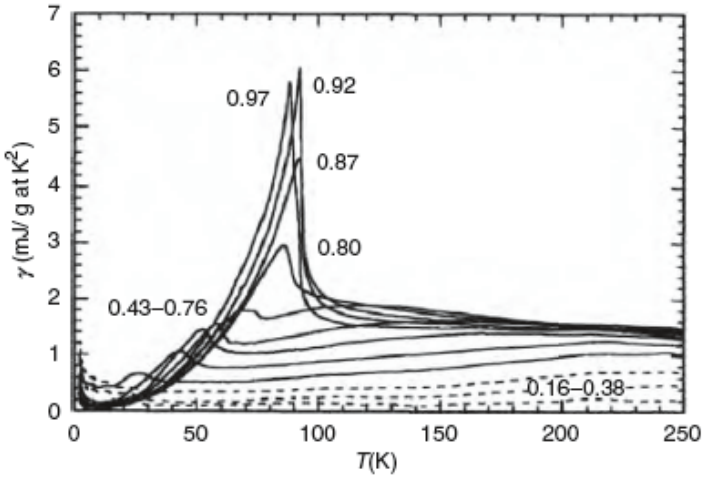

Figure 7.8: Electronic specific heat vs. T for $YBa_2Cu_3O_{6+x}$ for various doping levels x from [58]

of cuprates.[84] In the differential technique, the heat capacity of the sample of interest and the heat capacity of a reference sample are measured concurrently. The reference sample is chosen such that its phonon contribution to the specific heat is comparable to that of the sample. The reference sample is also assumed to have zero electronic specific heat. The authors obtained the specific heat difference between the sample of interest and the reference sample providing them with the measure of electronic specific heat. The complete analysis is more involved since a number of complications have to be accounted for. For example, oxygen doping in YBCO samples changes their phonon heat capacity and these effects need to be taken into consideration. They performed their experiments on YBCO and $Y_{0.8}Ca_{0.2}Ba_2Cu_3O_{7-\gamma}$ samples with various doping levels.[58, 59, 47] $Y_{0.8}Ca_{0.2}Ba_2Cu_3O_{7-\gamma}$ was measured because it is characterized by a wider range in the underdoped regime, having optimal doping at higher doping level then YBCO. Some of their results are shown in Figure 7.8 and Figure 7.9.

These results show interesting behaviour at temperatures above the critical temperature T_c. In overdoped samples, the normal state electronic specific heat seems to be independent of temperature and hole doping. This is in contrast with the behaviour observed for underdoped samples. The electronic specific heat starts to decrease at a temperature above T_c. This suggests that in underdoped samples, there is a loss of entropy at temperatures above T_c while the material is still in its normal state. Another noticeable difference in the electronic specific heat at various doping levels is the decrease in the specific heat jump at the critical temperature at higher doping levels. Similar results are obtained for the cuprate $La_{2-x}Sr_xCuO_4$.[47]

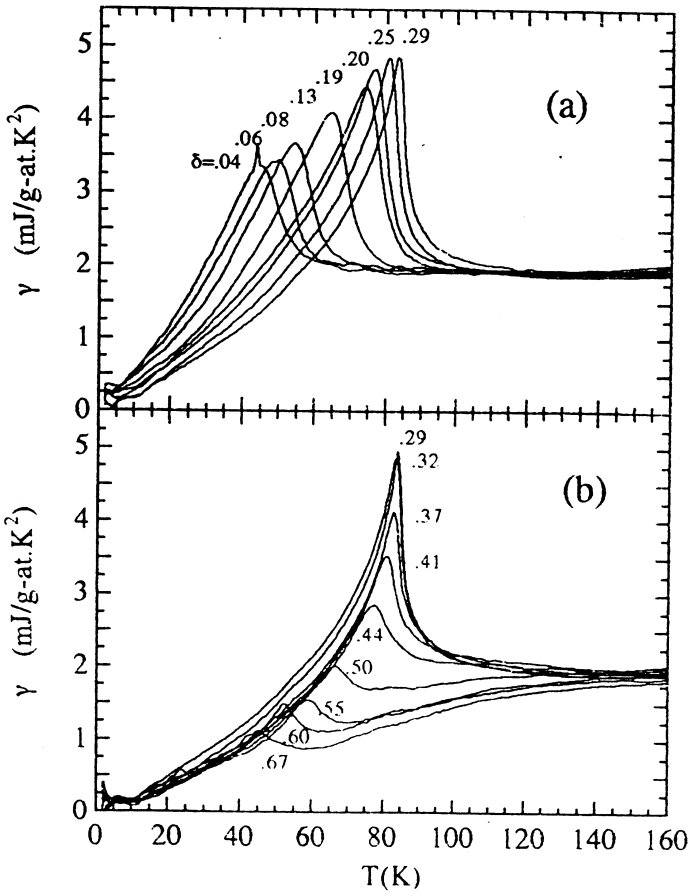

Figure 7.9: Electronic specific heat for (a) overdoped and; (b) underdoped $Y_{0.8}Ca_{0.2}Ba_2Cu_3O_{7-\gamma}$.[59]

The authors use the analysis of these specific heat results to argue that the pseudogap phase is not a precursor to the superconducting state, but rather is unrelated to it.[102, 103] Their argument is in support of the scenario (2) in Figure 7.5. They state that the pseudogap should be regarded as a separate phenomenon that is in competition with the superconducting state. Above T_c, the electronic specific heat data does not show any phase transition anomaly. Therefore, T^* is not a temperature at which the pseudogap appears. They suggest that T^* represents the energy scale for the pseudogap. They also argue that the T^* line cuts through the superconducting dome, ending at a quantum critical point at a doping level slightly above the optimal doping.

Chapter 8

YBCO Experiment

8.1 Specific Heat of YBCO

The goal of this project was to design and develop an experimental method to measure the specific heat of a high temperature superconductor and demonstrate it by determining the specific heat of a YBCO sample. Therefore, the temperature range of interest in this experiment is from about 10 K to approximately 200 K.

The essential methodology for the experiment is similar to the concepts and procedures described in Chapter 5. The experimental setup is illustrated in Figure 8.1. It consists of a dip probe constructed out of stainless steel. The central stainless steel rod contains regularly spaces baffles. These serve a number of purposes. They provide thermal contact to the stainless steel can that encloses the entire apparatus. They are also used for thermal anchoring of electrical leads going to the experiment stage. Thermal anchoring is achieved by winding the electrical leads around a small copper post. The copper post is then affixed to the baffles. Lastly, the baffles act as radiation shields preventing hot room temperature radiation from reaching the experiment stage.

At the bottom of the probe is a copper block used for mounting the experiment components. The heater resistor used for temperature control was attached to this block. The stage heater will be discussed in more details later. Additionally, all electrical wires were coupled to the copper block for heat-sinking purposes. The temperature control thermometer was a calibrated Cernox CX-1070 thermometer that was fixed to the sample holder. The sample holder that enclosed the experiment sample was fundamentally the same as the one described in Chapter 5. The sample heater was a very small ($0.5mm \times 1.0mm \times 0.254mm$) $10k\Omega$ thin-film resistor. The sample thermometer was a Cernox CX-1070 chip thermometer. Both components were directly coupled to the sample using a small amount of GE varnish. The electrical leads to the sample heater and the Cernox thermometer were six

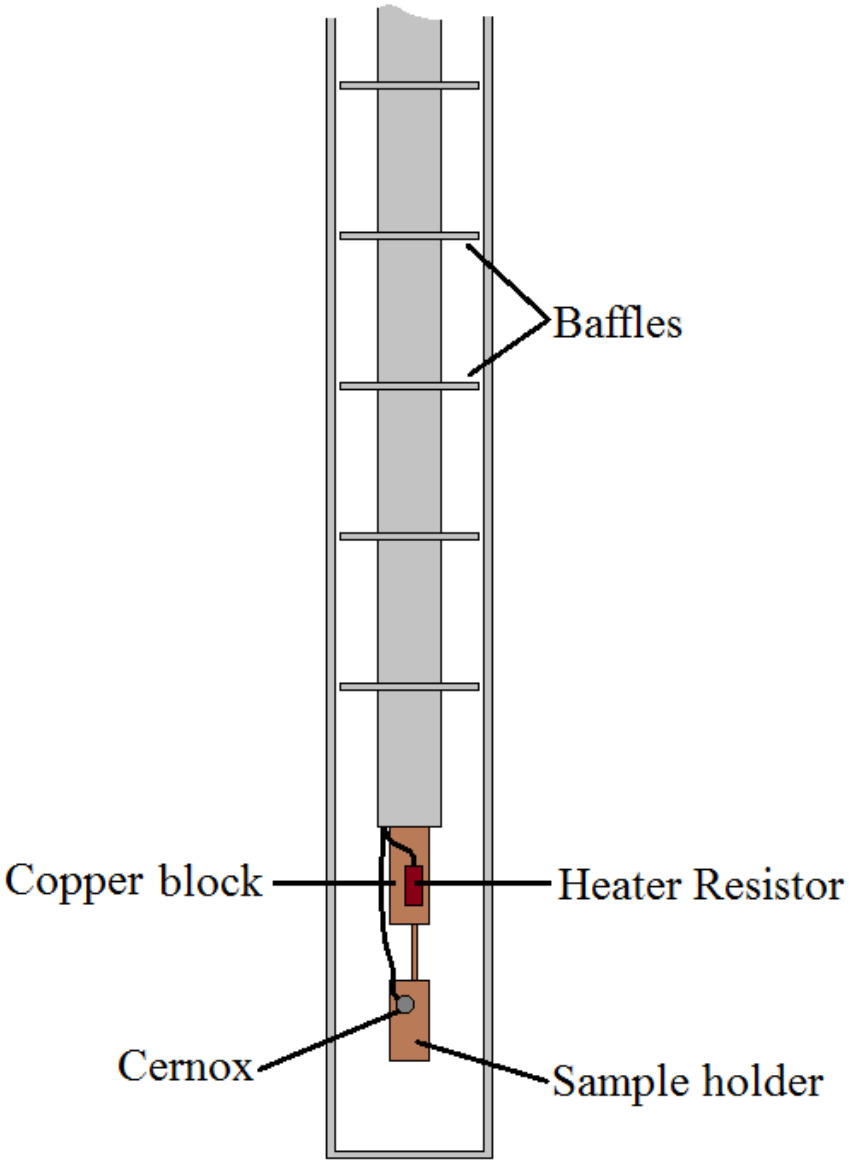

Figure 8.1: Illustration of the dip probe used for measuring the specific heat of a YBCO sample.

NbTi wires with $6\mu m$ diameter and length of approximately $5mm$. These wires were also used as the thermal weak link.

To perform the experiment, the apparatus was enclosed in the stainless steel case. The whole setup system is vacuum tight. A turbopump was used to remove the gas from the probe. The equipment was then cooled down in two steps. The apparatus was submerged into a dewar of liquid nitrogen reducing the temperature to approximately $80K$. Subsequently, it was submerged into a dewar containing liquid helium (^{4}He). Liquid nitrogen has a much greater latent heat of evaporation than liquid helium. Additionally, at temperatures about $80K$, most of the heat capacity of the apparatus has been removed. Therefore, it is considerably more cost and time efficient to pre-cool the experiment with liquid nitrogen before using liquid helium to reach lower temperatures. The base temperature of the equipment is approximately $16K$. This is where an equilibrium is reached between the cooling power of the liquid helium and heat leaks from the room temperature air surrounding the top of the probe sitting outside the dewar. For temperatures above $80K$, the only cryoliquid used for refrigeration was liquid nitrogen.

Specific heat measurements were performed using the quasi-adiabatic method. Temperature control, data acquisition, and data analysis were performed in the same manner as specified in sections 5.4, 5.6, and 5.7.

8.2 Magnetic Susceptibility of YBCO

Magnetic susceptibility of a material describes its response to an applied magnetic field. Magnetic susceptibility is defined as:[110]

$$\chi = \frac{\partial M}{\partial H} \tag{8.1}$$

where M is the magnetization density of the material, and H is the applied magnetic field. The behaviour of materials in the presence of a magnetic field can be classified in a number of major groups.

Diamagnetism When an external magnetic field is applied to a diamagnetic material, the object creates a magnetic field that counters the applied magnetic field, thus causing a repulsive effect. Most materials that are considered "non-magnetic" (such as water, wood, plastic, etc.) are diamagnetic. Diamagnetic materials consist of atoms that have zero net magnetic moment. Since diamagnetic materials oppose the applied magnetic field, their magnetic susceptibility is less than zero. Figure 8.2 illustrates the magnetization and the magnetic susceptibility of a diamagnetic material. It should be noted that the magnetic susceptibility is negative and independent of temperature.

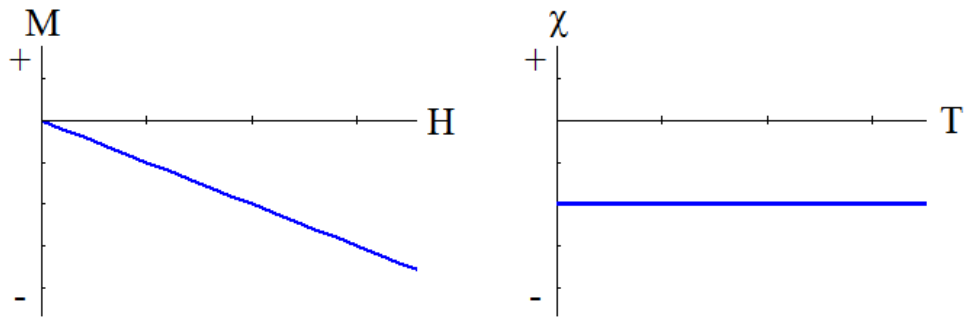

Figure 8.2: *Diamagnetism* Magnetization is opposite the externally applied magnetic field. Magnetic susceptibility is negative and independent of temperature.

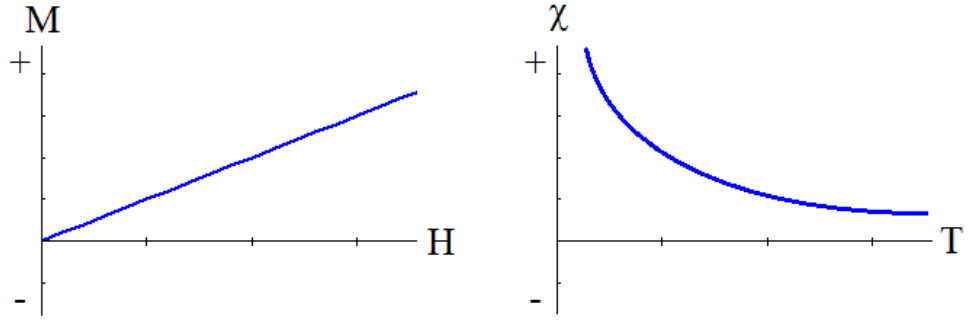

Figure 8.3: *Paramagnetism* Magnetization is in alignment with the applied magnetic field. Magnetic susceptibility is positive and decreases with temperature according to the Curie's law.

Paramagnetism Paramagnetic materials contain atoms or ions with non-zero net magnetic moments arising from the presence of unpaired electrons in partially filled orbitals. Therefore, in the presence of an externally applied magnetic field, the constituent atoms of a paramagnetic material align in the direction of the applied magnetic field. Figure 8.3 shows the magnetization and the magnetic susceptibility of paramagnetic materials. As the temperature is increased, heat thermally excited electrons creating thermal disorder and destroying the magnetic order. Hence, magnetic susceptibility decreases with temperature.[1]

The basic principle behind equipment used for measuring magnetic susceptibility is illustrated in Figure 8.4. A superconducting magnet is used to generate a static magnetic field. The applied magnetic field magnetizes the sample to be measured. The sample is

[1]This is Curie's law and it states that the magnetic susceptibility is inversely proportional to temperature ($\chi \propto 1/T$).

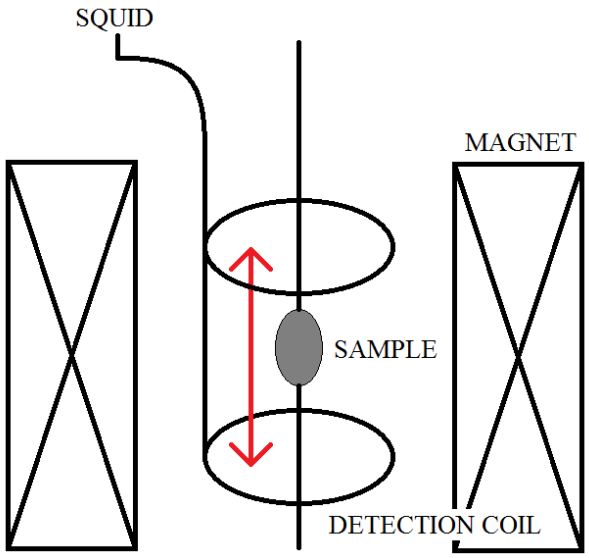

Figure 8.4: Simple illustration of a magnetometer.

made to oscillate in position relative to the detection coil. The purpose of the detection coil is to measure the flux change as the magnetized sample is moved up and down. The motion of the magnetic moment of the sample induces an electric current in the detection coil system. Therefore, the induced current in the pickup coil is proportional to the sample's magnetic moment. The output of the detection coil is sent to circuitry used to analyze the signal. Here, a superconducting quantum interface device (SQUID) acts as a very sensitive current-to-voltage converter. The current variations in the detection coils generate changes in the SQUID output. The SQUID output voltage then may be analyzed to determine the magnetic moment of the sample. Magnetic susceptibility may be measured in this way for various magnetic field strengths or as a function of temperature.

Susceptibility measurements can be used as a tool for determining the critical temperature of superconducting materials. Above the transition temperature, superconducting materials usually have small magnetic susceptibility. When in the superconducting state, the materials become perfect diamagnets. Hence, its magnetic susceptibility becomes $\chi = -1$. In actual experiments, the critical temperature is signaled by an appearance of a significant negative nonzero magnetic susceptibility.

For this experiment, magnetic susceptibility of a YBCO sample was measured using a commercial Quantum Desigh SQUID magnetometer at McMaster University by Paul Dube.

Chapter 9

YBCO Results and Discussion

9.1 Specific Heat of YBCO

The YBCO sample used in the experiment was $YBa_2Cu_3O_{6+x}$ with $x = 0.355$. The YBCO crystal were made by the self-flux method using $BaZrO_3$ crucibles[55] by Doug Bonn at University of British Columbia. The sample is in the underdoped region, ie. it is below optimal doping. The sample showed prominent discoloration. It was very brittle. When we tried to place it into the experimental assembly, the sample fragmented into a number of pieces. This led us to believe that the sample has been damaged. Chemical reactions of YBCO with water deteriorate the sample quality and have adverse effects on its superconducting properties.[60, 42] The products of these chemical reactions are non-superconducting Y_2BaCuO_5, copper oxide, barium hydroxide, and barium carbonate. We proceeded with the experiment as a proof of concept and to determine the performance of the equipment. We used the biggest piece of the remnants of our YBCO sample. Unfortunately, the sample was considerably smaller. The mass of the sample used in the experiment was $1.5mg$. The results of the heat capacity measurements are shown in Figure 9.1. The data show no signs of a superconducting transition. Instead, they exhibit behaviour consistent with a phonon contribution to the heat capacity.

Unfortunately, since the sample broke into smaller fragments, the specific heat of the addenda was not insignificant and had a sufficient contribution to the total heat capacity. There are a few steps that may be taken in order to minimize this contribution of the addenda. The ideal solution would be to use a bigger sample so that its heat capacity is the dominant term. Polishing the heater and the thermometer chip substrates would reduce their mass and hence their heat capacity contribution. Another option would be cutting the chips along their length. This may reduce their size considerably and smaller lead wires may be required and wire bonding may have to be utilized in order to make

electrical connections.

In order to estimate the contribution to the heat capacity of the addenda, we developed a crude model. Cernox thermometer chip is comprised of silicon oxynitride (Si_2N_2O) sensor material on alumina (Al_2O_3) substrate with gold pads for electrical connections. The heater resistor chip is made up of nichrome alloy (80% Ni, 20% Cr) resistor material on alumina substrate with gold soldering pads. Each chip has a mass of $\approx 1mg$. In our model, we assumed that each chip is mostly made up of the alumina substrate material; 70% of the mass was attributed to the substrate material. Gold soldering pads made up 10% of the mass of each chip. The remaining 20% were attributed to the oxynitride material for Cernox thermometer, and the nichrome for the heater chip. The specific heat contribution of the alumina substrate, nichrome and silicon oxynitride were modeled using the Debye model (Equation 3.26). The Debye temperatures Θ_D of alumina, nichrome, and silicon oxynitride are $980K$[3], $428K$[53], and $738K$[26] respectively. The data for specific heat of gold in our temperature range was taken from [33]. We also included an estimate of the heat capacity contribution of GE varnish used for fixing the chips to the sample. We estimated that the amount of GE varnish used was approximately $0.1mg$. There are reported data for specific heat of GE varnish from $1K$ to $4K$[81], $4K$ to $18K$[22], $2K$ to $80K$[37], and from $200K$ to $400K$[45]. In our analysis, we used the data from [37]. The amount of silver epoxy used for electrical connections is extremely small (smaller then the size of the chip gold pads) and we assumed that its contribution is negligible. The heat capacity from our measurements with an estimate of the addenda contribution are plotted in Figure 9.2. The addenda heat capacity is relatively small, however it is not insignificant. Figure 9.3 shows our specific heat data after the subtraction of the addenda contribution along with $YBa_2Cu_3O_7$ crystal specific heat data from [91]. Considering that the two samples are of different doping levels, our sample is damaged, and the very crude analysis of our addenda, the two results are in relatively close agreement.

As can be seen in the figures, there seems to be some noise in our heat capacity data. There are a few possibilities for sources of these fluctuations. One of our initial concerns was that there might be a discrepancy between the heat pulses requested by the software controlling the experiment and the actual applied heat pulses. We checked this by analyzing the output of the DAQ card using a digital oscilloscope and comparing them to the data stored by the software. Although the pulse lengths are different from what was specified in the software, they did match to the data recorded by the software; ie. if we requested a $20s$ heat pulse, the actual heat pulse applied was not precisely $20s$, however the software recorded the actual and correct length of the heat pulse in its data output. It is not likely that the source of the noise in the data is due to software since we used a similar program for data acquisition for $PrOs_4Sb_{12}$. If the noise was due to discrepancy in heat pulses it would be present in the low temperature data and it would be more evident since we applied shorter pulses for that set of data. Another possibility is that there is a radiation leak into

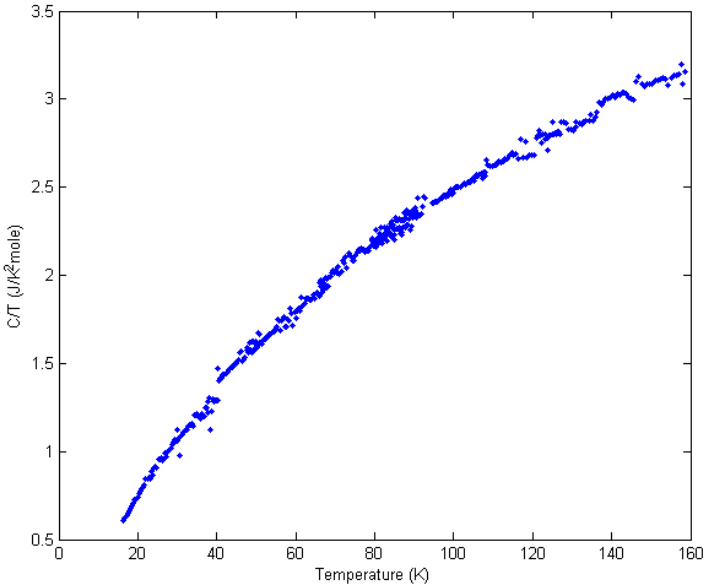

Figure 9.1: Specific heat of the YBCO sample.

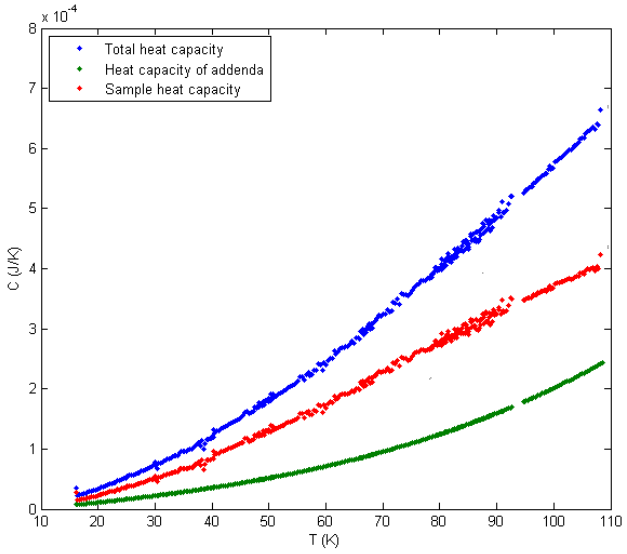

Figure 9.2: Total heat capacity of the YBCO sample and addenda (blue), an estimate of the addenda contribution to the heat capacity (green), and the total heat capacity of the sample minus the addenda heat capacity (red). Addenda heat capacity is relatively small, however it is not insignificant.

our sample holder causing the sample to warm up and be at different temperature then our calibrated thermometer. This seems an unlikely explanation. Our sample holder was enclosed and any holes were covered to prevent any stray radiation. There is another check for this. We calibrated our sample thermometer at almost every data point. If there were points during which stray radiation was warming up the sample we would see these points in the calibration data as noise. More precisely, there would be spikes in the calibration data curve where the sample thermometer has lower resistance (higher temperature) than would be expected. Figure 9.4 shows our resistance and temperature calibration data for the Cernox sample thermometer. We inspected the data, and there are no noticeable spikes or any noise in the data. Instead most data points follow a nice curve. However, there does seem to be a small shift in the calibration between some of the different data sets (shown in inset). This would not cause random noise in our final data. Additionally, noise in the data is present even in single data sets that have only a single calibration curve. Another possibility is that the noise is due to different settings (such as resistance range or excitation level) used on the LR700 ac resistance bridge. This is very unlikely since we kept these setting as consistent as possible. It is possible that our experiment is somehow sensitive to some outside sources of noise, such as radiation or vibrations. Perhaps the level of liquid helium cryoliquid present in the dewar has some unforseen effects. Though it seems unlikely that our experiment would be extremely sensitive to these effects since the temperature range of interest is relatively high. Another possibility is that the source of the noise is due to electronics. It is possible that the LR700 is the culprit; this particular device has been damaged and repaired before. My first suggestion for trying to pinpoint the cause of the noise is to replace the LR700 with a device that is known to behave correctly and produce reliable measurements. Another possibility is that sample's specific heat actually changes between different data sets. We tried to keep the sample in vacuum. However, we did have to bring it to outside atmosphere when we were working on setting up the experiment (for example, when fixing electrical connections). Also, the vacuum in the probe was not perfect and over long time some air would leak into the interior. Perhaps, the sample could react with water vapour or absorb some gases. This could alter its specific heat.

There are a few remarks that need to be made in regards to the experimental arrangement. One of the initial concerns was with the NbTi wires being used as the weak link for thermal relaxation. Due to the wide range in temperature of interest in the experiment, it was uncertain whether the properties of the weak link would need to be altered in order to provide a satisfactory time constant. As the experiment was performed and measurements were taken, we found that the NbTi wired maintained an adequate time constant in the entire temperature range.

In performing the experiment, we encountered an issue with temperature control. We used a $1k\Omega$ resistor as a temperature control heater. We found that the Lakeshore temper-

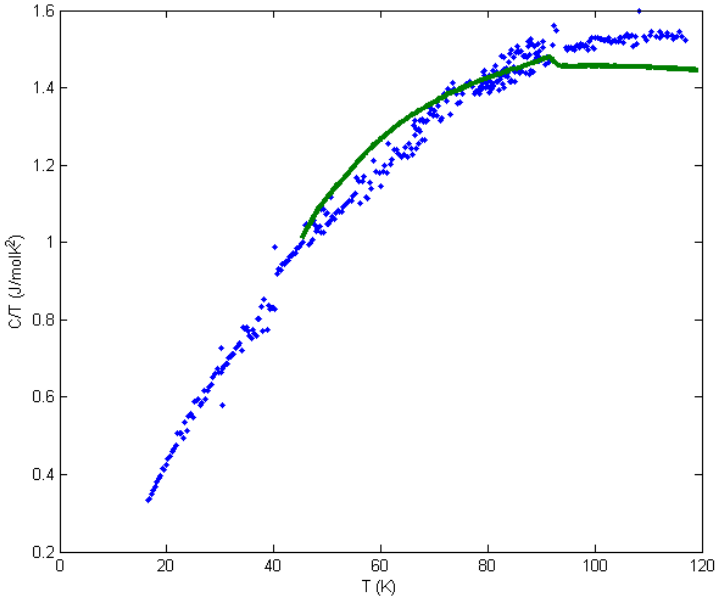

Figure 9.3: Heat capacity of the sample minus the addenda heat capacity from our measurements (blue). $YBa_2Cu_3O_7$ sample specific heat data from [91] (green).

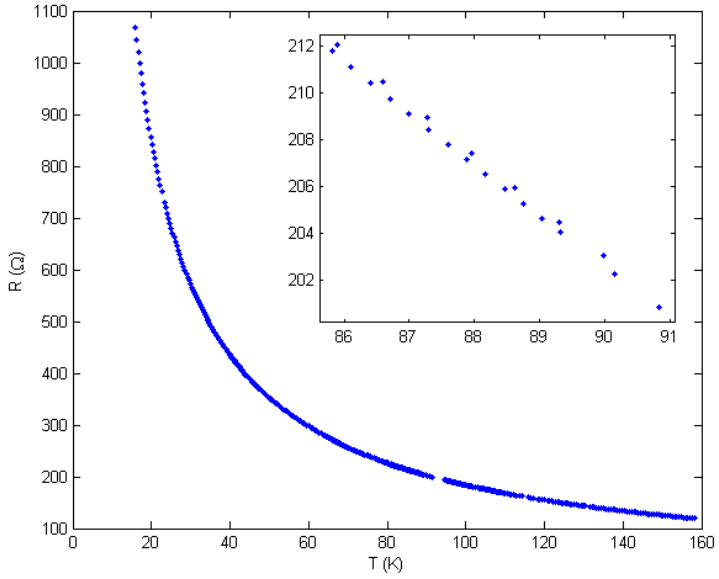

Figure 9.4: Resistance and temperature values used for calibration of the Cernox sample thermometer.

ature controller required a very long time to heat the experimental apparatus and change the temperature to a new setpoint. This problem started to occur at temperatures around $40 - 50K$. The Lakeshore output is $10V$ and up to $100mA$. This means that maximum power of $1W$ occurs for heater resistors of 100Ω. However, resistors we were using have power rating of $125mW$. To solve this problem, we connected another $1k\Omega$ resistor in parallel with the original heater resistor. After this alteration, the temperature controller was able to change the setpoint temperature in a reasonable amount of time. Similar issue occurred at temperatures about $140K$. Adding another $1k\Omega$ resistor in parallel resolved the issue once more.

Another issue that arose is that the output of the DAQ-card was not sufficient to provide adequate heat pulse to the sample heater. This problem developed at approximately $60K$. This difficulty was solved by changing the current limiting resistor from $600k\Omega$ to $200k\Omega$.

9.2 Magnetic Susceptibility of YBCO

Magnetic susceptibility may be used to test whether a material sample has undergone a superconducting transition and to determine its superconducting transition temperature. If a sample is in superconducting state, then it behaves as a diamagnet. Thus, the sample's magnetization is opposite the applied magnetic field. Figure 9.5 shows the output of the magnetization measurement on our YBCO sample at temperature of $5K$ and applied magnetic field $1000Oe$. The green line represents the applied magnetic field.[1] The blue data points represent the sample's magnetization. At this temperature, the YBCO sample should be in the superconducting state. Thus, the sample should be diamagnetic, and its magnetization should be reverse of the applied magnetic field. However, the data shows that the sample's magnetization is in alignment with the applied magnetic field.

Figure 9.6 shows YBCO magnetic susceptibility as a function of temperature. It is clear that the sample does not exhibit any sign of a superconducting transition. Instead, it behaves as a paramagnetic material. For contrast, Figure 9.7 shows YBCO magnetic susceptibility measurements from previously published work.[54]

[1] More accurately, the green line represents the magnetization of a paramagnetic material whose magnetic moments are aligned with the applied magnetic field.

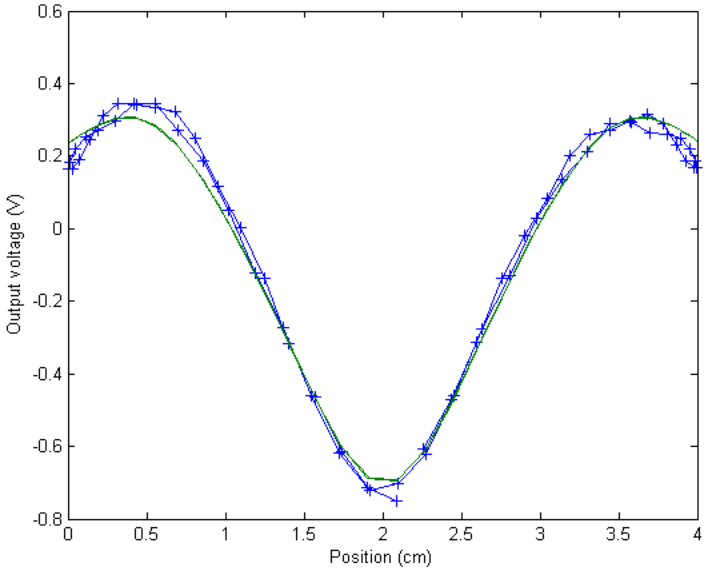

Figure 9.5: Output of a single magnetization measurement performed at $5K$ and magnetic field of $1000Oe$ (blue). Representation of the magnetization of a paramagnetic material (green).

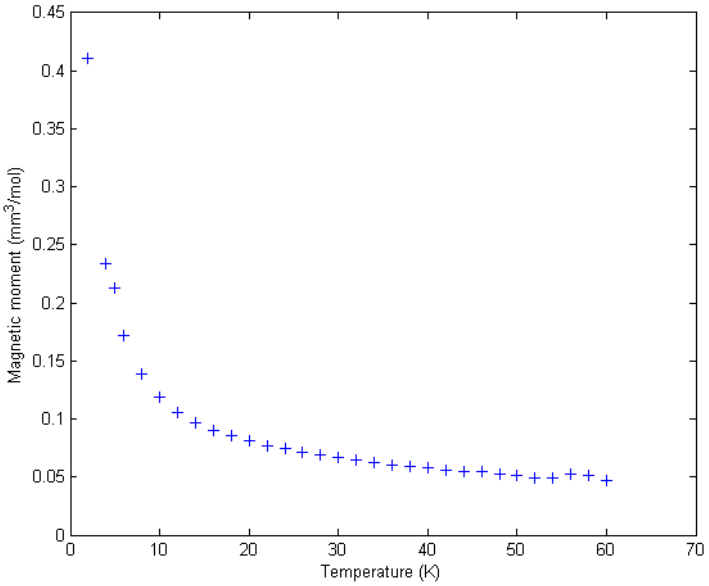

Figure 9.6: Magnetic susceptibility of the YBCO sample as a function of temperature measured under magnetic field of $1000Oe$. There is no sign of a superconducting transition. It is behaving as a paramagnetic sample.

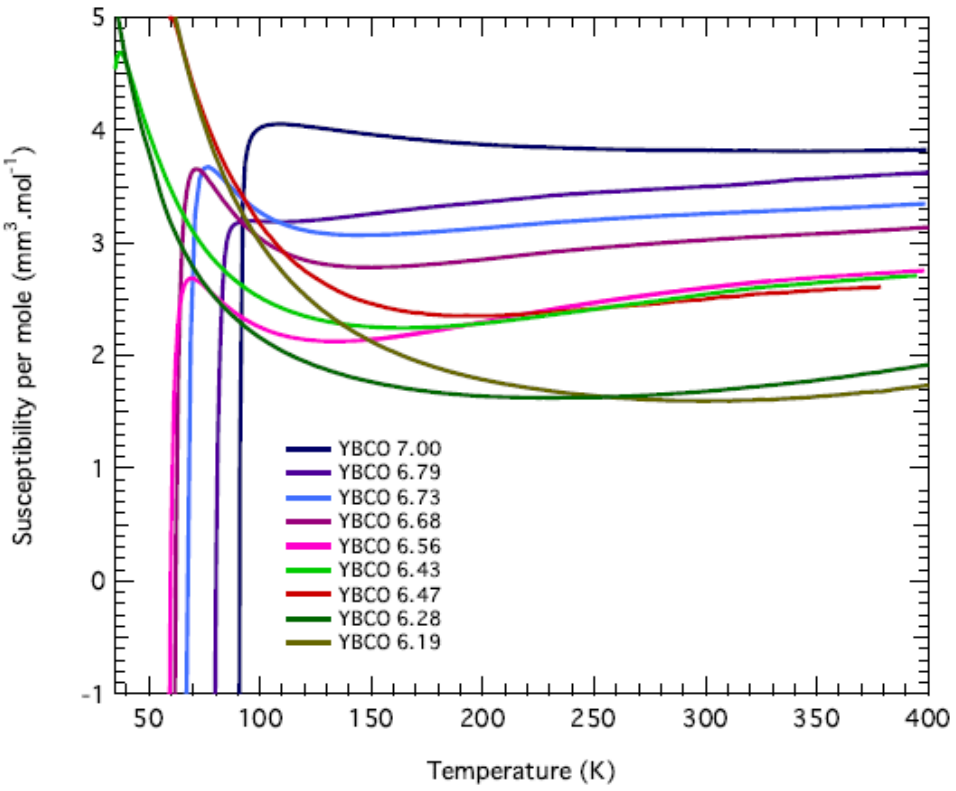

Figure 9.7: Magnetic susceptibility of YBCO samples measured under 1 T as a function of temperature from [54].

Chapter 10

Conclusion

The measurements of the specific heat of $PrOs_4Sb_{12}$ clearly indicate the double transition behaviour with the upper transition temperature of $1.87K$ and lower transition temperature of $1.63K$. The properties of the two transitions are generally in fair agreement with the previously reported results. The low temperature specific heat exhibits power law dependence. This property suggests presence of nodes in the superconducting gap indicating the possibility of unconventional superconductivity in this heavy fermion system. Additionally, the presence of multiple samples with equal upper transition temperatures but different lower transition temperatures suggest that the upper transition and lower transition are due to different phases. The lower transition is sensitive to sample quality which implies that the order parameter is asymmetric. In future work, it would be beneficial to expand the temperature range of the measurements so that modeling of the Schottky anomaly may be performed and included in the analysis of the data.

In the second part of our work, we have successfully developed an experimental apparatus and procedure for measuring the specific heat of a high temperature superconductor. The experimental method was demonstrated by measuring the specific heat of a sample from temperature of about $15K$ to about $160K$. The method can be easily extended to higher temperatures. Improvements are possible by reducing the size of the addenda. Polishing the substrates of the heater and thermometer chips would reduce their mass significantly. Additionally, it is possible to reduce their size by cutting them along their length. Having larger YBCO samples would also make the heat capacity of the addenda less significant. Suggestions for future work are to measure the specific heat of a number of YBCO samples with various doping levels. Additionally, it would be very beneficial to develop a method to account for the specific heat of the crystal lattice in order to determine the electronic specific heat. This would enable one to study the pseudogap properties in hopes of developing an accurate phase diagram for YBCO.

Appendices

Appendix A

Anomalous Results

While measuring the specific heat of $PrOs_4Sb_{12}$ on the dilution refrigerator, we noticed some unexpected and peculiar features in our results at approximately $500mK$. Other measurements have reported anomalous results in this temperature range. Ozcan et al. performed penetration depth measurements and observed a drop in the magnetic penetration depth at $T \approx 450mK$ that is indicative of a superconducting transition (see Figure A.1).[80] Another magnetic penetration depth study reported some strange results in this temperature range (see Figure A.2).[18] Nuclear quadrupole resonance measurements performed by Kotegawa et al. noticed an upturn of unknown origin in their results at temperatures around $600mK$.[51] These results are shown in Figure A.3. Cichorek et. al measured data that exhibit unexpected enhancement of the lower critical field and critical current at around $600mK$.[19] They speculate that these observations reflect a transition into another superconducting phase. Since we were aware of these unusual results, we decided to further investigate our specific heat measurements with more scrutiny.

We observed that at temperatures around $500mK$, we could apply a very large heat pulse without causing a great change in temperature of the sample. Instead, the sample would warm up to an "equilibrium" temperature and it would remain at that temperature as shown in Figure A.4. The sample would remain at approximately this temperature until the the heat pulse is turned off (see Figure A.5). However, sometimes it would suddenly and unexpectedly start to continuously warm up until the application of heat is stopped (shown in Figure A.6). This behaviour is somewhat reminiscent of a phase transition with latent heat. However, it is puzzling in many respects. During some measurements, the sample's temperature would be stable at the "equilibrium" temperature indefinitely; we have continuously applied the heat pulse to the sample for $3-4$ hours with the sample's temperature remaining stable. This indicates an extremely large latent heat. On the other hand, during some measurements, the sample temperature would remain stable only for a short time (few minutes) before it would suddenly and quickly begin to increase until

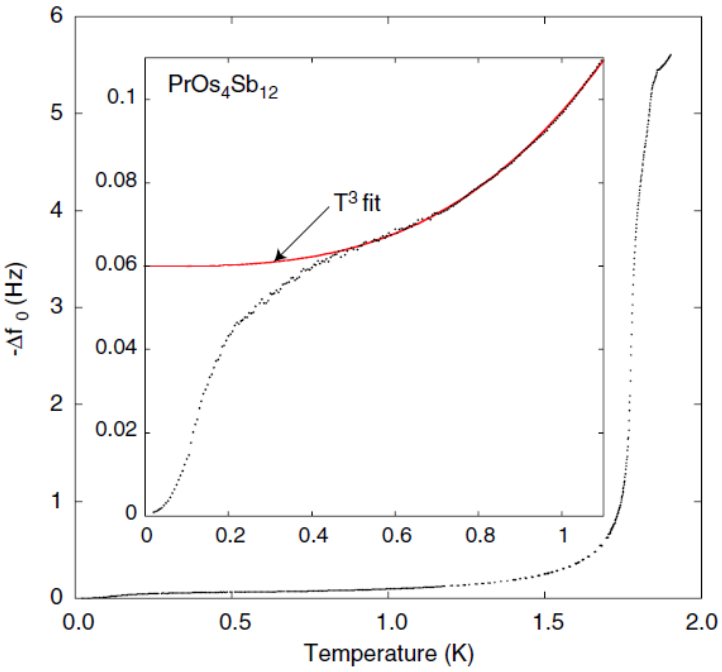

Figure A.1: Temperature dependence of the frequency shift due to the expulsion of magnetic flux from the interior of a $PrOs_4Sb_{12}$ sample. At $T \approx 450mK$, a supeconducting-transition-like drop in the magnetic penetration depth sets in.

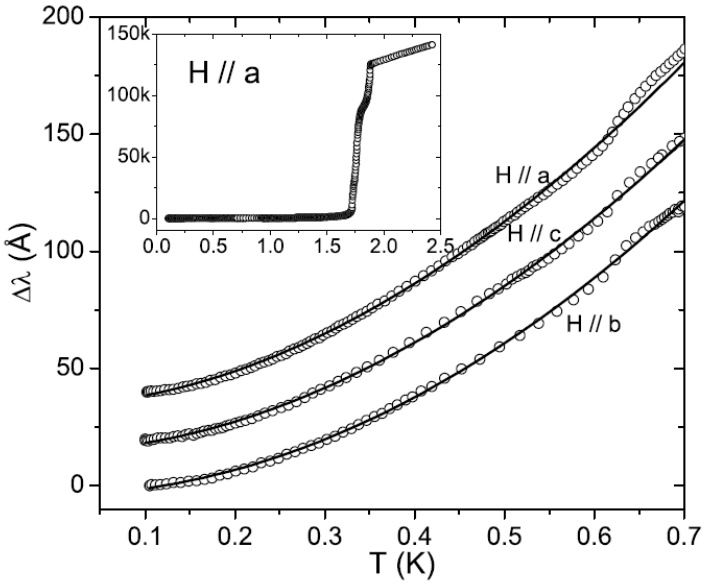

Figure A.2: Penetration depth variation at low temperatures.

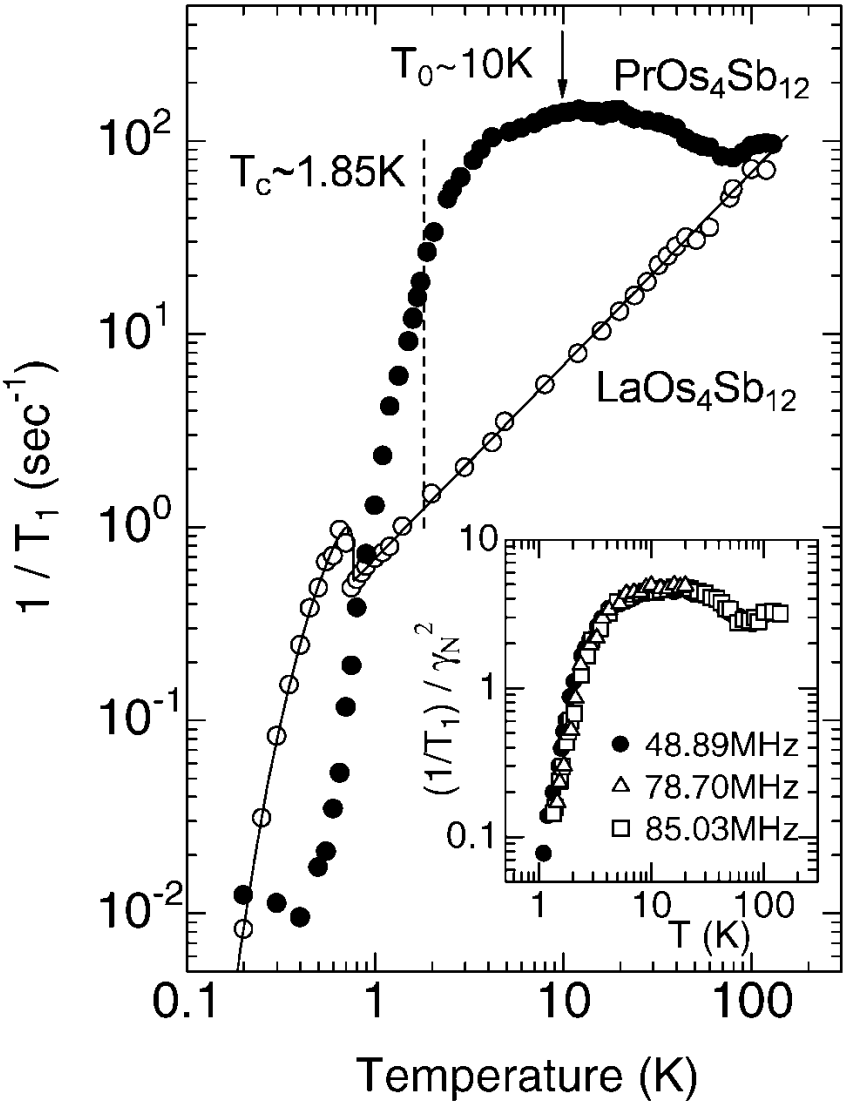

Figure A.3: $1/T_1$ as a function of temperature.

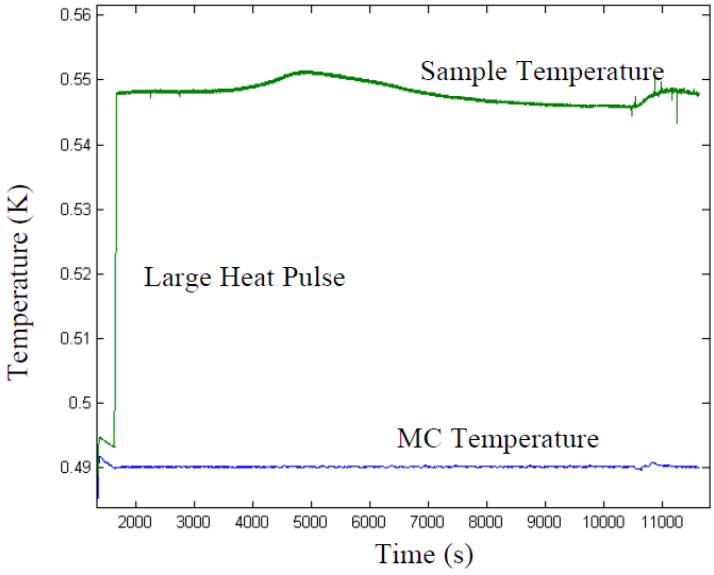

Figure A.4: Upon application of a large heat pulse, the sample's temperature (green) would reach an "equilibrium" and be stable for extended period.

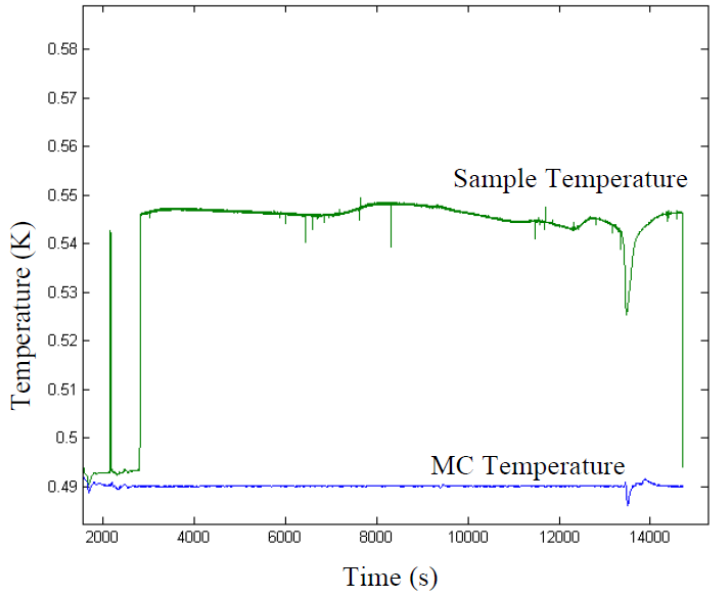

Figure A.5: If the heat pulse is turned off, the sample's temperature (green) would immediately return to the mixing chamber temperature (blue).

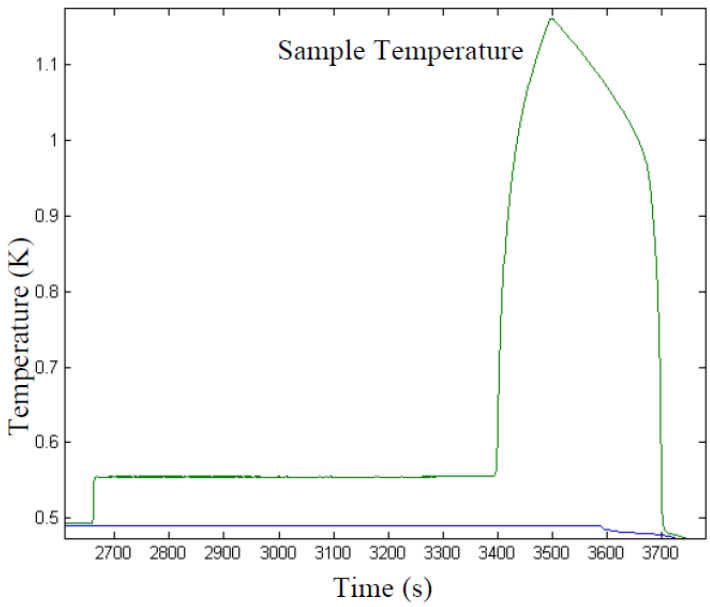

Figure A.6: Sometimes, the sample's temperature (green) would unexpectedly and quickly begin to increase until the heat pulse is turned off. Then it would decrease and fall back down to the mixing chamber temperature (blue).

the heat pulse was turned off. At this point, the sample would return to the background temperature of the mixing chamber. Additionally, if the sample's temperature remained at the "equilibrium" temperature for a very long time, and the heat pulse was turned off, it would immediately return to the setpoint temperature of the dilution refrigerator. This behaviour is inconsistent with a phase transition with latent heat. In this case, one would expect the sample's temperature to remain at the "equilibrium" temperature even after the termination of the heat pulse.

We spent a long time performing specific heat measurements trying to observe some consistent behaviour and make sense of the results we were obtaining. In order to eliminate the possibility that these anomalous results are an artifact caused by our equipment, we placed our $PrOs_4Sb_{12}$ sample on another dilution refrigerator. After repeating the specific heat measurements on a different dilution refrigerator, we did not observe any unusual behaviour at $T \approx 500mK$.

We came up with one explanation to resolve the original strange behaviour we observed. We believe that we had a very small ^{4}He leak in our dilution refrigerator. At these very small temperatures, ^{4}He would be a superfluid. We suspect that the superfluid ^{4}He would creep across the thermal link, dental floss, and electrical contacts and cover our sample. At about $500mK$, the heat pulse would cause the ^{4}He coating the sample to warm up and start

to evaporate. Therefore, what we were detecting was the latent heat of evaporation of ^{4}He film covering our sample. This model is consistent with the behaviour we observed. The "equilibrium" temperature could be stable for extended periods of time because there could be a continuous supply of superfluid ^{4}He creeping onto the sample. When the heat pulse is terminated, the sample temperature would return to the mixing chamber temperature as expected since there is no actual phase transition in the sample and no latent heat. Also, it is possible that the supply of superfluid ^{4}He may become discontinuous at some periods. Then, the heat pulse would quickly warm up the sample, suddenly increasing its temperature until the heat pulse is turned off.

Although this makes our initial findings wrong, it is fortunate that we were careful enough to detect and avoid a potential error in our results. It is also a very interesting effect to observe and clearly demonstrates some of the amazing properties of ^{4}He liquid. One could also imagine a possible way to utilize this effect in order to detect and check for very small helium leaks in dilution refrigerators.

References

[1] *http : //upload.wikimedia.org/wikipedia/commons/a/a1/YBCOstructure.jpg.* xiii, 81

[2] *http : //www.lakeshore.com/temp/sen/crtdts.html.* 63

[3] *http : //www.oxmat.co.uk/Crysdata/al2o3.htm.* 99

[4] H. Alloul, T. Ohno, and P. Mendels. *y89* nmr evidence for a fermi-liquid behavior in $YBa_2Cu_3O_{6+x}$. *Phys. Rev. Lett.*, 63(16):1700–1703, Oct 1989. 84

[5] P. W. Anderson. The Resonating Valence Bond State in La_2CuO_4 and Superconductivity. *Science*, 235(4793):1196–1198, 1987. 86

[6] P. W. Anderson. *The Theory of Superconductivity in the High-T_C Cuprates.* Princeton University Press, 1997. 86

[7] Yuji Aoki, Hitoshi Sugawara, and Hideyuki Sato. Heavy fermion behaviors in the pr-based filled skutterudites. *Journal of Alloys and Compounds*, 408-412:21 – 26, 2006. Proceedings of Rare Earths'04 in Nara, Japan, Proceedings of Rare Earths'04. 37

[8] R. Bachmann, Jr. F. J. DiSalvo, T. H. Geballe, R. L. Greene, R. E. Howard, C. N. King, H. C. Kirsch, K. N. Lee, R. E. Schwall, H.-U. Thomas, and R. B. Zubeck. Heat capacity measurements on small samples at low temperatures. *Review of Scientific Instruments*, 43(2):205–214, 1972. 58

[9] A. V. Balatsky, I. Vekhter, and Jian-Xin Zhu. Impurity-induced states in conventional and unconventional superconductors. *Rev. Mod. Phys.*, 78(2):373–433, May 2006. 33, 71

[10] J. Bardeen, L. N. Cooper, and J. R. Schrieffer. Theory of superconductivity. *Phys. Rev.*, 108(5):1175–1204, Dec 1957. 12

[11] T. H. K. Barron and Guy K. White. *Heat capacity and thermal expansion at low temperatures*. Kluwer Academic/Plenum, New York :, 1999. 62

[12] E. D. Bauer, N. A. Frederick, P.-C. Ho, V. S. Zapf, and M. B. Maple. Superconductivity and heavy fermion behavior in $PrOs_4Sb_{12}$. *Phys. Rev. B*, 65(10):100506.1–100506.4, Feb 2002. 37, 38, 40, 52, 75

[13] J. G. Bednorz and K. A. Mller. Possible high t_c superconductivity in the ba-la-cu-o system. *Zeitschrift fr Physik B Condensed Matter*, 64(2):189–193, 1986. 80

[14] K. H. Bennemann and J. B. Ketterson. *Superconductivity*. Springer, 2008. 80, 84

[15] Werner Buckel and Reinhold Kleiner. *Superconductivity Fundamentals and Applications*. WILEY-VCH Verlag GmbH and Co. KGaA, second edition, 2004. 40

[16] Sudip Chakravarty, R. B. Laughlin, Dirk K. Morr, and Chetan Nayak. Hidden order in the cuprates. *Phys. Rev. B*, 63(9):094503, Jan 2001. 87

[17] Jr. Charles P. Poole. *Handbook of Superconductivity*. Academic Press, 2000. 8

[18] Elbert E. M. Chia, M. B. Salamon, H. Sugawara, and H. Sato. Probing the superconducting gap symmetry of $PrOs_4Sb_{12}$: A penetration depth study. *Phys. Rev. Lett.*, 91(24):247003, Dec 2003. 40, 52, 108

[19] T. Cichorek, A. C. Mota, F. Steglich, N. A. Frederick, W. M. Yuhasz, and M. B. Maple. Pronounced enhancement of the lower critical field and critical current deep in the superconducting state of $PrOs_4Sb_{12}$. *Phys. Rev. Lett.*, 94(10):107002, Mar 2005. xii, 73, 108

[20] Leon N. Cooper. Bound electron pairs in a degenerate fermi gas. *Phys. Rev.*, 104(4):1189–1190, Nov 1956. 12

[21] Nathaniel Craig and Ted Lester. Hitchhikers guide to the dilution refrigerator. *http* : $//marcuslab.harvard.edu/how_to/Fridge.pdf$. xii, 56

[22] J.L. Cude and L. Finegold. Specific heat of ge 7031 varnish (4 - 18 k). *Cryogenics*, 11(5):394 – 395, 1971. 99

[23] Jeroen Custers, Yukie Namai, Takashi Tayama, Toshiro Sakakibara, Hitoshi Sugawara, Yuji Aoki, and Hideyuki Sato. Field-orientation dependence of the specific heat of $PrOs_4Sb_{12}$. *Physica B: Condensed Matter*, 378-380:179 – 181, 2006. Proceedings of the International Conference on Strongly Correlated Electron Systems - SCES 2005. 40, 52

[24] Bascom S. Deaver and William M. Fairbank. Experimental evidence for quantized flux in superconducting cylinders. *Phys. Rev. Lett.*, 7(2):43–46, Jul 1961. 16

[25] R. Doll and M. Näbauer. Experimental proof of magnetic flux quantization in a superconducting ring. *Phys. Rev. Lett.*, 7(2):51–52, Jul 1961. 16

[26] T. C. Ehlert. Thermal decomposition of the oxynitride of germanium and the heat capacity of the oxynitrides of silicon and germanium. *Journal of the American Ceramic Society*, 64(2):C–25 – C–26, 1981. 99

[27] Jörg Fink, Enrico Schierle, Eugen Weschke, Jochen Geck, David Hawthorn, Viktor Soltwisch, Hiroki Wadati, Hsueh-Hung Wu, Hermann A. Dürr, Nadja Wizent, Bernd Büchner, and George A. Sawatzky. Charge ordering in $La_{1.8-x}Eu_{0.2}Sr_xCuO_4$ studied by resonant soft x-ray diffraction. *Phys. Rev. B*, 79(10):100502, Mar 2009. 87

[28] R. A. Fisher, N. E. Phillips, A. Schilling, B. Buffeteau, R. Calemczuk, T. E. Hargreaves, C. Marcenat, K. W. Dennis, R. W. McCallum, and A. S. O'Connor. Evidence for line nodes in the energy gap for $(La_{1.85}Sr_{0.15})CuO_4$ from low-temperature specific-heat measurements. *Phys. Rev. B*, 61(2):1473–1476, Jan 2000. 89

[29] N. A. Frederick, T. D. Do, P.-C. Ho, N. P. Butch, V. S. Zapf, and M. B. Maple. Superconductivity and crystalline electric field effects in the filled skutterudite series $Pr(Os_{1-x}Ru_x)_4Sb_{12}$. *Phys. Rev. B*, 69(2):024523, Jan 2004. 53

[30] Neil Adam Frederick. *Superconductivity, Heavy Fermion Behavior, and Crystalline Electric Field Effects in the Filled Skutterudite Series* $Pr(Os_{1-x}Ru_x)_4Sb_{12}$. PhD thesis, University of California, San Diego, 2005. 39, 53

[31] M. Fujita, K. Yamada, H. Hiraka, P. M. Gehring, S. H. Lee, S. Wakimoto, and G. Shirane. Static magnetic correlations near the insulating-superconducting phase boundary in $La_{2-x}Sr_xCuO_4$. *Phys. Rev. B*, 65(6):064505, Jan 2002. 87

[32] J. R. Gavaler, M. A. Janocko, and C. K. Jones. Preparation and properties of high-t_c nb-ge films. *Journal of Applied Physics*, 45(7):3009–3013, 1974. 80

[33] T. H. Geballe and W. F. Giauque. The heat capacity and entropy of gold from 15 to 300 k. *Journal of the American Chemical Society*, 74(9):2368–2369, 1952. 99

[34] E. A. Goremychkin, R. Osborn, E. D. Bauer, M. B. Maple, N. A. Frederick, W. M. Yuhasz, F. M. Woodward, and J. W. Lynn. Crystal field potential of $PrOs_4Sb_{12}$: Consequences for superconductivity. *Phys. Rev. Lett.*, 93(15):157003, Oct 2004. 38, 52

[35] M. J. Graf and A. V. Balatsky. Identifying the pairing symmetry in the Sr_2RuO_4 superconductor. *Phys. Rev. B*, 62:9697–9702, Oct 2000. 33

[36] K. Grube, S. Drobnik, C. Pfleiderer, H. v. Löhneysen, E. D. Bauer, and M. B. Maple. Specific heat and ac susceptibility studies of the superconducting phase diagram of $PrOs_4Sb_{12}$. *Phys. Rev. B*, 73(10):104503, Mar 2006. xi, 40, 44, 45, 52

[37] J.T. Heessels. Specific heat of general electric 7031 varnish from 2 to 80 k. *Cryogenics*, Dec. 99

[38] R. W. Hill, Shiyan Li, M. B. Maple, and Louis Taillefer. Multiband order parameters for the $PrOs_4Sb_{12}$ and $PrRu_4Sb_{12}$ skutterudite superconductors from thermal conductivity measurements. *Phys. Rev. Lett.*, 101(23):237005, Dec 2008. xi, 42, 43, 52, 71

[39] R. W. Hill, Cyril Proust, Louis Taillefer, P. Fournier, and R. L. Greene. Breakdown of fermi-liquid theory in a copper-oxide superconductor. *Nature*, 414. 84

[40] P. Hirschfeld, D. Vollhardt, and P. Wlfle. Resonant impurity scattering in heavy fermion superconductors. *Solid State Communications*, 59(3):111 – 115, 1986. 33

[41] P.-C. Ho, N. A. Frederick, V. S. Zapf, E. D. Bauer, T. D. Do, M. B. Maple, A. D. Christianson, and A. H. Lacerda. High-field ordered and superconducting phases in the heavy-fermion compound $PrOs_4Sb_{12}$. *Phys. Rev. B*, 67(18):180508, May 2003. xi, 38, 39, 40, 52

[42] N. M. Hwang, G. W. Bahng, Y. K. Park, J. C. Park, H. G. Moon, and D. N. Yoon. Recovery of superconductivity in water-decomposed y-ba-cu-o superconductors by reheating. *Journal of Materials Science Letters*, 8(5):517–519, May 1989. 98

[43] K. Ishida, K. Yoshida, T. Mito, Y. Tokunaga, Y. Kitaoka, K. Asayama, Y. Nakayama, J. Shimoyama, and K. Kishio. Pseudogap behavior in single-crystal $Bi_2Sr_2CaCu_2O_{8+\delta}$ probed by cu nmr. *Phys. Rev. B*, 58(10):R5960–R5963, Sep 1998. 87

[44] K. Izawa, Y. Nakajima, J. Goryo, Y. Matsuda, S. Osaki, H. Sugawara, H. Sato, P. Thalmeier, and K. Maki. Multiple superconducting phases in new heavy fermion superconductor $PrOs_4Sb_{12}$. *Phys. Rev. Lett.*, 90(11):117001, Mar 2003. xi, 40, 44, 46, 52

[45] K D Jayasuriya, A M Stewart, and S J Campbell. The specific heat capacity of ge varnish (200-400k). *Journal of Physics E: Scientific Instruments*, 15(9):885, 1982. 99

[46] David C. Johnston. Magnetic susceptibility scaling in $La_{2-x}Sr_xCuO_{4-y}$. *Phys. Rev. Lett.*, 62(8):957–960, Feb 1989. 84

[47] Loram J.W. Evidence on the pseudogap and condensate from the electronic specific heat. *Journal of Physics and Chemistry of Solids*, 62:59–64(6), January 2001. 90

[48] R. Kleiner and P. Müller. Intrinsic josephson effects in high-t_c superconductors. *Phys. Rev. B*, 49(2):1327–1341, Jan 1994. 84

[49] Masahumi Kohgi, Kazuaki Iwasa, Motoki Nakajima, Naoto Metoki, Shingo Araki, Nick Bernhoeft, Jean-Michel Mignot, Arsen Gukasov, Hideyuki Sato, Yuji Aoki, and Hitoshi Sugawara. Evidence for magnetic-field-induced quadrupolar ordering in the heavy-fermion superconductor $PrOs_4Sb_{12}$. *Journal of the Physical Society of Japan*, 72(5):1002–1005, 2003. 38, 40, 52

[50] N. B. Kopnin and G. E. Volovik. Singularity of the vortex density of states in d-wave superconductors. *JETP Letters*, 64(9):69*0–694, Nov 1996. 88

[51] H. Kotegawa, M. Yogi, Y. Imamura, Y. Kawasaki, G.-q. Zheng, Y. Kitaoka, S. Ohsaki, H. Sugawara, Y. Aoki, and H. Sato. Evidence for unconventional strong-coupling superconductivity in $PrOs_4Sb_{12}$: An sb nuclear quadrupole resonance study. *Phys. Rev. Lett.*, 90(2):027001, Jan 2003. 40, 42, 52, 108

[52] K. Kuwahara, K. Iwasa, M. Kohgi, K. Kaneko, N. Metoki, S. Raymond, M.-A. Méasson, J. Flouquet, H. Sugawara, Y. Aoki, and H. Sato. Direct observation of quadrupolar excitons in the heavy-fermion superconductor $PrOs_4Sb_{12}$. *Phys. Rev. Lett.*, 95(10):107003, Sep 2005. 38, 52

[53] W.N. Lawless. Specific heat of nichrome, 2-30 k. *Cryogenics*, 20(9):527 – 528, 1980. 99

[54] B. Leridon, P. Monod, D. Colson, and A. Forget. Thermodynamic signature of a phase transition in the pseudogap phase of $YBa_2Cu_3O_x$ high-t_c superconductor. *EPL (Europhysics Letters)*, 87(1):17011, 2009. xiv, 103, 105

[55] Ruixing Liang, D. A. Bonn, and W. N. Hardy. Growth of high quality ybco single crystals using $BaZrO_3$ crucibles. *Physica C: Superconductivity*, 304(1-2):105 – 111, 1998. 98

[56] A. G. Loeser, Z.-X. Shen, D. S. Dessau, D. S. Marshall, C. H. Park, P. Fournier, and A. Kapitulnik. Excitation Gap in the Normal State of Underdoped $Bi_2Sr_2CaCu_2O_{8+delta}$. *Science*, 273(5273):325–329, 1996. 84

[57] F. London and H. London. The electromagnetic equations of the supraconductor. *Proceedings of the Royal Society of London.*, 149(866):71–88, Mar 1935. 11

[58] J. W. Loram, K. A. Mirza, J. R. Cooper, W. Y. Liang, and J. M. Wade. Electronic specific heat of $YBa_2Cu_3O_{6+x}$ from 1.8 to 300 k. *Journal of Superconductivity*, 7(1):243–249, Feb 1994. xiii, 90

[59] J. W. Lorama, K. A. Mirza, J. R. Cooper, and J. L. Tallon. Specific heat evidence on the normal state pseudogap. *Journal of Physics and Chemistry of Solids*, 59(10-12):2091 – 2094, 1998. xiv, 90, 91

[60] I. M. Low, S. S. Low, and C. Klauber. Chemical reactivity of ybacuo and bi(pb)srcacuo superconductors in water. *Journal of Materials Science Letters*, 12(20):1574–1576, Jan 1993. 98

[61] D. E. MacLaughlin, J. E. Sonier, R. H. Heffner, O. O. Bernal, Ben-Li Young, M. S. Rose, G. D. Morris, E. D. Bauer, T. D. Do, and M. B. Maple. Muon spin relaxation and isotropic pairing in superconducting $PrOs_4Sb_{12}$. *Phys. Rev. Lett.*, 89(15):157001, Sep 2002. 40, 42, 52

[62] K. Maki and E. Puchkaryov. Impurity effects in p -wave superconductors. *EPL (Europhysics Letters)*, 50(4):533, 2000. xi, 33

[63] M B Maple, P-C Ho, N A Frederick, V S Zapf, W M Yuhasz, E D Bauer, A D Christianson, and A H Lacerda. Superconductivity and the high-field ordered phase in the heavy-fermion compound $PrOs_4Sb_{12}$. *Journal of Physics: Condensed Matter*, 15(28):S2071, 2003. xii, 40, 52, 73, 76

[64] M. B. Maple, P.-C. Ho, V. S. Zapf, N. A. Frederick, E. D. Bauer, W. M. Yuhasz, F. M. Woodward, and J. W. Lynn. Heavy fermion superconductivity in the filled skutterudite compound $PrOs_4Sb_{12}$. *Journal of the Physical Society of Japan*, 71S(Supplement):23–28, 2002. 37, 38, 40, 52, 76

[65] M E McBriarty, P Kumar, G R Stewart, and B Andraka. Superconductivity and disorder in $PrOs_4Sb_{12}$. *Journal of Physics: Condensed Matter*, 21(38):385701, 2009. xi, xii, 47, 48, 52, 73, 75

[66] M.-A. Measson, D. Braithwaite, J. Flouquet, G. Seyfarth, J. P. Brison, E. Lhotel, C. Paulsen, H. Sugawara, and H. Sato. Superconducting phase diagram of the filled skuterrudite $PrOs_4Sb_{12}$. *Phys. Rev. B*, 70(6):064516, Aug 2004. xi, 37, 38, 62

[67] M.-A. Méasson, D. Braithwaite, G. Lapertot, J.-P. Brison, J. Flouquet, P. Bordet, H. Sugawara, and P. C. Canfield. Double superconducting transition in the filled skutterudite $PrOs_4Sb_{12}$ and sample characterizations. *Phys. Rev. B*, 77(13):134517, Apr 2008. xii, xiii, 47, 49, 50, 71, 73, 74, 75, 76

[68] M.-A. Measson, D. Braithwaite, B. Salce, J. Flouquet, G. Lapertot, J. Pcaut, G. Seyfarth, J.-P. Brison, H. Sugawara, and H. Sato. Nature of the double superconducting transition in $PrOs_4Sb_{12}$? *Physica B: Condensed Matter*, 378-380:56 – 57, 2006. Proceedings of the International Conference on Strongly Correlated Electron Systems - SCES 2005. 47

[69] M.-A. Measson, D. Braithwaite, B. Salce, J. Flouquet, G. Lapertot, H. Sugawara, H. Sato, and Y. Onuki. Pressure dependence of the double superconducting transition of the filled skutterudite $PrOs_4Sb_{12}$. *Journal of Magnetism and Magnetic Materials*, 310(2, Part 1):626 – 628, 2007. Proceedings of the 17th International Conference on Magnetism, The International Conference on Magnetism. 44, 52

[70] M.-A. Measson, J.P. Brison, G. Seyfarth, D. Braithwaite, G. Lapertot, B. Salce, J. Flouquet, E. Lhotel, C. Paulsen, H. Sugawara, H. Sato, P.C. Canfield, K. Izawa, and Y. Matsuda. Superconductivity of the filled skuterrudite $PrOs_4Sb_{12}$: Phase diagram and characterisations. *Physica B: Condensed Matter*, 359-361:827 – 829, 2005. Proceedings of the International Conference on Strongly Correlated Electron Systems. xi, 44, 45, 52

[71] M. W. Meisel, G. R. Stewart, and E. D. Adams. Thick film chip resistors as millikelvin thermometers. *Cryogenics*, 29(12):1168 – 1169, 1989. 76

[72] Prasanta Misra. *Heavy-Fermion Systems*. Elsevier, 2008. 17, 36, 37

[73] Kathryn A. Moler, David L. Sisson, Jeffrey S. Urbach, Malcolm R. Beasley, Aharon Kapitulnik, David J. Baar, Ruixing Liang, and Walter N. Hardy. Specific heat of $YBa_2Cu_3O_{7-\delta}$. *Phys. Rev. B*, 55(6):3954–3965, Feb 1997. 88

[74] H. Monien, K. Scharnberg, L. Tewordt, and D. Walker. Specific heat, thermal conductivity, and ultrasound attenuation in d-wave superconductors. *Solid State Communications*, 61(9):581 – 585, 1987. 33, 88

[75] M. Nishiyama, T. Kato, H. Sugawara, D. Kikuchi, H. Sato, H. Harima, and G.-Q. Zheng. Evidence for nodes in the superconducting energy gap of the skutterudite compound $PrOs_4Sb_{12}$. *Physica B: Condensed Matter*, 378-380:192 – 193, 2006. Proceedings of the International Conference on Strongly Correlated Electron Systems - SCES 2005. 40, 52

[76] M. R. Norman, H. Ding, M. Randeria, J. C. Campuzano, T. Yokoya, T. Takeuchi, T. Takahashi, T. Mochiku, K. Kadowaki, P. Guptasarma, and D. G. Hinks. Destruction of the fermi surface in underdoped high-t_c superconductors. *Nature*, 392(6672):157–160, 1998. 84

[77] M. R. Norman, D. Pines, and C. Kallin. The pseudogap: friend or foe of high t_c? *Advances in Physics*, 54(8):715–733, 2005. xiii, 82, 83, 88

[78] M R Norman and C Ppin. The electronic nature of high temperature cuprate superconductors. *Reports on Progress in Physics*, 66(10):1547, 2003. 82, 86

[79] N. Oeschler, P. Gegenwart, F. Weickert, I. Zerec, P. Thalmeier, F. Steglich, E. D. Bauer, N. A. Frederick, and M. B. Maple. B-t phase diagram of $PrOs_4Sb_{12}$ studied by low-temperature thermal expansion and magnetostriction. *Phys. Rev. B*, 69(23):235108, Jun 2004. 40

[80] S. Ozcan, W.M. Yuhasz, N.A. Frederick, and M.B. Maple. Magnetic penetration depth measurements of the heavy-fermion superconductor $PrOs_4Sb_{12}$. *Physica B: Condensed Matter*, 378-380:182 – 183, 2006. Proceedings of the International Conference on Strongly Correlated Electron Systems - SCES 2005. 108

[81] Norman E. Phillips. Heat capacity of aluminum between 0.1 k and 4.0 k. *Phys. Rev.*, 114(3):676–685, May 1959. 99

[82] Frank Pobell. *Matter and Methods at Low Temperatures*. Springer, third edition, 2007. xii, 29, 55, 61, 62

[83] A V Puchkov, D N Basov, and T Timusk. The pseudogap state in high-t_c superconductors: an infrared study. *Journal of Physics: Condensed Matter*, 8(48):10049, 1996. 87

[84] A V Puchkov, D N Basov, and T Timusk. The pseudogap state in high-t_c superconductors: an infrared study. *Journal of Physics: Condensed Matter*, 8(48):10049, 1996. 90

[85] Vollmer R., Faisst A., Pfleiderer C., V Lhneysen H, Bauer E. D., Ho P. C., Zapf V., and Maple M. B. Low-temperature specific heat of the heavy-fermion superconductor $PrOs_4Sb_{12}$. *Phys Rev Lett.*, 90(5):057001–1–057001–4, 2003. xi, 37, 38, 40, 41, 52

[86] S Rahimi, M B Maple, and R W Hill. Thermal conductivity of the superconducting filled skutterudite compounds $PrOs_4Sb_{12}$ and $PrRu_4Sb_{12}$. *Journal of Physics: Condensed Matter*, 20(21):215209, 2008. 42, 52, 62, 71

[87] B. Revaz, J.-Y. Genoud, A. Junod, K. Neumaier, A. Erb, and E. Walker. $d-wave$ scaling relations in the mixed-state specific heat of $YBa_2Cu_3O_7$. *Phys. Rev. Lett.*, 80(15):3364–3367, Apr 1998. 88

[88] P. L. Richards and M. Tinkham. Far infrared energy gap measurements in bulk superconductors. *Phys. Rev. Lett.*, 1(9):318–320, Nov 1958. x, 10

[89] Turel C. S., Wei J. Y. T., Djurkovic B., Kycia J. B., Yuhasz W. M., Baumbach R., and Maple M. B. Andreev spectroscopy study of multigap pairing in $PrOs_4Sb_{12}$. *APS Meeting Abstracts*, pages 12002–+, mar 2008. 42, 52, 71, 76

[90] Brian C. Sales. Filled skutterudites. volume 33 of *Handbook on the Physics and Chemistry of Rare Earths*, pages 1 – 34. Elsevier, 2003. xi, 36, 37

[91] A. Schilling and O. Jeandupeux. High-accuracy differential thermal analysis: A tool for calorimetric investigations on small high-temperature-superconductor specimens. *Phys. Rev. B*, 52(13):9714–9723, Oct 1995. xiv, 99, 102

[92] S. Schmitt-Rink, K. Miyake, and C. M. Varma. Transport and thermal properties of heavy-fermion superconductors: A unified picture. *Phys. Rev. Lett.*, 57(20):2575–2578, Nov 1986. 33

[93] J. Robert Schrieffer and James S. Brooks. *Handbook of High-Temperature Superconductivity: Theory and Experiment*. Springer, 2007. 84, 87, 88

[94] G. Seyfarth, J. P. Brison, M.-A. Méasson, D. Braithwaite, G. Lapertot, and J. Flouquet. Superconducting $PrOs_4Sb_{12}$: A thermal conductivity study. *Phys. Rev. Lett.*, 97(23):236403, Dec 2006. xiii, 42, 47, 52, 74

[95] G. Seyfarth, J. P. Brison, M.-A. Méasson, J. Flouquet, K. Izawa, Y. Matsuda, H. Sugawara, and H. Sato. Multiband superconductivity in the heavy fermion compound $PrOs_4Sb_{12}$. *Phys. Rev. Lett.*, 95(10):107004, Sep 2005. xi, 42, 43, 52

[96] M. E. Simon and C. M. Varma. Detection and implications of a time-reversal breaking state in underdoped cuprates. *Phys. Rev. Lett.*, 89(24):247003, Nov 2002. 87

[97] H. Suderow, S. Vieira, J. D. Strand, S. Bud'ko, and P. C. Canfield. Very-low-temperature tunneling spectroscopy in the heavy-fermion superconductor $PrOs_4Sb_{12}$. *Phys. Rev. B*, 69(6):060504, Feb 2004. 42, 52

[98] H. Sugawara, S. Osaki, S. R. Saha, Y. Aoki, H. Sato, Y. Inada, H. Shishido, R. Settai, Y. Ōnuki, H. Harima, and K. Oikawa. Fermi surface of the heavy-fermion superconductor $PrOs_4Sb_{12}$. *Phys. Rev. B*, 66(22):220504, Dec 2002. 38

[99] Paul F. Sullivan and G. Seidel. Steady-state, ac-temperature calorimetry. *Phys. Rev.*, 173(3):679–685, Sep 1968. 58

[100] Mike Sutherland, D. G. Hawthorn, R. W. Hill, F. Ronning, S. Wakimoto, H. Zhang, C. Proust, Etienne Boaknin, C. Lupien, Louis Taillefer, Ruixing Liang, D. A. Bonn, W. N. Hardy, Robert Gagnon, N. E. Hussey, T. Kimura, M. Nohara, and H. Takagi.

Thermal conductivity across the phase diagram of cuprates: Low-energy quasiparticles and doping dependence of the superconducting gap. *Phys. Rev. B*, 67(17):174520, May 2003. 85, 86

[101] Mike Sutherland, S. Y. Li, D. G. Hawthorn, R. W. Hill, F. Ronning, M. A. Tanatar, J. Paglione, H. Zhang, Louis Taillefer, J. DeBenedictis, Ruixing Liang, D. A. Bonn, and W. N. Hardy. Delocalized fermions in underdoped cuprate superconductors. *Phys. Rev. Lett.*, 94(14):147004, Apr 2005. 84

[102] J. L. Tallon and J. W. Loram. The doping dependence of t^* - what is the real high-t_c phase diagram? *Physica C: Superconductivity*, 349(1-2):53 – 68, 2001. 87, 92

[103] J. L. Tallon, J. W. Loram, G. V. M. Williams, J. R. Cooper, I. R. Fisher, J. D. Johnson, M. P. Staines, and C. Bernhard. Critical doping in overdoped high-t_c superconductors: a quantum critical point? *physica status solidi (b)*, 215(1):531–540, Sep 1999. 87, 92

[104] Takashi Tayama, Toshiro Sakakibara, Hitoshi Sugawara, Yuji Aoki, and Hideyuki Sato. Magnetic phase diagram of the heavy fermion superconductor $PrOs_4Sb_{12}$. *Journal of the Physical Society of Japan*, 72(6):1516–1522, 2003. 38, 44, 52

[105] Tom Timusk and Bryan Statt. The pseudogap in high-temperature superconductors: an experimental survey. *Reports on Progress in Physics*, 62(1):61, 1999. 84

[106] Michael Tinkham. *Introduction to Superconductivity*. McGraw-Hill, Inc., 1975. 4, 9, 10, 13, 16, 80

[107] C. C. Tsuei, J. R. Kirtley, C. C. Chi, Lock See Yu-Jahnes, A. Gupta, T. Shaw, J. Z. Sun, and M. B. Ketchen. Pairing symmetry and flux quantization in a tricrystal superconducting ring of $YBa_2Cu_3O_{7-\delta}$. *Phys. Rev. Lett.*, 73(4):593–596, Jul 1994. 84

[108] R. E. Walstedt, W. W. Warren, R. F. Bell, R. J. Cava, G. P. Espinosa, L. F. Schneemeyer, and J. V. Waszczak. Cu63 nmr shift and linewidth anomalies in the $t_c = 60k$ phase of y-ba-cu-o. *Phys. Rev. B*, 41(13):9574–9577, May 1990. 84

[109] Yuxing Wang, Bernard Revaz, Andreas Erb, and Alain Junod. Direct observation and anisotropy of the contribution of gap nodes in the low-temperature specific heat of $YBa_2Cu_3O_7$. *Phys. Rev. B*, 63(9):094508, Feb 2001. 88

[110] Neil W.Ashcroft and N. David Mermin. *Solid State Physics*. Thomson Learning, Inc., 1976. 3, 13, 26, 28, 29, 61, 82, 84, 95

[111] D. A. Wollman, D. J. Van Harlingen, W. C. Lee, D. M. Ginsberg, and A. J. Leggett. Experimental determination of the superconducting pairing state in ybco from the phase coherence of ybco-pb dc squids. *Phys. Rev. Lett.*, 71(13):2134–2137, Sep 1993. 84

[112] D. A. Wright, J. P. Emerson, B. F. Woodfield, J. E. Gordon, R. A. Fisher, and N. E. Phillips. Low-temperature specific heat of $YBa_2Cu_3O_{7-\delta}$, $0 \leq \delta \leq 0.2$: Evidence for d-wave pairing. *Phys. Rev. Lett.*, 82(7):1550–1553, Feb 1999. xiii, 88, 89

[113] M. K. Wu, J. R. Ashburn, C. J. Torng, P. H. Hor, R. L. Meng, L. Gao, Z. J. Huang, Y. Q. Wang, and C. W. Chu. Superconductivity at 93 k in a new mixed-phase y-ba-cu-o compound system at ambient pressure. *Phys. Rev. Lett.*, 58(9):908–910, Mar 1987. 80